To the Graduate Council:

I am submitting herewith a dissertation written by Alvin Ray Womac entitled "Fluid Fertilizer Injector Development Based Upon Dynamic Response of *In Situ* Soil Subjected to Impact Loading." I have examined the final copy of this dissertation for form and content and recommend that it be accepted in partial fulfillment of the requirements for the degree of Doctor of Philosophy, with a major in Agricultural Engineering.

Fred D. Tompkins, Major Professor

We have read this dissertation
and recommend its acceptance:

Accepted for the Council:

Vice Provost
and Dean of The Graduate School

FLUID FERTILIZER INJECTOR DEVELOPMENT BASED UPON DYNAMIC RESPONSE OF *IN SITU* SOIL SUBJECTED TO IMPACT LOADING

A Dissertation

Presented for the

Doctor of Philosophy

Degree

The University of Tennessee, Knoxville

Alvin Ray Womac

December 1988

To:

My Wife, Eleanore,

for her devotion and support.

My Mother, the late Mrs. Jean W. Womac,

for her noble exhortation.

My Father, Mr. Neal R. Womac,

for his spirited encouragement.

My Brother, Mr. Jeffrey S. Womac,

for his courageous support.

ACKNOWLEDGMENTS

The author appreciates the immeasurable technical and moral support provided by the entire staff of the Agricultural Engineering Department and by staff members from other departments.

The author thanks Dr. Houston Luttrell who generously made departmental resources available for the project.

Dr. Fred D. Tompkins served as major professor with superb leadership and is deeply appreciated.

Dr. Eric C. Drumm, committee member from the Civil Engineering Department, provided invaluable insight for solving the soil dynamics problem.

Dr. Robert S. Freeland rendered much assistance for proper data acquisition by the microcomputer-based system.

Dr. Donald D. Howard, committee member from the Plant and Soil Science Department, contributed to the design of the fertilizer injector.

Drs. Luther R. Wilhelm and Bobby L. Bledsoe, committee members, provided valuable information regarding data acquisition and analysis and machine design.

Dr. William E. Hart, Dr. John B. Wilkerson, Mr. Lannie O. Hillon, and Mr. J. Walter Hitch helped the author with many important details of the project.

Mr. Paul E. Elliott, Mr. Walker Garner, and Mr. Craig Wagoner provided practical advice and patiently assisted with fabrication of the instrumented probe and fertilizer injector.

Dr. Robert D. Freeland, Dr. John G. Graveel, Dr. William L. Parks, Mr. John F. Bradley, and Mr. Bobby McKee provided information about soils used in this project.

Mr. Yung Chung, Civil Engineer with Tennessee Valley Authority, was consulted about resonant column test procedures. Tennessee Valley Authority provided the resonant column device.

Finally, the author would also like to thank fellow graduate students who gave help and suggestions.

ABSTRACT

An experimental machine for injecting fluid fertilizer into the soil at discrete increments with minimal soil disturbance was developed. The design featured a probe-type injector, the design of which was based upon measurements of dynamic soil response to impact loading.

A microcomputer-based data acquisition system was developed and employed for high-frequency monitoring of a probe impacted into the *in situ* surface of clay loam, fine sandy loam, and silt loam soils. Data defining impact force on the probe versus depth of penetration were obtained for probe diameters ranging from 9.5 to 19.1 mm and probe striking velocities ranging from 2.0 to 5.0 m/s. Results showed that final probe penetration depth strongly affected peak probe force. A regression model based upon input energy, probe diameter, and penetration depth was developed to predict peak impact force on a probe.

Dynamic soil characteristics were measured to quantify the soil conditions used in the penetration tests. Soil specimens were tested in a torsional-type resonant column device, employing a method developed to test agricultural soils at low confining stresses. Measured shear modulus, damping ratio, and strain amplitude ranged from 13.1 to 38.1 MPa, 0.89 to 4.04 percent, and 4.9×10^{-5} to 11.9×10^{-5} cm/cm, respectively. Generally, shear modulus decreased and damping ratio increased with an increase in strain amplitude.

A prototype injector employing a kinematically inverted slider-crank mechanism was evaluated. Vertical orientation of the mechanism allowed a member, or probe, to engage soil during injector travel. Horizontal probe tip velocity offset injector travel velocity. A hydraulic-based actuator system controlled this velocity relationship. The probe released fluid through the tip during soil penetration. A custom-built fluid dispenser system integrated with the probe mechanism consisted of a pressure-regulated source, rotary timing valve, rotary fluid distributor, and probe tip valve. Fluid injection occurred at 400-mm intervals at a soil depth of 65 mm. Steady flow through the probe tip was described with a modified orifice flow equation. Reduction in intermittent flow rate with increasing crank speed was described with a decaying exponential function.

TABLE OF CONTENTS

LIST OF TABLES

LIST OF FIGURES

FIGURE PAGE

CHAPTER I

INTRODUCTION

1. BACKGROUND AND STATEMENT OF THE PROBLEM

No-tillage cropping systems accomplish planting without the use of moldboard plows, disk harrows, or chisel plows to prepare a seedbed. Crop residue is left on the surface of the ground after no-till planting because: 1) soil erosion is decreased (McGregor and Greer, 1982; Dickey et al., 1983); and 2) soil moisture is conserved (Blevins et al., 1971; Gallaher, 1977). Since fertilizers are typically incorporated into the soil with the above implements, fertilizers have been surface applied to many no-till crops (McDowell and McGregor, 1980; Fee, 1982; Touchton and Hargrove, 1982). Surface applications of phosphorus (P) and potassium (K) have yielded satisfactory plant responses (Singh et al., 1966; Shear and Moschler, 1969; Triplett and Van Doren, 1969; Moschler et al., 1972; Kang and Yunusa, 1977; Yost et al., 1979). However, surface application of nitrogen (N) has not been as effective as subsurface placement (Bandel et al., 1980; Mengel et al., 1982; Dowding et al., 1984).

Two major problems are associated with surface application of N: 1) N is lost due to NH_3 volatilization (Terman and Hunt, 1964; Mengel et al., 1982; Touchton and Hargrove, 1982); and 2) N becomes immobilized within the organic crop residues (Doran, 1980; Touchton and Hargrove, 1982). The magnitude of each problem depends on the specific environment (soil moisture content, organic matter content, soil temperature, soil pH, etc.) (Ernst and Massey, 1960; Terman and Hunt, 1964) and on the applied form of N (Mengel et al., 1982; Touchton and Hargrove, 1982). These problems emphasize the need to incorporate N sources used for no-till crops.

Ammonium nitrate (NH_4NO_3) has been a popular N source (Slack, 1972) for granular surface application because of low volatilization losses, but it has become expensive and less common on the fertilizer market (Fee, 1983; Lessiter, 1984a). Anhydrous ammonia (NH_3) has also been commonly applied by subsurface injection (Fee, 1982; Fee, 1983), because it has been an economical N source. Lack of handling and storage convenience and safety problems have hindered widespread acceptance of anhydrous ammonia as an N source (Pesek et al., 1971). Urea (NH_2CONH_2) solutions (especially urea-ammonia nitrate, UAN) are expected to become important future N sources (Pesek et al., 1971; Bridges, 1982). Urea solutions have been surface applied and found to have a high volatilization (Ernst and Massey, 1960; Terman and Hunt, 1964; Hargrove and Kissel, 1979; Mengel et al., 1982; Touchton and Hargrove, 1982), especially if substantial rainfall did not soon follow application to transport the solution into the soil (Fox and Hoffman, 1981).

Contrary to rainfall being a benefit for fertilizer application, rainfall intensity that exceeds infiltration can result in N losses by surface runoff (Angle et al., 1984; Owens et al.,1984; Baker et al., 1986). Infiltrated water may also leach N from the root zone into subsurface water supplies (Hubbard and Sheridan, 1983; Owens et al., 1983; Cameron and Wild, 1984; Lowrance et al., 1984a;

Lowrance et al., 1984b; Timmons, 1984; Schreiber, 1985; Schreiber and McDowell, 1985; Hergert, 1986). Proper timing of N application, with respect to anticipated nutrient uptake by the crop, should help minimize leaching.

N sources can be difficult to incorporate in a no-tillage system at the proper time with conventional applicators because: 1) field residue interferes with knives and firm soil inhibits sealing of the knife slot (Fee, 1983); and 2) conventional applicators inherently disturb established crop stands. The difficulties with knives have been partially overcome by using coulters ahead of the knives, knife sealing wings, and packing wheels (Fee, 1983; Lessiter, 1984b). However, conventional applicators significantly disturb the soil structure which is contrary to the objectives of no-tillage cropping systems.

Probe-type mechanisms that penetrate the soil and inject fluid at distinct intervals offer an alternative method for incorporating N sources. Use of the probe minimizes soil disturbance and crop damage; consequently, fluid nutrients can be readily applied at the most efficient time for plant uptake.

Prediction models for dynamic soil penetration resistance are incomplete (Sanglerat, 1972; Perumpral, 1983) and only useful for making relative comparisons at a particular site (Lambe and Whitman, 1979). Consequently, there exists a lack of design information for dynamic probe-type mechanisms.

2. OBJECTIVES

The purpose of this study was to design, construct, and evaluate a probe-type applicator for subsurface placement of fluid fertilizers for no-till crop fertilization. Specific objectives were:

1. To obtain design data for a probe-type applicator based upon the dynamic response of impact loaded *in situ* soil.
2. To design, construct, and evaluate a prototype probe-type fluid fertilizer applicator.

CHAPTER II

REVIEW OF LITERATURE

1. FLUID FERTILIZER INJECTION EQUIPMENT

Commercially Available Units

Most crop producers use a simple, yet reliable, soil opener device to inject fertilizer solutions. These devices are pulled through the soil at considerable tractor operation expense and soil structure damage. A tube is attached to the back side of the opener to deposit fluid fertilizer behind the opener as it travels through the soil. When much plant residue covers the soil surface, applicators usually mount a coulter in front of the opener so that the opener trails in a slot or cleared path. Many commercial coulter/opener assemblies are available in a variety of shapes and sizes (Colby Mfg. Co.; DMI, Inc.; Fleischer Mfg. Inc.; Harlan Mfg.; Werts Corp.; Yetter Mfg. Co.). Chichester et al. (1984) evaluated, using magnitude of soil disturbance as a basis, several commercial coulter/opener combinations.

Curley and Smith (1985) described the grain drill built by Colby Manufacturing Company that used dual fertilizer injection knife assemblies per crop row. One knife assembly deposited a formulation of fluid starter fertilizer below and without direct contact to deposited seeds. A second assembly injected the starter formulation and/or UAN between rows at a depth up to 150 mm, which was deeper than the injection by the in-row assembly. The design was claimed to eliminate the danger of seedling injury due to seedling contact with fertilizer.

DMI, Inc. (1985) marketed a spring-loaded, fertilizer applicator coulter/knife assembly. The knife trailed the 510-mm diameter coulter by approximately 150 mm and penetrated about 75 mm deeper than the coulter. The assembly was mounted on a 100-mm square toolbar. Each coulter/knife assembly required approximately 10 to 12 kw of power-take-off-rated tractor power for operation in typical soils.

Fleischer Manufacturing Inc. (1985) marketed a fertilizer applicator equipped with cutting disks having depth-control bands or smooth coulters and depth-control wheels. The applicator could be outfitted with either a rigid or spring-mounted knife that trailed the disk or coulter a distance of about 890 mm. Penetration depth of the knife was adjustable. Either cutter and knife combination was secured to a mounted toolbar which also served as a hitch for anhydrous ammonia and/or liquid fertilizer tank wagons.

Allied Chemical Co. developed an applicator that blasts liquid fertilizer through crop residue into the ground at 13800 kPa pressure (Lessiter, 1984c). Fertilizer flowed through a nozzle attached to a floating slide shoe that followed the ground contour when pulled through the field. Only high-quality, clear liquid fertilizers were recommended for use with the applicator, since the nozzle orifices were prone to abnormal abrasive wear due to high operation pressure.

John Blue Co. marketed the applicator, under the trade name Nutri-Blast, as a mounted unit, an attachment for no-till planters and grain drills, or as a caddy unit. The caddy unit could be used alone or in conjunction with soil-engaging implements trailing the unit (Solutions, Inc, 1984). Possible problems with using this unit include inadequate and erratic soil penetration depths.

Experimental Units

Fluid injectors using probes attached to a wheel or drum have been patented, including U.S. Patents numbered 3,602,166, 3,025,806, 2,649,061, and 2,649,060. Each of these machines use multi-soil openers, or probes, fixed to a component that rotates about an axle. Development of a simpler version of this concept is described in the following paragraph.

James Baker, at Iowa State University, designed an injector (Point Injector) that metered and punched fluid fertilizer through crop stubble and into soil (Dawelbeit et al., 1981). The primary components of the apparatus were a rotary valve (wheel hub), a hollow-tined wheel, and a pump. The wheel resembled a spoked wagon wheel with the spokes protruding through the outer rim. As it rotated over the ground, the spokes (probes) in contact with soil aligned with a fluid supply port in the wheel hub. During this alignment, fluid was forced through the probe and into the soil. The injector could be used as an independent unit or be mounted on and used in conjunction with another implement, such as a planter or cultivator. No provision for sealing the holes in the soil resulting from operation was provided. Subsequent agronomic evaluation of point-type injection indicated increased crop yields when fertilizer was applied by this method (Baker et al., 1983; Baker and Timmons, 1984; Baker et al., 1985; Baker et al., 1986).

However, Baker encountered problems with the Point Injector, including wheel warping, rotary valve leaks, and undesirable soil disturbance. Several generations of the Point Injector have been built. With each generation, they have increased the number of spokes in the wheel. The first had six. The most recent had twelve. Also, the diameter of the wheel has been increased with each generation. These changes may indicate that reductions in soil disturbance were being attempted. Baker noted that the wheel turns through the soil on the spoke tips. The spokes on the most recent generation enter and exit the soil at an angle of about 45 degrees. Consequently, a 70-mm streak of soil disturbance forms at the surface. A field version of the Point Injector was trial marketed by Cady Systems, Inc. (Wanzel, 1988). This market study was not concluded before the publication of this dissertation.

Wilkins et al. (1982) modified a John Deere HZ deep furrow grain drill opener to place liquid fertilizer 50 mm below deposited seeds. Nitrogen applied with the modified opener at rates as high as 45 kg/ha did not reduce stands of wheat. Under the test conditions encountered, fertilizer banded below the seed with the modified opener sometimes increased, but never reduced, wheat yields.

Townsend and Bethge (1984) developed a rotary furrow opener used for minimum-tillage planting and fertilizer placement. The opener formed a furrow with a rotating, toothed disk. The soil lifted by the disk was split into two streams and then each stream was redeposited into the furrow on top of fertilizer and seed, respectively. Upon operating a prototype through extreme surface residues and relatively hard soils, they concluded that the concept was feasible.

Rogers and Rinholm (1987) investigated developing a high-pressure (40000 kPa) applicator similar to the Nutri-Blast. The investigated applicator, referred to as the Pulse Bander, incorporates a nozzle-mounted, solenoid-actuated valve to allow intermittent fluid flow. The applicator nests fluid fertilizer every 150 mm. Depth of soil penetration, durability of the solenoid, and other pertinent details of the system were not disclosed.

2. SOIL DYNAMICS

Mechanics of Soil Penetration

Prandtl's Theory

Ludwig Prandtl (1875-1953), a German physicist, theorized that the penetration of a homogeneous, isotropic media by a rigid punch could be analyzed in terms of plastic equilibrium (Jumikis, 1969). This established the basis for present-day calculation of bearing capacity and pile capacity. Prandtl assumed that bodies having elastic deformations could be treated as rigid bodies and that plastic deformations had zero volume change. Figure 1 illustrates Prandtl's assumed failure zone with streamlines of plastic displacement shown on the right and stress-trajectories shown on the left. This theory disregards the weight of the triangular wedge directly below the load and assumes that this wedge acts like a rigid body. Consequently, Prandtl's ultimate stress equation at plastic equilibrium is written in the following form (Jumikis, 1969):

$$\sigma_u = c \cot(\phi)\{[\tan^2(\pi/4 + \phi/2)]e^{\pi \tan(\phi)} - 1\} \qquad (2.1)$$

where,

σ_u = ultimate compressive stress
c = cohesion of soil
ϕ = friction angle of soil.

Terzaghi (1943) modified Prandtl's equation to prevent the ultimate compressive stress from becoming equal to zero when cohesion equalled zero (Jumikis, 1969). Terzaghi suggested that the factor c' should be added to the original quantity c in Prandtl's equation. The factor c' is computed as follows:

$$c' = \gamma\ t \tan(\phi) \qquad (2.2)$$

where,

c'= added cohesion factor
t = equivalent soil surcharge height
γ = unit weight of soil.

Jumikis (1969) discussed Prandtl's Theory with Terzaghi's contribution and provided illustrative examples of bearing capacity computation using this model.

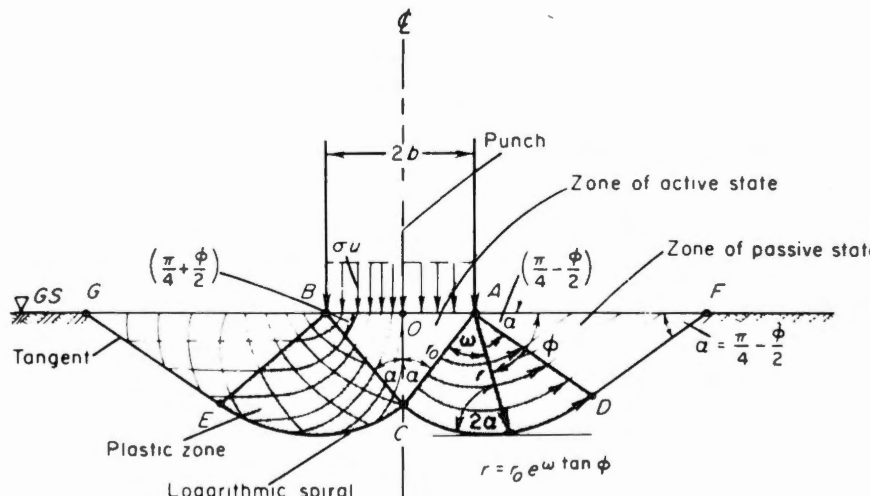

LEGEND

AB = loaded region
FDCEG = boundary of plastic region against the elastic one
DF = GE = tangents to curves CD and CE
CD = CE = logarithmically spiraled curves
$\alpha = \pi/4 - \theta/2$
θ = friction angle of soil

(from Jumikis, 1969)

FIGURE 1. Prandtl's failure zone of plastic equilibrium beneath a punch.

Bearing Capacity

Das (1983) reviewed the general equation of ultimate bearing capacity for static vertical loading. The equation is expressed as follows:

$$q_u = cN_cS_cd_c + qN_qS_qd_q + 0.5\ \gamma BN_\gamma S_\gamma d_\gamma \qquad (2.3)$$

where,

q_u = ultimate load per unit area of the foundation
c = cohesion of soil
γ = effective unit soil weight below foundation
q = γD_f
D_f = depth of foundation
B = width of foundation
N_c, N_q, N_γ = bearing capacity factors [$f(\phi)$]
ϕ = friction angle of soil
S_c, S_q, S_γ = shape factors
d_c, d_q, d_γ = depth factors.

Numerous researchers evaluated the bearing capacity, shape, and depth factors based on variations of the Prandtl soil failure surface. Bowles (1982) reviewed the most common equations used to calculate these factors.

Das (1983) also showed that ultimate dynamic bearing capacity has been experimentally correlated to ultimate static bearing capacity. However, he cautioned that the development of models describing dynamic loading was limited. Consequently, only general approximations for ultimate dynamic bearing capacity are available. For example, the bearing capacity factors for sands increased for impact type loadings; the increase was greater for dense saturated sand because of possible development of negative pore water pressure in the soil. Also, the undrained cohesion of saturated clays for dynamic loading was approximated as fifty percent greater than the undrained cohesion for static loading.

Pile Capacity

Lambe and Whitman (1979) noted that the static load capacity of a pile is the sum of the point resistance plus the frictional shaft resistance. Point resistance is equivalent to bearing capacity and is computed similarly (see preceding paragraphs). Shaft resistance is due to soil-pile friction along the length of driven pile and is equal to the area of pile surface in contact with the soil times a unit shaft resistance. Figure 2 shows several assumed soil failure patterns used to compute the static load capacity of a pile. Note the soil deformations related to point resistance and shaft resistance. Lambe and Whitman (1979) noted that a pile is statically indeterminate and that a precise analysis is difficult. Thus, most computations of pile capacity are based on empirical knowledge and the results of pile tests performed at the actual site for pile installation.

Winterkorn and Fang (1975) showed that dynamic pile formulas were developed to determine the static load capacity of a pile. These formulas were based on the following energy balance:

$$\text{Energy input} = \text{Energy used} + \text{Energy lost} \qquad (2.4)$$

where,

Energy input = energy delivered by pile driver
Energy used = driving resistance times pile movement
Energy lost = unaccounted energy estimated on the basis of past experiences.

Lambe and Whitman (1979) noted that this formula is unreliable for relating dynamic to static pile capacity. Winterkorn and Fang (1975) also stated that this formula was pseudoscientific because of basic

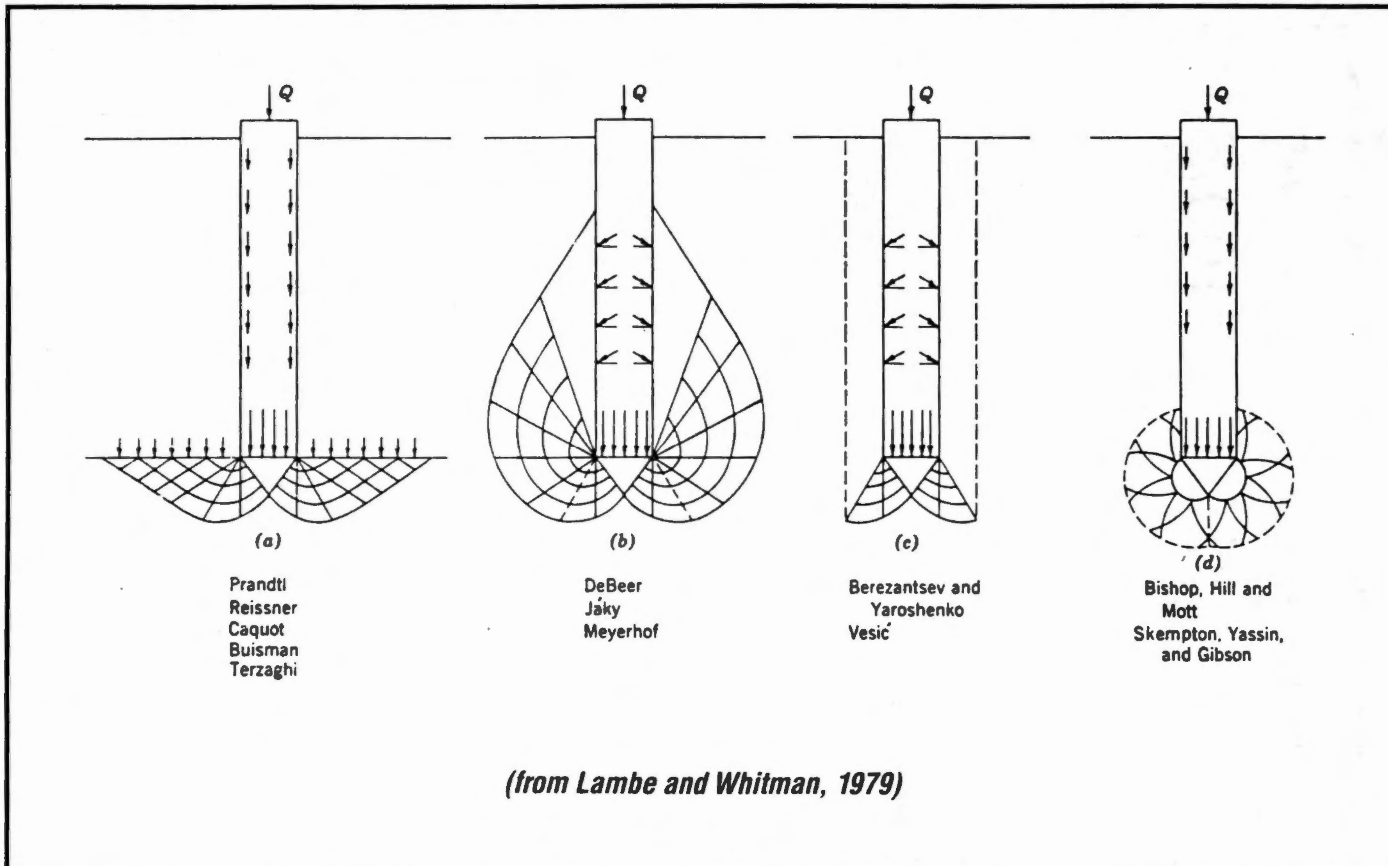

FIGURE 2. Assumed soil failure patterns used to compute the static load capacity of a pile.

differences between static and dynamic behavior of soil. However, the formula was considered appropriate for comparing the dynamic resistance of piles at one site.

Effects of Strain Rate on Soil Penetration

Soil Strength Parameters

Fountaine and Brown (1959) evaluated a torsional shear box operated within an *in situ* sandy clay loam, sandy loam, and clay soil. Of particular interest, the shear strength of these soils was measured at rotational speeds of 51 deg/s and 1.2 deg/s. For these operating conditions, the rate of straining did not have a significant effect on shear strength.

Hendrick and VandenBerg (1961) investigated the effects of tensile load application rate upon the ultimate strength and energy requirements associated with the failure of a clay soil. These tensile strength determinations were performed at various soil moisture contents and loading rates ranging from near zero to 0.06 $kg/mm^2/s$. Stress and strain in the soil samples were monitored during the determinations. Loading rate had no effect upon ultimate strength, but increased loading rates resulted in smaller energies required to cause failure because the rapidly-loaded samples strained less before failure.

Aref et al. (1975) investigated the dynamic shear strength properties of unsaturated soils by the method of deformation energy partition (Chancellor et al., 1969). This method used stress-strain data obtained from confined and unconfined axial compression tests to compute total input energy, volume strain energy, shear strain energy, and energy transmitted to sample surroundings. A clay loam soil was tested at various moisture contents using strain rates of 0.0003/s and 0.0042/s. As strain rate increased, higher axial stresses at failure were observed. However, the proportions of input compressive energy used for volumetric strain, shear strain, or lateral expansion were not affected by strain rate.

Flenniken et al. (1977) studied dynamic soil strength parameters from unconfined compression tests. The unconfined compression device consisted of three parts: a carriage, a guide track, and a stand to support the soil sample and piezo-electric force transducer. Rate of strain was varied by adjusting the drop height of the carriage; carriage velocity at the soil sample ranged from 0.60 to 7.20 m/s. The data signal from the transducer was routed to an amplifier and then to a storage oscilloscope which displayed a force-time trace and a displacement-time trace from a magnetic pickup. Force-time data were superimposed onto a high speed movie film exposed to the soil deformation process and to corresponding timing marks provided by a pulse generator. Axial and radial deflections of the soil samples were then analyzed. Results indicated the following: 1) peak dynamic stresses were 100 to 500 percent greater than the maximum stresses obtained in quasi-static tests; 2) energy under the stress-strain curve increased with increasing strain rate; 3) an increase in soil density increased peak stresses, energy to peak stress, and a dynamic strength parameter; and 4) dynamic unconfined soil strength parameters were generally independent of sample size.

Stafford and Tanner (1983a) investigated the effect of deformation rate on the shear strength of a sand and a clay soil. A rotating annular shear device and a rotating plane friction annulus were used to shear soil in the speed range equivalent to 0.0015 to 5.000 m/s linear sliding speed. Soil cohesion was found to vary logarithmically with deformation rate over a wide range of moisture contents. Soil internal friction angle was independent of deformation rate and residual shear strength did not vary in a consistent manner with deformation rate.

Soil-Metal Sliding Resistance

Stafford and Tanner (1983b) studied the effect of sliding speed on the soil-metal friction between steel and a clay and a sandy clay loam soil. The effect was analyzed by use of the following Coulomb-type equation:

$$\tau = C_a + \sigma \tan(\delta) \tag{2.5}$$

where,

τ = frictional stress
C_a = soil adhesion
σ = normal stress
δ = angle of soil to metal friction.

Measurements of soil-metal frictional stress were made over a normal stress range of 23.0 to 540.0 kPa. Sliding speed was varied from 0.0015 to 5.000 m/s. Test results showed a logarithmic increase in the friction angle with speed over a wide range of soil moisture contents. Adhesion did not exhibit a clear relationship with speed. Consequently, the soil-metal frictional stress increased with speed for these operating conditions.

Soil-Tool Interactions

Rowe and Barnes (1961) investigated the relationship between speed and tillage tool draft. They measured the soil-metal frictional resistance and shear strength of a sand, silt loam, clay loam, and silty clay soil. Rate of shear was varied from 0.20 to 6.80 m/s. For the soil conditions tested, the frictional resistance was considered independent of speed. Shear strength increased with increases in speed. Also, the shear strength increase became progressively larger in the soils with higher clay content.

The force required to push a probe through soil at a constant velocity has been extensively studied. Turnage and Freitag (1969) studied the effects of cone velocity and size on soil penetration resistance. Penetration tests were conducted with six sizes of 30-degree, right circular cones and three sizes of flat, circular plates in three fine-grained saturated soils. Vertical penetration tests were conducted at constant velocities which ranged from 0.0003 to 3.4933 m/s. Horizontal penetration tests were performed at a velocity that increased linearly from zero to maximum velocities that ranged from 3.50 to 45.3 m/s. ASAE standard penetration tests (conical tip having 30-degree included angle and 323 mm^2 projected area pushed at a speed of 0.03 m/s) were made on each soil sample used for vertical or horizontal penetration. The results were summarized by the following expression:

$$(CI_x)/(CI_s) = [((v/d)_x)/((v/d)_s)]^k \qquad (2.6)$$

where,

CI_x = cone index of specific cone, kPa
CI_s = cone index of an ASAE standard cone, kPa
v = penetration rate, m/s
d = base diameter of 30-degree right circular cone, mm
v_s = standard penetration rate = 0.03 m/s
d_s = standard cone base diameter = 20.3 mm
k = exponent of shear rate factor.

This relation was valid for velocities which ranged from 0.02 to 43.2 m/s, diameters from 13.0 to 79.0 mm, and saturated soils ranging from silt to heavy clay. The exponent ranged from 0.091 to 0.109 for these conditions.

Wismer and Luth (1972) used a horizontal penetrometer to predict the performance of plane soil cutting blades operating in clay soil. Of particular interest, they examined the relationship between cone index, penetration speed, and cone diameter. Penetration speed of the penetrometer was varied from 0.02 to 35.6 m/s for two different sized 30-degree cones operated in saturated clay. The results indicated a velocity/diameter ratio of 0.100. These results also agreed with those obtained by Turnage and Freitage (1969).

Stafford (1979) observed the performance of a rigid tine in relation to soil properties and tine speed. A tine was operated in a sandy clay loam and a clay soil contained in a laboratory bin. Tine velocity was varied from 0.005 to 5.50 m/s. Draft force deviated 5 to 10 percent from the mean value for most soil conditions, and

Stafford noticed a periodic deviation of 10 to 40 percent (from mean) during tests with dry soil conditions. He observed two force-speed relationships. First, at low moisture contents, force increased at an increasing rate with speed; these data were fitted with polynomial curves. Second, at high moisture contents, the force increased at a decreasing rate with speed; these data were fitted with decaying exponential curves. Increase in soil cohesion with speed was determined to be the most significant component affecting the increase in draft force with speed.

Clark and Wagner (1983) used performance equations derived for inclined blades (Soehne, 1956) to simulate these tools operating under numerous conditions. For example, the effects of blade velocity and soil type on draft force were isolated. A flat blade was simulated to operate in sand, sandy loam, and loam soils in a velocity range from zero to 4.17 m/s. Draft force required to operate the blade increased with increases in velocity for each soil type. Draft forces in the sandy soil were most sensitive to changes in velocity, as compared to the other tested soils. They attributed this greater sensitivity to a lack of cohesive forces and to greater percentages of acceleration forces.

Nicholson et al. (1984) tested the draft requirements for four different implements operated in silt loam and silty clay soils. Draft forces, implement speeds, and depths of operation were measured in the study. They also measured soil parameters, including moisture content, bulk density, and cone index. For a tandem disk harrow operated in the speed range of 0.278 to 2.22 m/s, draft was not significantly affected by speed. However, the draft of sweep and chisel plows was significantly affected by speed, depth, and an interaction of speed and depth. As the depth of these plows increased, the rate at which draft increased with speed also increased.

Adeli et al. (1986) reviewed the current techniques, including numerical methods, for predicting the soil penetration depth of free falling impactors. They concluded that the Sandia Laboratories' empirical formula was a very effective depth prediction technique. The Sandia formula is expressed as follows:

$$Xp = 162.1\ SK(W/A)^{0.5}\ \ln(1 + 21.53\ V^2/10^5) \tag{2.7}$$

where,

- Xp = predicted soil penetration depth, mm
- S = soil dependent penetrability index
- K = nose shape factor of impactor
  - = 0.56 for flat nose
  - = 1.33 for conic nose
- W = projectile weight, N
- A = cross-sectional area of impactor, mm^2
- V = impactor velocity upon impact (< 61.0), m/s.

This equation is only applicable when the depth of penetration is equal to or greater than three projectile diameters plus one nose length, because surface effects complicate the prediction at shallow depths. Adeli et al. noted that the penetrability index S is determined from full-scale penetration tests at the site, or from a site with similar soil conditions. This Sandia formula is valid for impactor velocities equal to or less than 61.0 m/s and for impact normal to the soil surface. Another Sandia formula similar to Equation 2.7 was listed by Adeli et al. for velocities which exceed 61.0 m/s.

Soil response to impact loads caused by high-velocity penetration can be quantified using parameters which have already been successfully employed to model the dynamic response of other geologic materials, such as rock. Pertinent parameters include the force-time trace, force-penetration trace, peak force, penetration depth, and input energy (Pang et al., 1986; Rogers et al., 1986).

Prediction of impact forces on a probe with the Turnage-Freitag model is not appropriate because of the inherent differences between penetration at constant velocity and that due to impact. The main difference is due to the additional soil resistance required to equilibrate the inertia force created by decelerating an impacting probe.

Wave Propagation Characteristics of Soil

Background

Application of dynamic loads to an object or media, such as soil, causes stress waves to propagate at a predictable velocity through the material. The stress wave hypothesis allows theoretical solutions to be derived and verified for bounded elastic media (Richart and Woods, 1970; Das, 1983); however, the concept also applies to problems having irrecoverable strain (Kolsky, 1963) and has been extended to soil tillage dynamics.

Gupta and Pandya (1967) developed a draft prediction model based on stress wave propagation velocity. They measured the propagation velocities of compression and shear waves caused by the motion of a simple implement, computed average compression and shear stresses based on these velocities, and showed that the computed stresses were in close agreement with the average stresses indicated by implement draft measured coincident with wave velocities.

Hendrick and VandenBerg (1961) noted that frequency of tool oscillation and soil resonant frequency are two major factors affecting the reduction in draft realized by vibratory tillage tools. Resonant frequency is a unique function of wave velocity and effective sample length. Thus, the measurement of stress wave velocity and/or resonant frequency in agricultural soils is crucial to understanding and modeling soil-tool dynamics.

Resonant Column Test

The resonant-column test is a laboratory procedure (Richart and Woods, 1970) used to measure the resonant frequency of soil. The resonant-column apparatus excites and monitors the low amplitude vibration of a cylindrical soil specimen supported within a triaxial test cell. The specimen is excited in one of two ways; longitudinal or torsional excitement imparts compression or shear waves, respectively. Excitation frequency is adjusted to produce system resonance; Young's modulus can then be calculated from soil density and compression wave velocity, while shear modulus can be calculated from soil density and shear wave velocity. The resonant column test also serves to determine the vibration damping characteristics of soil. Since the shear response of soil is an important aspect of tillage and traction, the study reported herein focuses on shear modulus and damping measured with the torsional-based device.

Several factors affect the determination of shear modulus and damping in soils. Hardin and Drnevich (1972a) reported that strain amplitude, effective mean principal stress, and void ratio are the most important factors that influence these determinations. They reported the following: (1) shear modulus decreases and damping ratio increases with increasing strain amplitude; (2) shear modulus increases and damping ratio decreases with increasing effective mean principal stress; and (3) shear modulus decreases and damping ratio decreases with increasing void ratio in undisturbed cohesive soils. Sample disturbance also affects the determinations, particularly for saturated clays. Seed and Idriss (1970) stated, "*in situ* moduli (for saturated clays) are two or three times greater than the laboratory test values at comparable strains."

Resonance testing methods for agricultural soils subjected to loads representative of field conditions are not clearly defined in the literature. Shear moduli and damping ratios were primarily determined for non-agricultural soils subjected to higher principal stresses and smaller void ratios than those of most agricultural soils (Hardin and Drnevich, 1972b). Principal stresses close to zero should be assumed for agricultural soil loads because of relatively shallow soil depths, unlike subsurface soils subjected to the confining stresses caused by overburden. The effect of wheel loads on confining stress at a soil-tool interface is probably minimal for interface-to-wheel distances greater than approximately one meter (Nichols et al.,1985).

CHAPTER III

STANDARD SOIL PROPERTY MEASUREMENTS

1. CLASSIFICATION PROPERTIES

The soil impact loading device described in the next chapter was operated in the surface of an *in situ* Etowah clay loam, a Hartsells fine sandy loam, and a Grenada silt loam soil. Selected properties of these soils are given in Table 1. Elapsed time since tillage, which may affect penetration resistance, was one year greater for the fine sandy loam than for the other two soils.

Average bulk density, moisture content, and organic matter content for each soil type (Table 1) were determined from ten replicated measurements. Soil bulk density, or dry density, was determined from 146-mm diameter by 149-mm deep samples removed from the soil surface with a section of steel tubing which had the leading edge beveled away from the sample. Soils included in the tests had similar bulk densities. Moisture content (dry basis) was determined by a standard oven-drying method (MacIver and Hale, 1970); the measurements indicated similar moisture contents among soils. However, if pore pressure had been monitored, it would have probably varied significantly because of the different grain size distributions of these soils. Moisture release curves documented for these soils (Longwell et al., 1963) confirm substantial differences among soil moisture tensions for the examined soils at the measured moisture contents. The effective stresses within the soil depend on

TABLE 1. Selected properties of tested soils.

Soil	Years Since Tillage	Bulk Density (g/cc)	Moisture Content (% d.b.)	Organic Matter (%)	% Passing Sieve No. 10 2.00 mm	% Passing Sieve No. 40 0.42 mm	% Passing Sieve No. 200 0.074 mm	Liquid Limit	Plas-ticity Index	USCS Identifi-cation
Clay loam	2	1.54	16.04	1.63	98	90	69	42	19	CL
Fine sandy loam	3	1.64	16.78	2.61	94	83	42	18	6	SM-SC
Silt loam	2	1.61	17.27	1.25	97	97	87	24	6	CL-ML

pore pressures and total applied stresses (Lambe and Whitman, 1979). Organic matter percentage was established from total carbon content determinations made by the Leco Dry Combustion Method (Smith, 1983). The assumed relationship between carbon and organic matter was that total carbon constituted 58 percent of the organic matter (Jackson, 1958). The soils tested had been last treated with lime several years prior to this study. Thus, effects of calcium carbonate on the carbon determinations should have been minimal.

Results of sieve analyses and Atterberg limit tests are also shown in Table 1. These analyses and tests were performed by the methods outlined by MacIver and Hale (1970). The soils were then classified using the Unified Soil Classification System (USCS) (Holtz and Kovacs, 1981); these results are listed in Table 1.

Cone penetrometer readings obtained with a manual instrument for each test site are listed in Table 2. These measurements were made in accordance with the procedures outlined in ASAE Standard S313.2 (ASAE Standards, 1987) with a penetrometer having a 20.3-mm cone-base diameter. Mean values for the penetrometer readings were calculated from 20 penetrations per soil type. The clay loam and silt loam had similar penetration resistances, which were less than that for the fine sandy loam. This difference will also be observed in the dynamic response data. Standard deviations of the readings are also reported in Table 2. These calculations indicate a smaller variability among cone indices for the fine sandy loam.

TABLE 2. Soil cone penetrometer readings for each soil type.

	Clay Loam		Fine Sandy Loam		Silt Loam	
Depth	Mean (kPa)	Standard Deviation (kPa)	Mean (kPa)	Standard Deviation (kPa)	Mean (kPa)	Standard Deviation (kPa)
Cone base	752	76	1441	98	690	43
51 mm	1289	206	2344	72	1255	90
102 mm	1731	278	2855	79	1696	101
152 mm	2131	103	2951	54	1917	125

2. DYNAMIC PROPERTIES

Resonant Column Device

The torsional-type resonant column device illustrated in Figure 3 was employed to determine the shear modulus and damping ratio of agricultural soils. The device consisted of a triaxial test cell containing a Soil Dynamics Instruments, Inc., Hardin oscillator positioned above and coupled to a soil specimen (Richart and Woods, 1970). Vibratory characteristics of the oscillator are listed in Table 3. The soil specimen was held in a membrane and installed on a rigid pedestal located below the oscillator. Shear waves generated by the oscillator passed from the coupler, through the specimen, and to the pedestal where they were reflected back into the specimen. The end restraints of the soil specimen provided vibration boundary conditions considered as a fixed-free system. A Columbia Research Laboratories, Inc. Model 902 accelerometer, mounted on the oscillator near the oscillator-specimen coupling, sensed the vibration amplitude of the system.

Pneumatic cylinders (Fig. 3) were used to support the oscillator above the soil specimen during configuration of the device. Thus, unconfined samples were not subjected to the weight of the oscillator. A counterbalance mechanism (Fig. 3) supported the oscillator during testing.

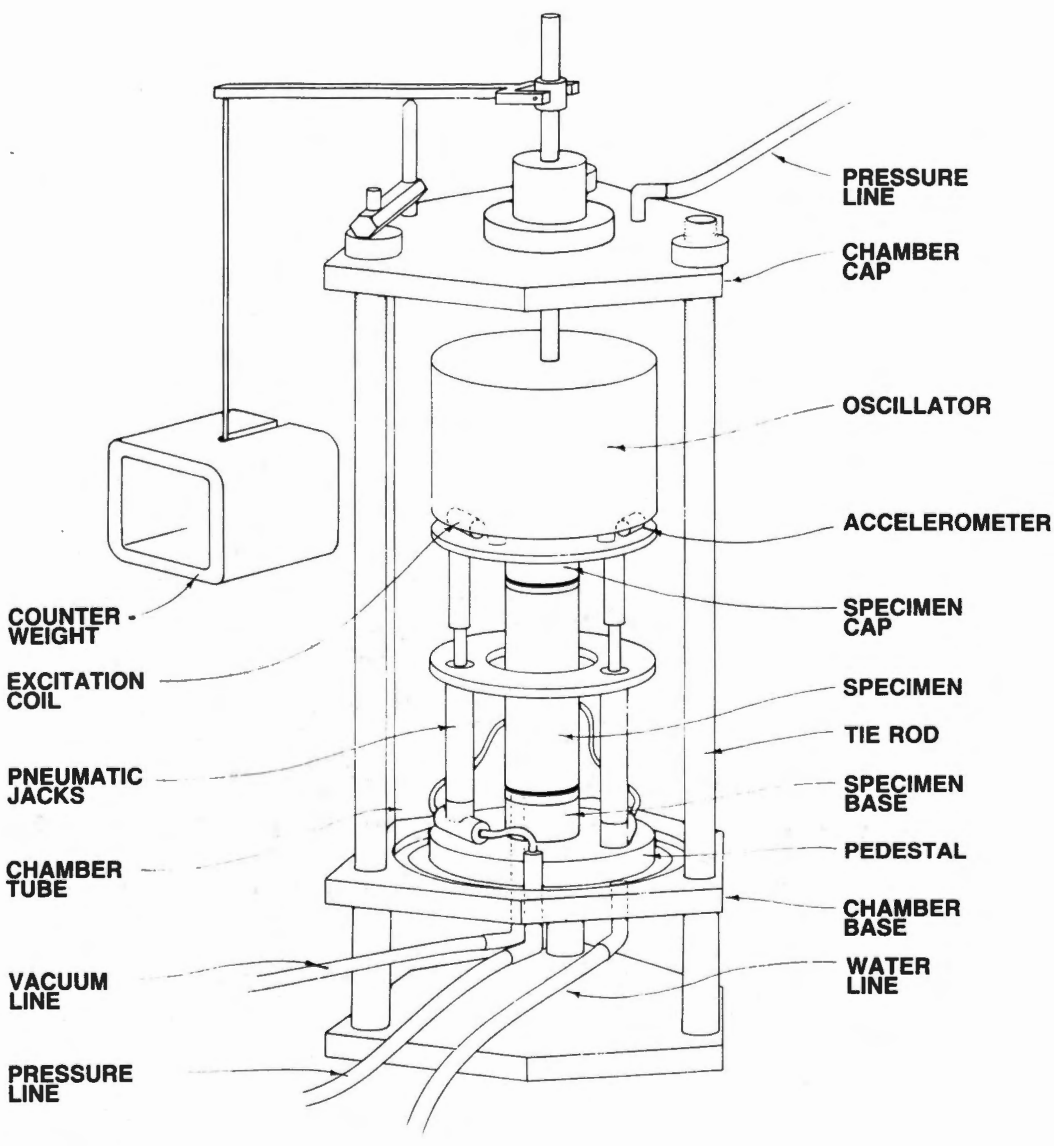

FIGURE 3. Torsional-type resonant column device used to test agricultural soils.

TABLE 3. Description and vibratory characteristics of the resonant column oscillator.

Parameter	Value
Brand Name	Soil Dynamics Instruments, Inc.
Model	Hardin Oscillator (U. S. Patent No. 3,362,316)
Active End Mass (w/Top Cap)	8.2 kg
Rotational Inertia	2.54214 g-cm sec^2
Torsional Apparatus Resonant Frequency	174.9 cps
Torsional Apparatus Logarithmic Decrement	0.011
Torque/Current Constant	831 g-cm/amp
Motion Transducer Calibration Factor	2500 mV/g

Signal Monitoring Apparatus

The signal monitoring apparatus connected to the resonant column device is shown in Figure 4. The oscillator was powered by a variable-output Waveforms, Inc. Model 512F sine wave generator. The signal frequency provided by the generator was monitored by a Dynascan Corp. digital frequency counter. The voltage potential across a precision (1 percent) resistor placed in series with the driving coils of the oscillator was monitored on the X-axis (horizontal) of a Tektronix, Inc. Type 564B storage oscilloscope. This potential was in phase with the forcing torque applied to the system (TVA, 1978). The accelerometer output, after being directed through a Columbia Research Laboratories, Inc. Model 4102 charge amplifier, was monitored on the Y-axis of the oscilloscope. The signal frequency output from the sine wave generator was varied until the resonant frequency was indicated as a vertical axis ellipse displayed on the oscilloscope (TVA, 1978). Furthermore, strain amplitude of the specimen was varied via the voltage level supplied to the oscillator.

Damping ratio was primarily determined by the steady-state method (TVA, 1978) based on system energy monitored during resonance. Several test results from the steady-state method were verified with the logarithmic decrement method (Wu, 1971); the latter involved re-configuration of the oscilloscope to plot accelerometer output on the Y-axis versus elapsed time displayed on the X-axis. Once resonance

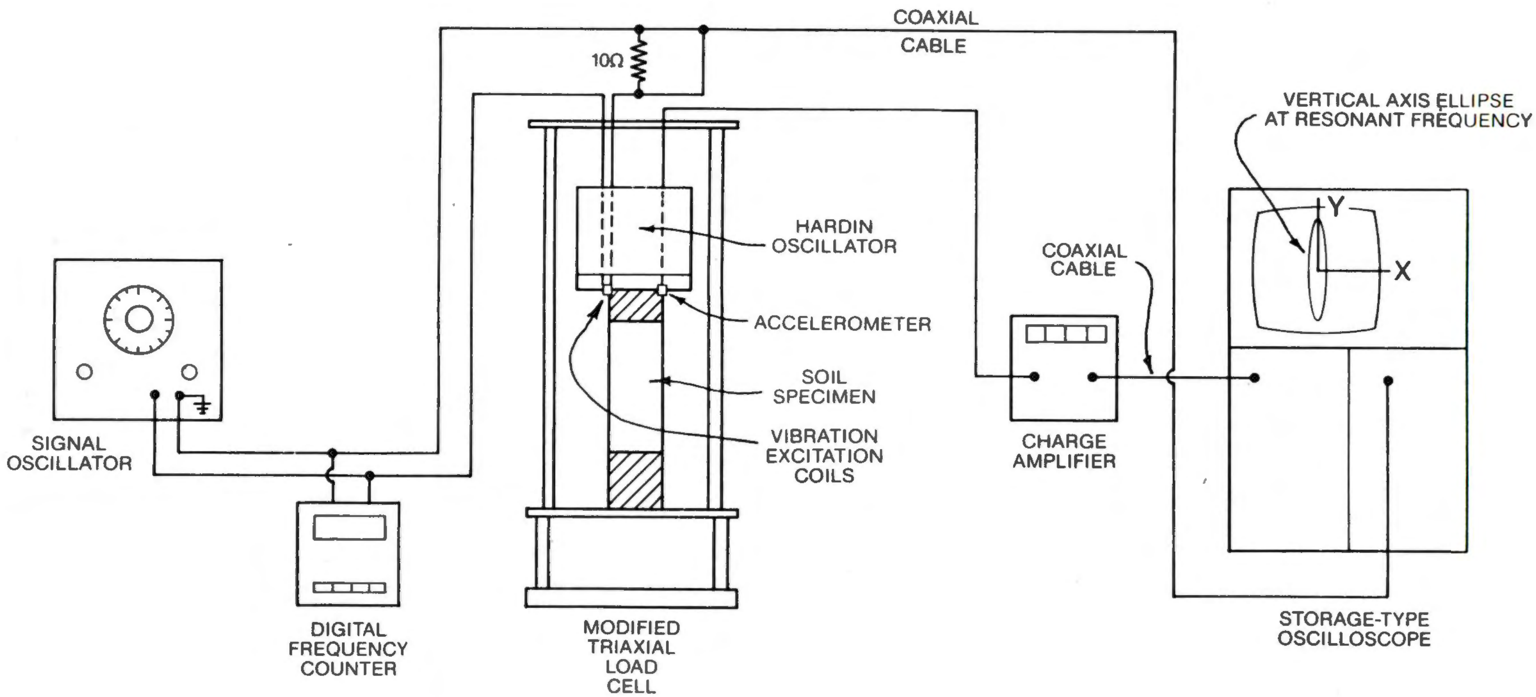

FIGURE 4. Schematic of signal monitoring apparatus connected to the resonant column device.

was established for the logarithmic decrement method, the oscillator current was then turned off and the amplitude decay was examined using the oscilloscope operating in storage mode.

Soil Specimen Preparation Methods

Two soil specimen preparation methods were examined. One half of the tests were performed with remolded specimens, whereas the remaining tests were performed with minimally-disturbed samples that were extracted from *in situ* deposits.

The first specimen preparation method was to remold the soil sample by compaction to a void ratio and moisture content similar to *in situ* conditions. Use of a split-type sample mold, having a negative backpressure applied, aided the formation of the specimen. The soil samples used to construct the specimens were transported and stored in heavy duty food freezer bags equipped with zipper-type seals. During storage in a room maintained at approximately 24 degrees Celsius and with minimal humidity control, the bagged soil samples typically lost one to two moisture percentage points (dry weight basis) per week. Consequently, the soils were completely dried in an oven and re-wetted to the appropriate moisture content immediately prior to resonance testing. The appropriate moisture content was assumed to equal the mean moisture content of the *in situ* condition for each soil type (Table 1, p.26). Each specimen was then formed in an ultra-thin latex membrane supported in the split-type sample mold positioned over the pedestal of the resonant column device. The specimens were constructed with 36-mm diameters and heights ranging from 72 to 81 mm.

The second specimen preparation method consisted of removing minimally-disturbed samples from *in situ* soil with an in-house fabricated sample removal tool. The tool consisted of a 36-mm i.d. by 83-mm tall cylindrical tube and a core removal plunger. The leading edge of the tube was beveled away from the sample. Sampling included forcing the tube into the selected *in situ* soil surface and then excavating the filled tube from the ground. The soil specimen was subsequently plunger-extracted from the tube into an ultra-thin latex membrane. During the extraction, 36-mm-diameter polyvinyl chloride (PVC) plugs were installed at each end of the sample to protect fragile corners. Membraned samples were then wrapped and sealed in food freezer bags and stored in a humidity-controlled sample chamber prior to testing. The success rate for obtaining these samples without visible signs of disturbance, such as cracks, was approximately 50 percent. Disturbance due to installation of the samples onto the resonant column pedestal also resulted in a cull rate of about 50 percent. Thus, only about one in four original samples was actually tested. Since observation of sample cracks was very subjective and some degree of disturbance was inevitable, these specimens are referred to as being minimally-disturbed rather than undisturbed. Moisture content and density were measured upon completion of resonance testing.

Resonant Column Test Procedures

Calibration of the resonant column device was verified by testing a dry Ottawah sand and comparing the test results with data published by Hall and Richart (1963) and Hardin and Black (1968). Three examples of compared data are presented in Table 4; examples A, B, and C were tested at similar void ratios and vibration strain amplitudes, but at the different confining stresses of 96, 48, and 24 kPa, respectively. Resonant frequency and measured shear modulus decreased, as expected, with decreasing confining stress. Predicted shear modulus was calculated using the following equation reported by Hardin and Black (1968):

$$G = 6908\ (2.17-e)^2\ s^{0.5}\ /\ (1+e) \qquad (3.1)$$

where,

G = shear modulus, kPa
e = void ratio expressed as a decimal
s = specimen confining stress, kPa.

In each example, this equation under-predicted the modulus as compared to the measured value. The prediction equation applies to round grained sands tested at low amplitudes of vibration. Hardin and Black (1968) defined low amplitudes of vibration as having a magnitude of 10^{-4} rad/rad or less. The error in modulus prediction may be because of small differences between strain amplitudes for predicted and measured moduli (Table 4). Damping ratio increased as confining stress decreased. The predicted damping ratio was calculated with logarithmic decrement versus double amplitude data reported by Hall and Richart (1963). The measured values for damping ratio were always greater than the predicted values in these

TABLE 4. Comparison between measured and predicted values of shear moduli and damping ratio of dry Ottawah sand.

Parameter	Test A	Test B	Test C
Specimen Height (mm)	82.6	83.1	82.0
Specimen Mass (gm)	143.6	144.3	141.4
Void Ratio	0.51	0.52	0.53
Confining Stress (kPa)	96	48	24
Measured Strain Amplitude (cm/cm) ($x10^{-5}$)	12.1	11.3	11.7
Resonant Frequency (cps)	238	223	209
Measured Shear Modulus (MPa)	144.1	107.2	71.6
Predicted Shear Modulus (MPa)	123.8	85.9	59.6
Modulus Prediction Difference (%)	-16.6	-24.8	-20.2
Measured Damping Ratio (%)	1.9	2.7	3.6
Predicted Damping Ratio (%)	1.5	2.4	3.1
Ratio Prediction Difference (%)	-26.7	-12.5	-16.1

examples; the error was attributed to differences between void ratios of the sand samples used to obtain prediction data and the samples tested for measured values.

A remolded Grenada silt loam sample was tested at cell pressures of 10 and 49 kPa. These results were compared to Lick Creek silt data compiled by Hardin and Drnevich (1972b). Respectively, the values of shear moduli for cell pressures of 10 and 49 kPa were: Grenada silt loam, 21, 37 MPa; and Lick Creek silt, 15, 33 MPa. Moduli differences were attributed to the silt loam having coarser particles than that of the silt, which caused the silt loam to be rigid like a sand. Both soils had void ratio values close to unity and strain amplitudes with an order of magnitude of 10^{-4} cm/cm. This simple comparison of moduli served as an additional check of the apparatus and testing methods.

The resonant column test consisted of the following steps: (1) prepare specimen on pedestal, (2) position top cap on specimen, (3) install pneumatic-based support for Hardin oscillator, (4) raise pneumatic cylinders, (5) connect oscillator to top cap, (6) install plastic cylinder for triaxial cell, (7) connect sensor leads from triaxial-cell top to oscillator, (8) install cell top, (9) connect counter-balance device to oscillator, (10) disable pneumatic-based oscillator support, (11) activate signal monitoring equipment, (12) adjust power to oscillator, (13) adjust frequency to achieve resonance, (14) record test data, (15) check strain amplitude, (16) increase power and adjust frequency until visible sample disturbance or strain amplitude greater than $1x10^{-4}$ cm/cm occurs.

For simulated conditions involving long durations (days) of saturated sample testing, such as primary consolidation, soil specimens are often subjected to a liquid confining media to reduce air migration through the membrane (Drnevich, 1978). However, Drnevich et al. (1978) stated, "(an) air confining media may be used for dry or partially saturated specimens." Since the agricultural soils were only partially saturated, specimens were tested using air as the confining media.

Drnevich (1978) noted that coupling between the top cap and soil specimen was a possible problem, especially for stiff soil samples. This potential problem was examined. Tests were conducted at strain amplitudes up to 1.4×10^{-4} cm/cm for each soil type by using a coat of Ottawah sand glued to the soil-contacting surface of the top cap. No appreciable differences between shear moduli or damping ratios were detected between tests conducted with and without the glued sand. Thus, the standard cap was used to obtain the test results reported herein.

Results of Resonance Testing

Test results are tabulated according to soil type in Tables 5, 6, and 7. In each table, the sample preparation symbols REM and MIN-D refer to remolded and minimally-disturbed specimens, respectively. Samples used for more than one test condition are identified as having the same height and mass. Other test conditions listed are void ratio, moisture content (dry weight basis), and confining stress. Void ratio and moisture content ranged from 0.87 to 1.03 and

TABLE 5. Summary of resonant column tests performed on Etowah clay loam soil.

Sample Preparation*	Specimen Height (mm)	Specimen Mass (gm)	Void Ratio	Moisture Content (% d.b.)	Confining Stress (kPa)	Resonant Frequency (cps)	Shear Modulus (MPa)	Damping Ratio (%)	Strain Amplitude (cm/cm) ($x10^{-5}$)
REM	77.3	123.6	0.93	16.1	3	184	20.6	2.54	6.3
REM	77.3	123.6	0.93	16.1	3	182	17.0	3.04	7.3
REM	77.3	123.6	0.93	16.1	3	181	15.0	3.47	9.1
REM	77.3	123.6	0.93	16.1	3	180	13.1	4.04	9.3
MIN-D	82.5	132.4	0.93	16.8	0	186	26.0	2.53	4.9
MIN-D	82.5	132.4	0.93	16.8	0	185	24.4	2.43	8.7
MIN-D	82.5	132.4	0.93	16.8	0	184	21.8	2.60	9.1
MIN-D	82.5	132.4	0.93	16.8	0	183	20.1	2.46	10.9

*REM refers to remolded samples.

MIN-D refers to minimally-disturbed samples.

TABLE 6. Summary of resonant column tests performed on Hartsells fine sandy loam soil.

Sample Preparation*	Specimen Height (mm)	Specimen Mass (gm)	Void Ratio	Moisture Content (% d.b.)	Confining Stress (kPa)	Resonant Frequency (cps)	Shear Modulus (MPa)	Damping Ratio (%)	Strain Amplitude (cm/cm) ($x10^{-5}$)
REM	79.0	121.2	1.03	17.0	3	192	36.5	1.70	5.0
REM	79.0	121.2	1.03	17.0	3	188	28.2	2.18	6.9
REM	79.0	121.2	1.03	17.0	3	187	26.4	2.24	9.3
REM	77.6	118.1	1.04	16.9	3	186	24.3	2.59	9.5
MIN-D	74.2	119.7	0.92	16.5	3	194	38.1	0.89	8.9
MIN-D	74.2	119.7	0.92	16.5	3	192	33.8	1.28	10.0
MIN-D	77.8	128.0	0.87	16.3	3	191	34.2	1.27	11.1
MIN-D	80.5	132.7	0.88	16.6	3	189	30.9	1.60	11.2

*REM refers to remolded samples.

MIN-D refers to minimally-disturbed samples.

TABLE 7. Summary of resonant column tests performed on Grenada silt loam soil.

Sample Preparation*	Specimen Height (mm)	Specimen Mass (gm)	Void Ratio	Moisture Content (% d.b.)	Confining Stress (kPa)	Resonant Frequency (cps)	Shear Modulus (MPa)	Damping Ratio (%)	Strain Amplitude (cm/cm) ($x10^{-5}$)
REM	73.1	116.8	0.94	17.0	3	186	22.6	1.45	10.4
REM	72.0	115.0	0.94	16.9	3	185	20.6	1.84	11.1
REM	81.1	128.1	0.97	17.5	3	181	16.0	2.78	11.2
REM	75.0	121.3	0.92	17.5	3	181	14.3	3.13	11.4
MIN-D	82.0	129.6	0.95	16.3	0	186	26.0	1.47	8.5
MIN-D	82.0	129.6	0.95	16.3	0	184	21.8	1.75	9.7
MIN-D	78.5	123.7	0.97	17.5	0	184	20.9	2.25	11.2
MIN-D	81.3	129.0	0.95	16.9	0	183	19.8	2.28	11.9

*REM refers to remolded samples.

MIN-D refers to minimally-disturbed samples.

16.1 to 17.5 percent, respectively. Most tests required about 3 kPa of confining stress to minimize sample bulging, although the minimally disturbed clay loam and silt loam samples had sufficient structural strength to allow about one minute of testing at zero confining stress before the occurrence of visible plastic deformation (bulging). Observed resonant frequency, shear modulus, damping ratio, and strain amplitude ranged from 180 to 194 cps, 13.1 to 38.1 MPa, 0.89 to 4.04 percent, and 4.9×10^{-5} to 11.9×10^{-5} cm/cm, respectively.

Shear moduli measured for the remolded soil specimens are plotted as a function of strain amplitude in Figure 5. The moduli for the silt loam appear to be more sensitive to changes in amplitude as compared to the moduli of the other soils; this greater sensitivity is evidenced by the steeper curve slope. However, these tests were not conducted within the same range of strain amplitude, although the operating parameters, such as sample condition and resonant frequency, were similar (see Tables 5, 6, and 7). A common characteristic exhibited by each soil was a reduction in shear modulus as the maximum strain amplitude was attained. This reduction is observed as a taper on the extreme right of each curve. The taper was probably due to some combination of the following: (1) an undetected physical change may have occurred in the sample, (2) the data represent elements from a widely scattered band response, and (3) the soils may have similar nonlinear response curves for the examined strain amplitudes. Of these three possible reasons, some combination of reasons (1) and (2) was most likely.

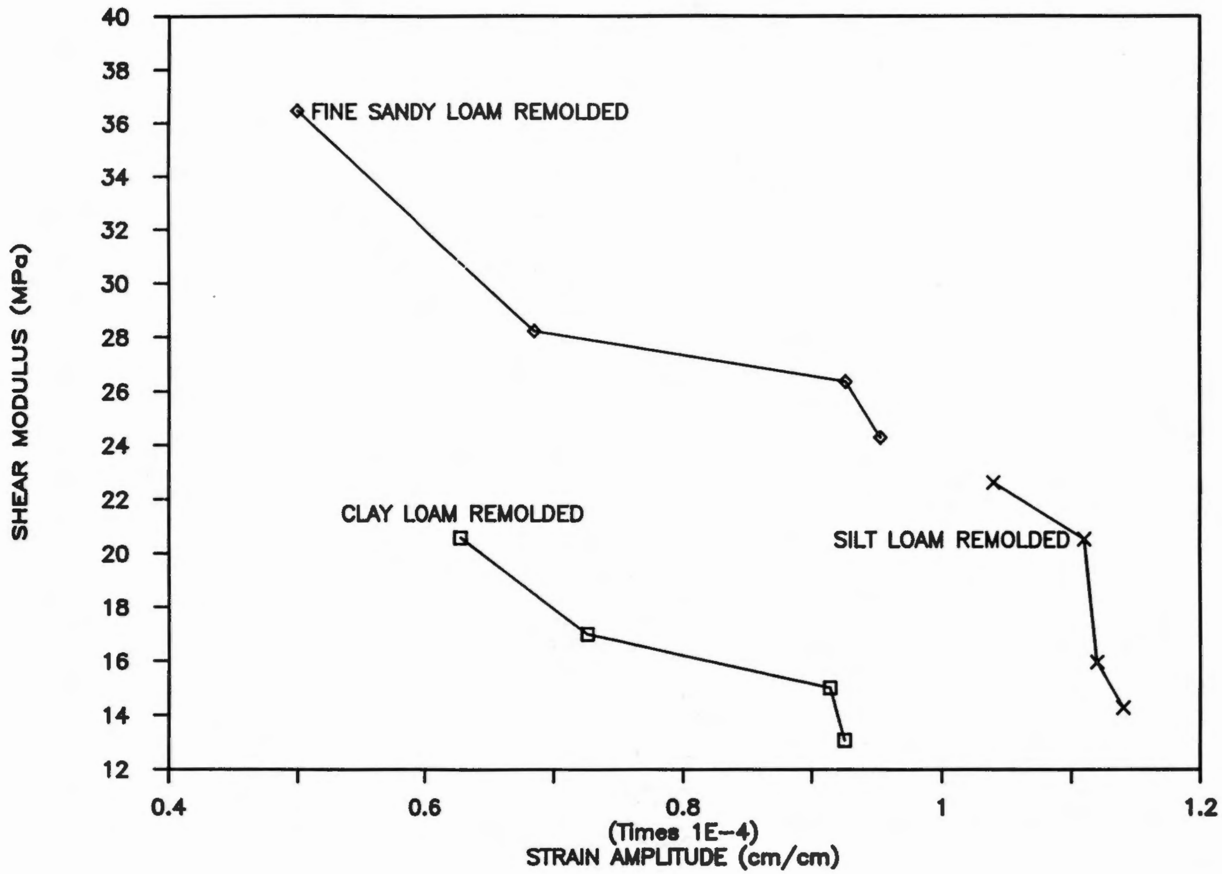

FIGURE 5. Shear modulus versus strain amplitude for remolded soil columns.

Shear moduli of minimally-disturbed soil samples are mapped versus strain amplitude in Figure 6. The moduli for the clay loam and silt loam were relatively unaffected by the amplitude changes observed in these tests; in fact, these two responses were nearly identical to each other. The moduli versus amplitude curve for the fine sandy loam is difficult to interpret on a point-by-point basis; however, this soil had a greater sensitivity and higher modulus than the other soils. The 3-kPa confining stress contributed to the high moduli of the fine sandy loam; whereas, the zero confining stress contributed to the low moduli of the clay loam and silt loam. The lack of smoothness of these curves was attributed to the lack of homogeneity of *in situ* surface soil.

As anticipated, shear modulus for all tests was greatest at the lowest strain amplitude and then generally decreased with increasing strain amplitude. Hardin and Drnevich (1972a) stated, "for practical purposes a value of shear modulus measured accurately for a strain amplitude of about 0.25×10^{-4} (cm/cm) or less can be taken to equal G_{max} (maximum shear modulus)." G_{max} was intended to be used in the calculation of a reference strain; nevertheless, a maximum modulus was implied at a low strain amplitude. The greatest modulus observed in each curve of Figures 5 and 6 probably did not correspond to G_{max}, although the greatest for the minimally-disturbed clay loam could easily be misinterpreted as G_{max} because it was only slightly larger than the adjacent point, making the left portion of the curve

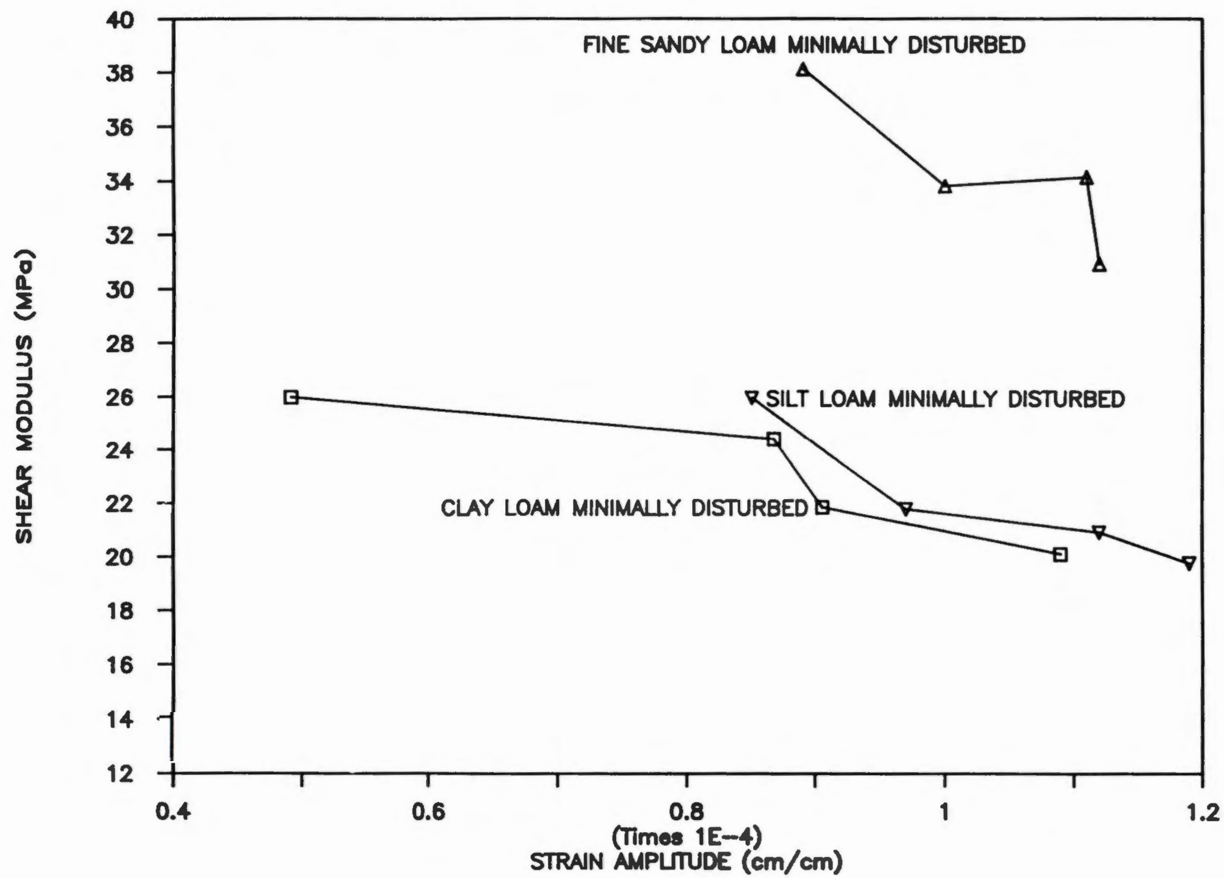

FIGURE 6. Shear modulus versus strain amplitude for minimally-disturbed soil columns.

(Fig. 6) appear insensitive to changes in amplitude. Consequently, the greatest modulus of the clay loam is also examined in a subsequent paragraph in which damping ratio is discussed.

By comparing the relative positioning of the shear modulus curves in Figures 5 and 6, the minimally-disturbed samples appeared stiffer than the remolded specimens. This difference can also be seen with the same shear modulus data in Tables 5 (p.40), 6 (p.41), and 7 (p.42). Stiffness is directly proportional to shear modulus, because shear modulus is defined as the slope of a line through the end points of the stress-strain hysteresis loop. The stress-strain relationship indicates the rigidity of the material. Perhaps the resonant column test could be used to indicate the degree of disturbance of remolded soil samples. The observed stiffness difference between remolded and minimally-disturbed specimens demonstrated the effects of structure on dynamic shear response.

The damping ratio versus strain amplitude relationships for the remolded soil samples are shown in Figure 7. Each damping ratio curve favors a reciprocal curve of modulus versus amplitude. For example, the fine sandy loam had high shear moduli values and low values for damping ratio, especially when compared to the clay loam. The sensitivity of damping ratio to strain amplitude of the silt loam was higher than that of the other soils. The taper of shear modulus observed in Figure 5 is revealed in Figure 7 as a sharp inclination of damping ratio, prevalent at the highest strain amplitude of each curve.

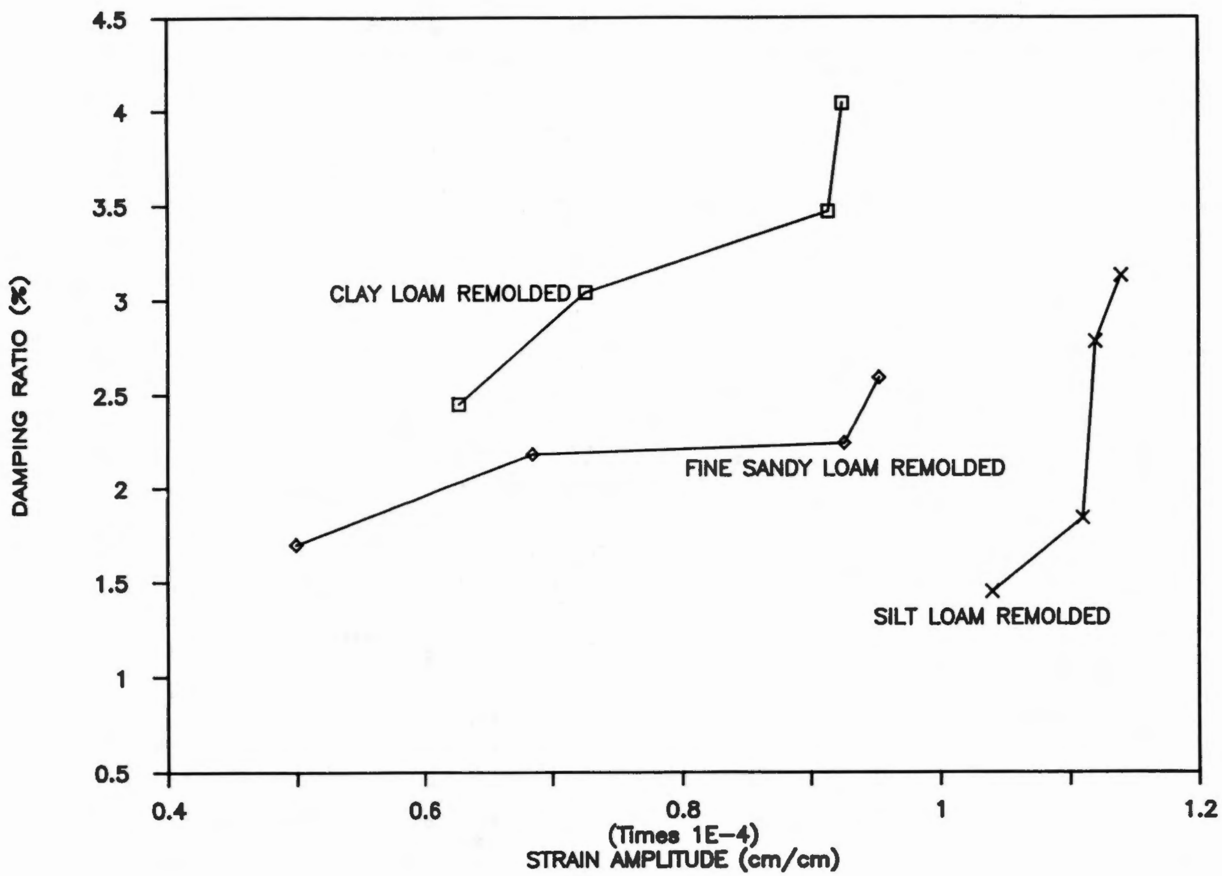

FIGURE 7. Damping ratio versus strain amplitude for remolded soil columns.

Figure 8 shows damping ratio versus amplitude plotted for the minimally-disturbed soil samples. Damping ratio versus amplitude again resembles a reciprocal curve of modulus versus amplitude. The clay loam and silt loam curves do not exhibit the close similarity as the shear modulus curves show for these same soils (Fig. 6). The clay loam curve behaves in a rather peculiar manner since it does not increase with amplitude. Damping ratio is expected to equal zero for zero strain amplitude and increase asymptotically to a maximum value as amplitude is increased; as a result, damping ratio versus strain amplitude has been described with a modified hyperbolic relationship (Hardin and Drnevich, 1972a).

Except for the minimally-disturbed clay loam, damping ratio of the tested specimens increased with amplitude as expected. The unusual behavior of the clay loam was also manifested with the greatest shear modulus mentioned in a previous paragraph. Since the greatest modulus coincided with a high damping ratio, the greatest modulus most likely did not represent G_{max}.

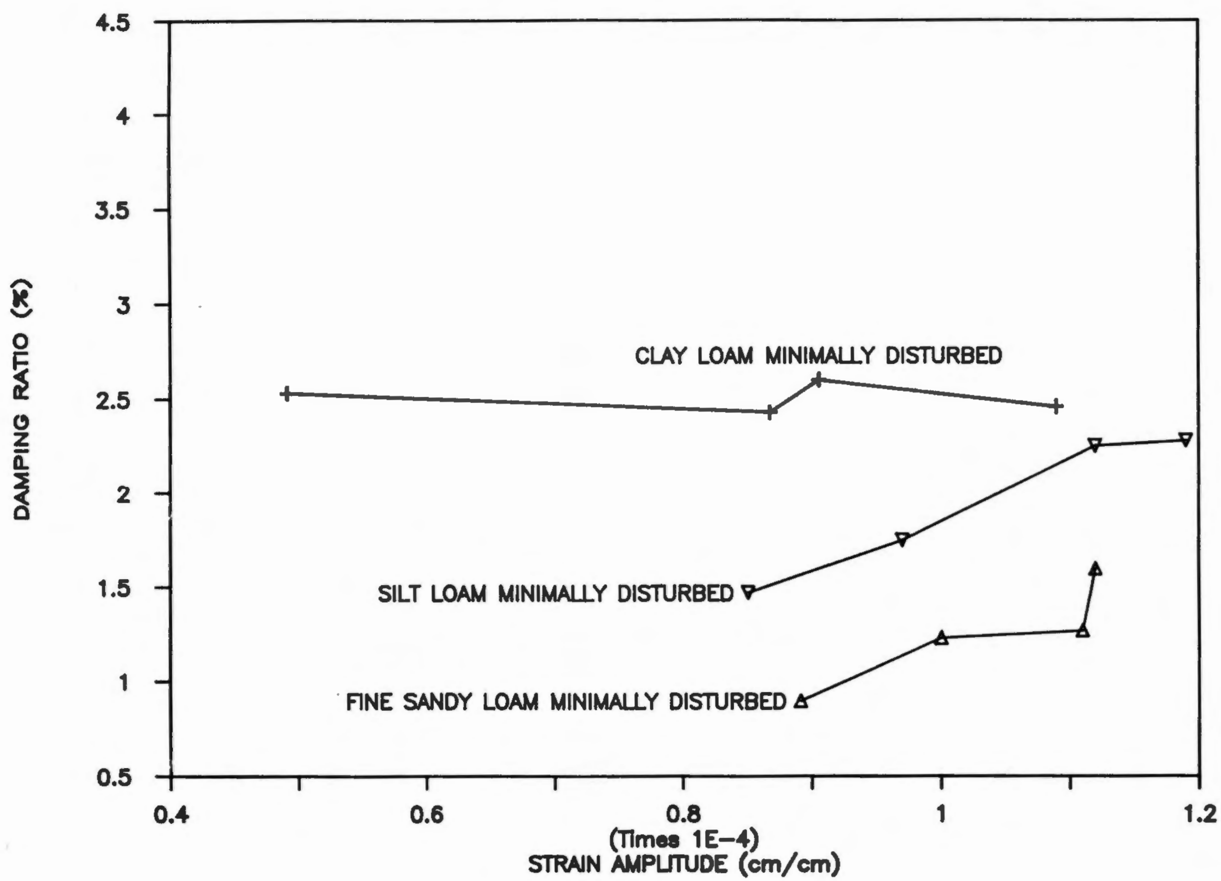

FIGURE 8. Damping ratio versus strain amplitude for minimally-disturbed soil columns.

Resonant Column Test Conclusions

Resonant column testing of three agricultural soils prepared by two methods yielded the following conclusions:

1. The developed resonance testing method proved to be effective for agricultural soils.
2. Shear modulus decreased with strain amplitude.
3. Damping ratio increased with strain amplitude.
4. The effects of sample structure on shear response were demonstrated.

CHAPTER IV

EQUIPMENT AND PROCEDURES FOR SOIL IMPACT TESTS

1. DEVICE FOR IMPACT LOADING OF *IN SITU* SOIL

The device illustrated in Figure 9 was fabricated to allow impacting a probe into *in situ* soil. The probe-supporting drop carriage was fitted with linear bearings that traveled on vertical guide members affixed to a work platform. The carriage was suspended by a winch and cable assembly prior to activation of a release mechanism and subsequent dropping. Impact velocity of the probe was varied by adjusting the drop height of the carriage. Momentum of the carriage was further varied with an array of precision mass plates that could be added.

An exploded view of the drop carriage is provided in Figure 10. The drop carriage supported a vertical load guide shaft aligned with linear bearings; the shaft transmitted impact force from the soil-engaging probe to an impact force transducer. Soil-engaging probes having various diameters could be connected to the bottom end of the vertical load guide shaft. Four cylindrical-shaped soil probes with diameters of 9.5, 12.7, 15.9, and 19.1 mm were fabricated. Each probe had a 30-degree included angle conical tip.

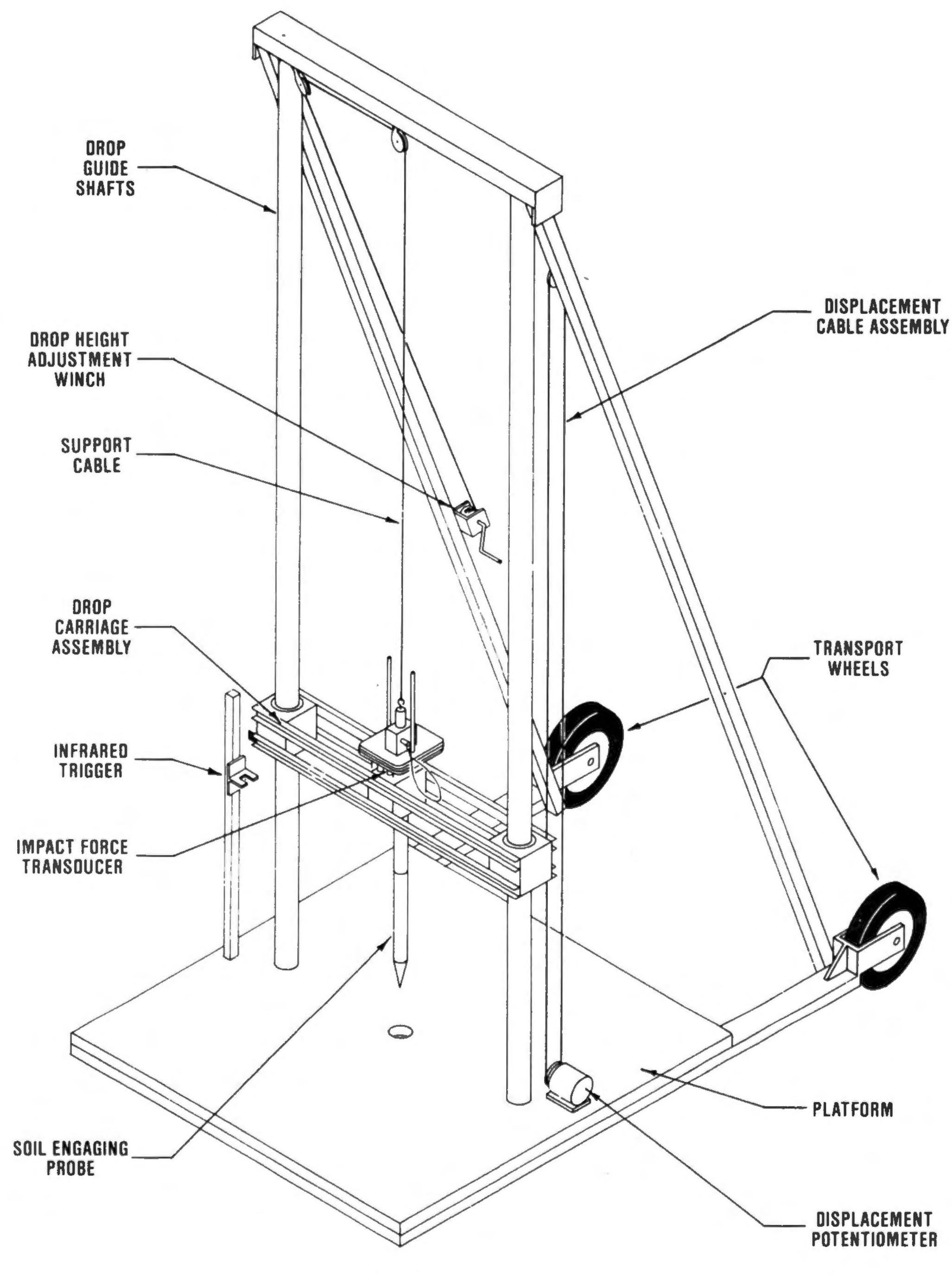

FIGURE 9. Instrumented device used for impact loading of soil.

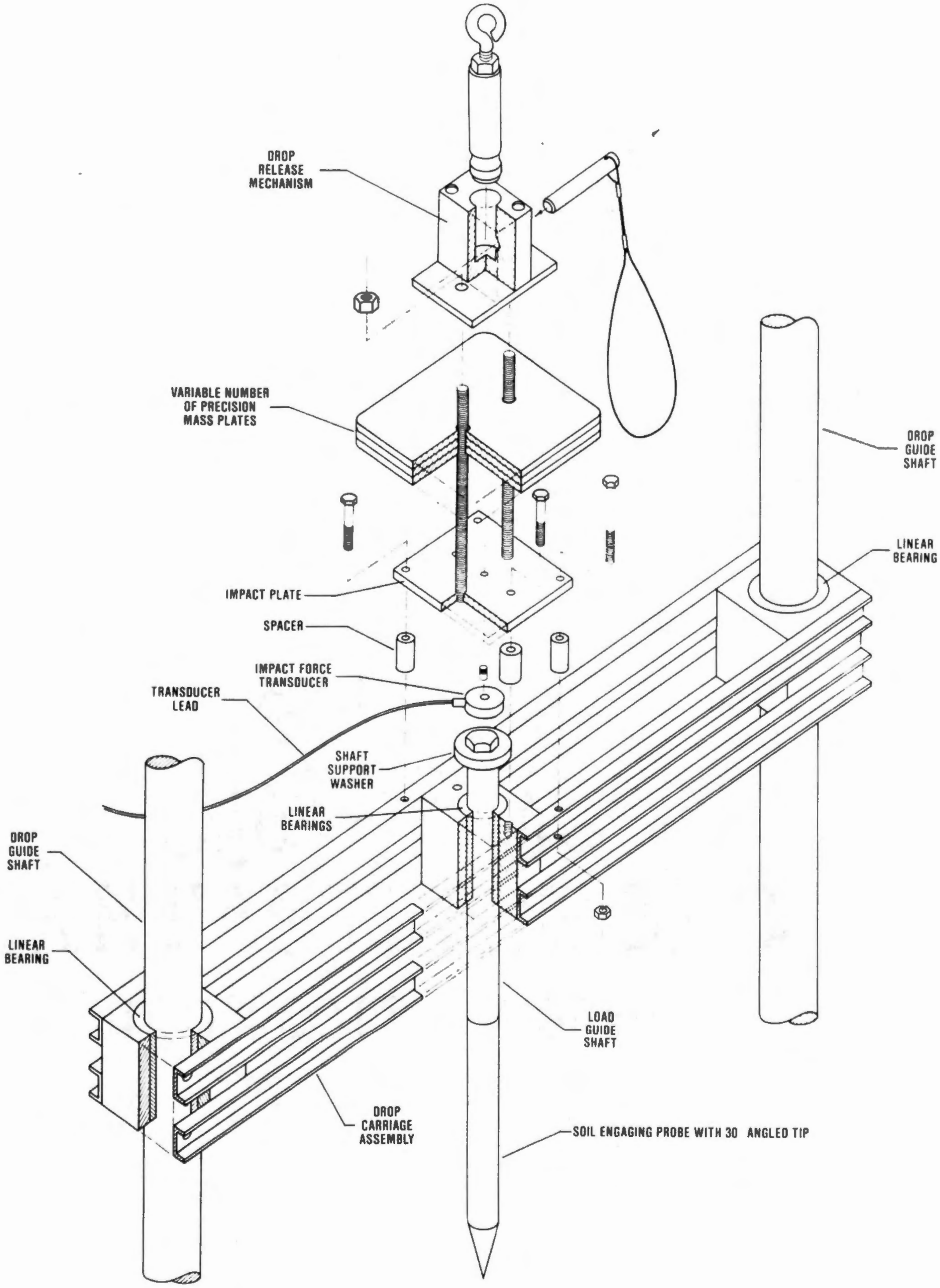

FIGURE 10. Drop carriage components shown with impact force transducer.

2. INSTRUMENTATION OF LOADING DEVICE

Impact force on the probe and probe displacement were monitored by the microcomputer-based data acquisition system illustrated in Figure 11. A quartz-based, 2200-N capacity impact force transducer (PCB Piezotronics, Inc.) was mounted between the upper end of the vertical load shaft and an impact plate rigidly fastened to the drop carriage (Fig. 10). Thus, the probe force was transmitted through the transducer to the drop carriage. A precision potentiometer, connected to the carriage with a pulley and cable system (Fig. 9), continuously indicated drop carriage position during data acquisition. A 1.6-mm o.d. plastic-coated steel cable was used to insure a positive grip between the pulleys and cable. Probe displacement was the position difference between the ground surface and punched depth readings; these displacement limits coincided with the initial detection of force and the first zeroing of force after a peak.

Output signals from the force transducer and position indicator were passed through low-pass active filters (Fig. 11) custom built by Frequency Devices, Inc. Data sampling errors were minimized (Freeland et al., 1987) with these seventh-order Cauer elliptic filters which had a ripple frequency of 5 kHz. A Digital Equipment Corp. LSI-11 based microcomputer was equipped with a Data Translation, Inc. Model 2782 12-bit analog/digital (A/D) converter for data sampling. The resolution of the A/D least significant bits for impact force and position were 1.02 N and 0.89 mm, respectively.

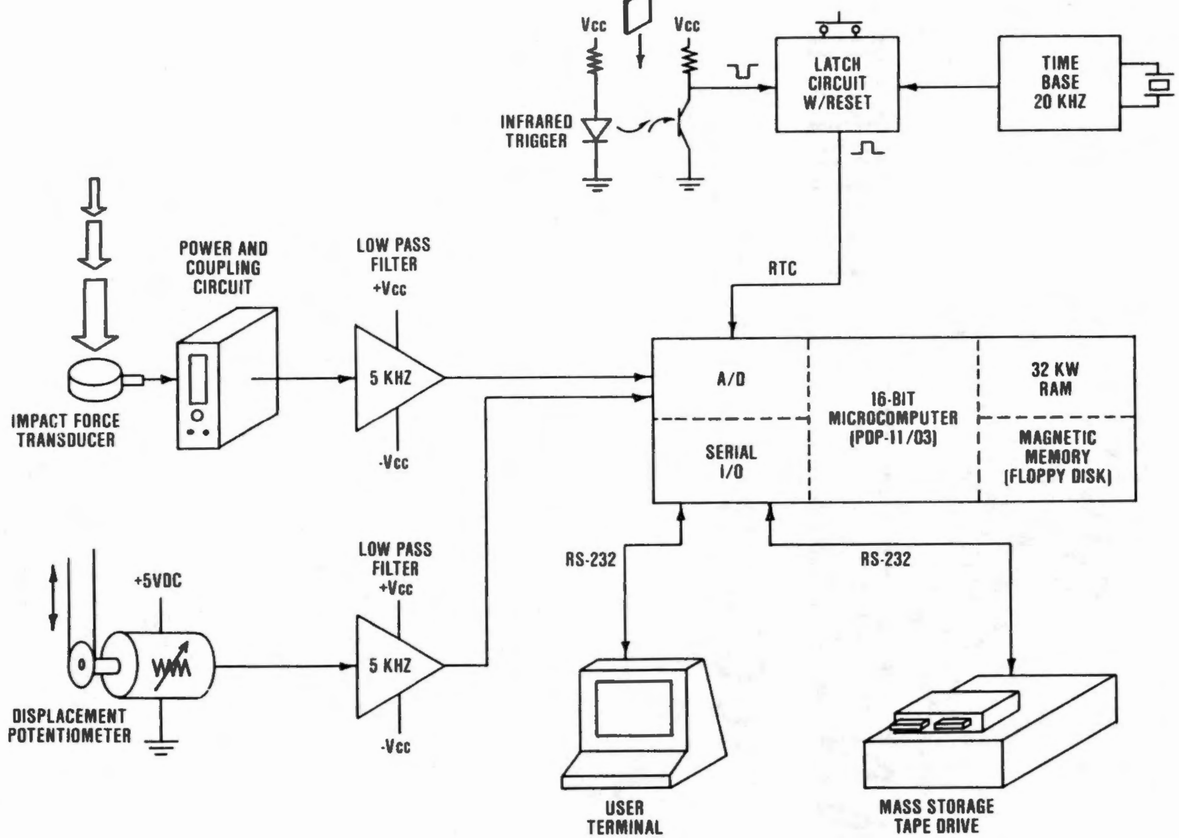

FIGURE 11. Schematic of microcomputer-based data acquisition system used to measure the dynamic response of soil.

The impact force transducer had a resolution of 0.04 N. Resolution of the position indicator, as estimated from the linearity of the displacement potentiometer (±0.25%), was ±4 mm. The actual resolution of position may have been better than ±4 mm depending on where the listed linearity error fell within the full-scale output range. This application primarily used that portion of the full-scale output range which corresponded to position measurement during penetration. The full-scale range represented the maximum drop carriage travel distance.

Data acquisition was initiated at approximately 10 ms prior to probe impact to obtain displacements for calculation of probe striking velocities. Triggering occurred when the falling carriage interrupted a beam of infrared radiation directed onto an infrared detector (Fig.9). Height of the trigger above the ground surface was variable and was adjusted to provide for proper trigger timing. Interruption of the infrared beam toggled a latch circuit to direct the output from a quartz-based pulse generator to the A/D board (Fig. 11). This stream of pulses regulated the start of data acquisition and the frequency of sampling. Force and displacement were then monitored at a frequency of 10 kHz until a predetermined number of samples had been taken. Probe striking velocity was determined analytically from displacement and sampling interval time prior to impact. Velocity was verified by equating the kinetic energy prior to impact to the energy expended as measured by integration of instantaneous probe force and displacement values.

Frequency of sampling was determined by examining the change of the least significant bit for preliminary sampling frequencies that ranged from 10 Hz to 100 kHz. The upper frequency limit was dictated by the rise time of the force transducer. These preliminary tests were performed without a low-pass filter and were thus used to determine filter specifications. Based upon the Nyquist Criterion of the Sampling Theorem (Freeland et al., 1987), the 10-kHz sampling frequency was twice the highest known system frequency of 5 kHz regulated by the low-pass filters.

Computer software in assembly language allowed the data acquisition system to initialize the A/D converter and to write the sampled test data onto a magnetic memory board (bubble memory) that emulated a floppy disk. Prior to each impact test, system initialization included the following: (1) loading the number of samples to be taken; (2) loading the first location of memory for A/D data storage; (3) loading the address of the A/D conversion completion routine; and (4) enabling the external trigger for automatic data conversion. Once initialized, the A/D waited for the stream of digital pulses from the pulse generator (Fig. 11). When the pulses began, each pulse triggered an A/D conversion and automatic storage by the A/D into computer memory through use of direct-memory-access (DMA). After the pre-selected sample count was reached, the A/D interrupted the computer out of a wait loop.

3. IMPACT TEST PROCEDURES

An impact test consisted of the following steps: (1) position and level impact device, (2) raise and secure drop carriage to predetermined drop height, (3) install soil probe, (4) position infrared trigger and reset trigger latch circuit, (5) modify the sample number displayed by the computer if necessary, (6) ready analog to digital conversion, (7) release drop carriage, (8) preview data for validity, and (9) repeat same test if data were invalid.

The impact tests for each soil were performed at drop heights of approximately 230, 460, 790, 1020, 1370, and 1680 mm, thereby producing average impact velocities of 2.0, 2.9, 3.8, 4.2, 4.7, and 5.0 m/s, respectively. The number of mass plates bolted to the drop carriage was reduced as the drop height was increased to achieve a penetration depth of approximately 100 mm. The total of 216 impact tests included six velocities, four probe diameters, and three soil types with three replications of each combination of these three variables. Turnage and Freitag (1969) performed only two replications of dynamic penetration tests; however, their tests were performed on remolded soil samples in which soil structure uniformity was more controllable than that in this study.

CHAPTER V

SOIL IMPACT TEST RESULTS

Figure 12 illustrates typical force-time traces observed for the three tested soils. The time scale represents the elapsed time after probe impact. Zero time was the instant the probe contacted the soil and an impact force was detected. Although the probe sometimes rebounded, the tests were only examined up to the first zeroing of force after a peak was observed. The tests illustrated were performed with a 19.1-mm diameter probe operated at a mean striking velocity of 4.83 m/s. The fine sandy loam soil was less penetrable than the other soils; this fact was also indicated by standard penetrometer readings (Table 2, p.28). Elastic deformation or a point of frictional slip was observed as the probe began to penetrate the surface, as evidenced by the brief relaxation of force, or dip in the force-time trace. Evidently, the initial peak that occurred at a force of approximately one-fifth the overall peak coincided with the proportional limit of the soil. The relatively large ratio of plastic to elastic deformation exemplifies the difficulty in describing this response with an analytical model. The exact shape of the response curve for each of the 216 tests is unique, thus showing the non-homogeneity of *in situ* soil. Clark and Reid (1984) reported similar difficulty in mapping cone index. Preliminary tests on remolded samples indicated less variability than with *in situ* soil, but duplication of two to three-year old soil structure with remolded samples proved to be difficult to verify. Preliminary test results differed between remolded and *in situ*

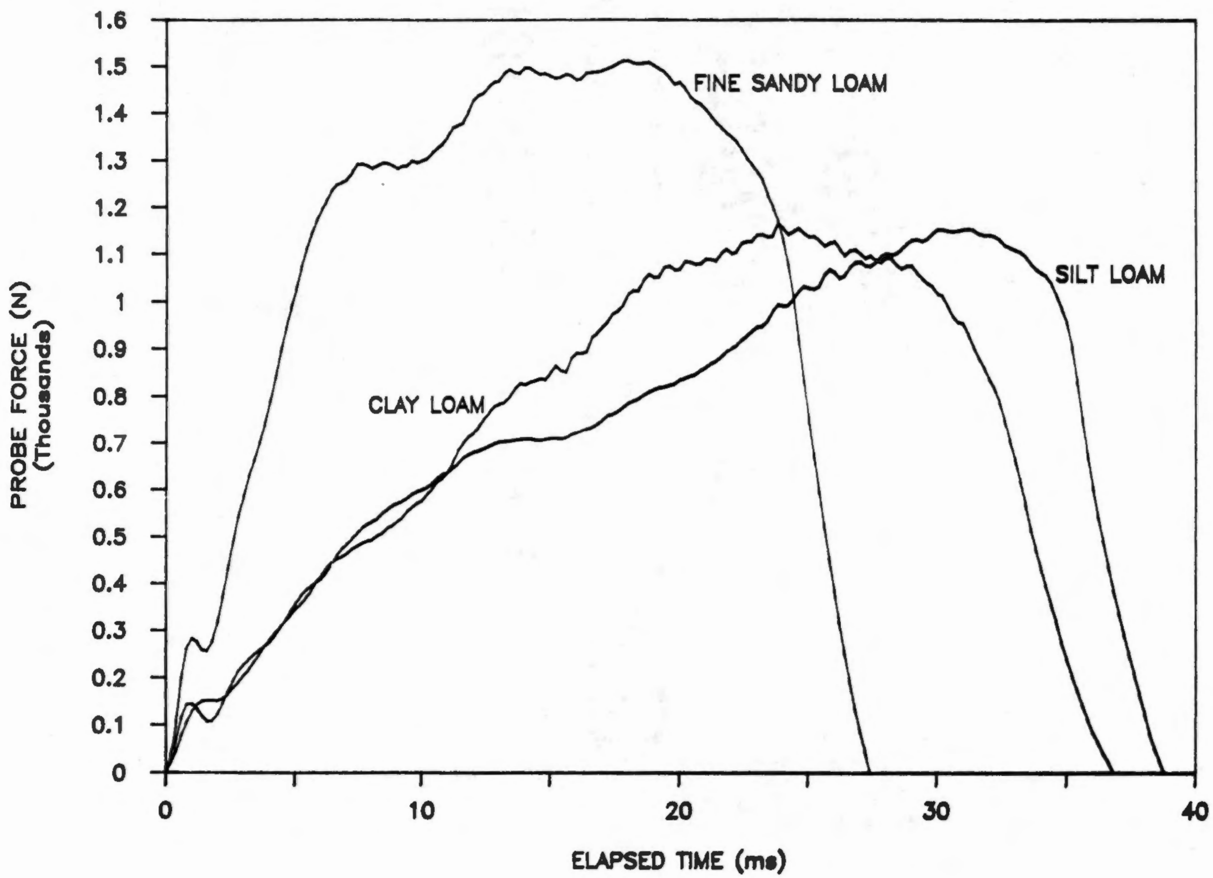

FIGURE 12. Typical force-time traces observed for the three tested soils.

soil samples, although density and moisture were similar for each condition. Compaction alone does not seem to duplicate the natural process involved with soil structure development. Consequently, *in situ* soil deposits were used for the impact tests.

Figure 13 is a plot of probe impulse as a function of probe striking velocity for the 216 tests according to soil type. The operating parameters associated with these tests are listed in the Appendix. Impulse is defined as the integral of force and time. Thus, the area bounded by each irregular force-time trace is represented as a plotted point. The uniqueness of each response within the 216 tests is partially shown in this figure. Velocity was chosen as the independent variable for two reasons. First, the variability of the striking velocity is exposed, even though the drop height and uniformity of drop carriage release were monitored closely. The six clusters of data coincide with the different drop heights. The second reason is to show the decrease in impulse as velocity increases. By integration (with respect to time) of the equation representing Newton's law stating that force equals the rate of change of linear momentum, impulse equals the change of momentum (Hartog, 1948). Assuming zero probe momentum after impact, probe impulse equals the product of probe striking velocity and mass. Examination of the data points in Figure 13 indicates that the impactor mass ranges from about 5 to 21 kg, which was verified from the masses recorded during the tests. Ratio of mass to velocity was much greater at lower velocities than at higher velocities to maintain similar penetrations. The amount of mass required at low velocity had to be increased more than the amount needed for constant momentum among

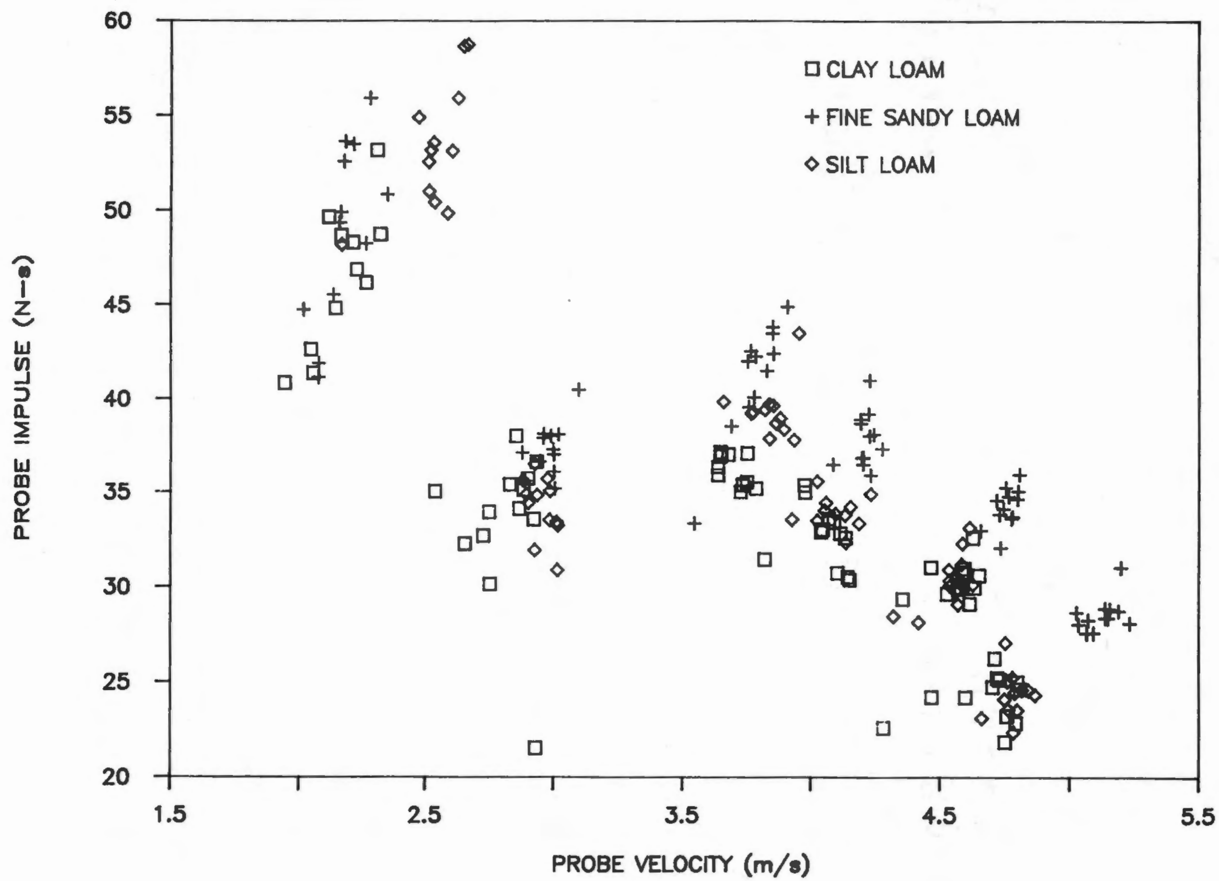

FIGURE 13. Probe impulse versus probe striking velocity for the 216 impact tests conducted at similar soil penetration depths.

tests. This occurred because the kinetic energy required for penetration at different velocities is similar; kinetic energy depends on one-half the product of mass times the square of velocity. Mass at a low velocity must be increased accordingly to compensate for the low value of velocity squared. The cluster of data second from the abscissa has an impulse lower than expected. Tests represented by the data in this cluster should have been conducted with more mass. Increasing the mass would have increased the carriage momentum and measured impulse. To reiterate the reason for varying the mass among tests, momentum of the carriage affected the maximum penetration depth of the probe. Substantially different penetration depths may affect dynamic soil response. The effects of the ratio of point resistance to frictional shaft resistance acting upon the dynamic probe were not investigated in this study.

Figure 14 is a plot of the force-penetration trace for the three tests depicted in Figure 12. The curves for each soil type differ only slightly between Figures 12 and 14, indicating a nearly linear velocity-time trace. A soil dependent frequency associated with penetration was observed and is illustrated by the unique ruggedness of each curve in Figure 14. The frequencies may depend somewhat on the idiosyncrasies of linear bearing travel down the guide shafts of the impact device, although Young et al. (1984) studied a similar characteristic with the cyclic variation of tillage forces on a vertical chisel.

Tables 8, 9, and 10 summarize impact test results on the Etowah clay loam, Hartsells fine sandy loam, and Grenada silt loam soil,

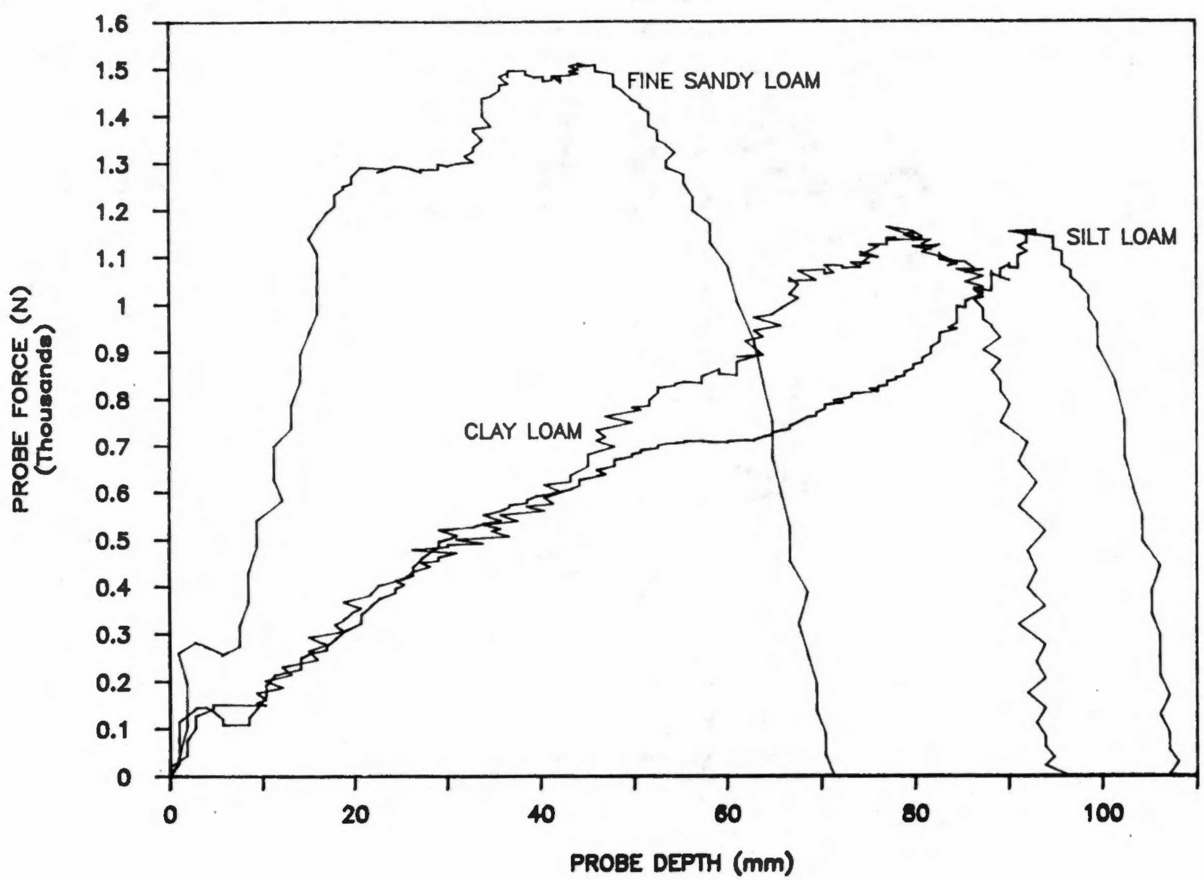

FIGURE 14. Typical force-penetration traces observed for the three tested soils.

TABLE 8. Summary of impact tests performed on Etowah clay loam soil.

Parameter	Probe Diameter (mm)			
	9.5	12.7	15.9	19.1
Probe Striking Velocity Range (m/s)	(2.16-4.79)	(2.21-4.81)	(1.94-4.72)	(2.04-4.60)
Input Energy Range (J)	(48.4-78.6)	(46.6-78.4)	(39.0-77.6)	(43.5-78.4)
Measured Peak Force Range (N)	(635-904)	(552-1140)	(673-1466)	(804-1306)
Mean Peak Force (N)	759	860	1006	1066
Measured Penetration Range (mm)	(116-217)	(96-259)	(60-135)	(69-111)
Mean Penetration (mm)	158	131	101	96

TABLE 9. Summary of impact tests performed on Hartsells fine sandy loam soil.

Parameter	Probe Diameter (mm) 9.5	12.7	15.9	19.1
Probe Striking Velocity Range (m/s)	(2.17-5.15)	(2.13-5.20)	(2.16-5.23)	(2.01-5.09)
Input Energy Range (J)	(49.0-83.8)	(47.2-84.4)	(48.4-82.7)	(42.3-85.6)
Measured Peak Force Range (N)	(623-983)	(861-1191)	(865-1466)	(1248-1766)
Mean Peak Force (N)	797	988	1210	1535
Measured Penetration Range (mm)	(77-157)	(69-122)	(46-121)	(39-85)
Mean Penetration (mm)	117	96	83	68

TABLE 10. Summary of impact tests performed on Grenada silt loam soil.

Parameter	Probe Diameter (mm) 9.5	12.7	15.9	19.1
Probe Striking Velocity Range (m/s)	(2.63-4.84)	(2.51-4.87)	(2.51-4.80)	(2.17-4.79)
Input Energy Range (J)	(55.8-83.5)	(52.9-78.6)	(51.9-80.7)	(40.9-84.2)
Measured Peak Force Range (N)	(620-931)	(624-1117)	(759-1292)	(895-1483)
Mean Peak Force (N)	716	860	1046	1127
Measured Penetration Range (mm)	(118-241)	(107-169)	(95-146)	(82-107)
Mean Penetration (mm)	168	135	108	95

respectively. Ranges of input parameters and dynamic response parameters are tabulated by probe size for each tested soil. The upper and lower limits of one range do not necessarily correspond to the upper and lower limits of another range. For example, input energy is affected by impact mass as well as striking velocity; thus, the lowest energy limit may not correspond to the lowest velocity limit. Mean values of peak force and penetration are also tabulated. The mean peak force increases with probe diameter for all tested soil types, with the greatest increase occurring in the fine sandy loam soil. Dynamic responses of clay loam and silt loam were similar for the soil conditions considered. Particularly important, an inverse relationship was observed between mean peak force and mean penetration. The primary forces acting during penetration are indeed inertia forces, since the forces are closely dependent upon penetration depth. Penetration depth determines the time required for the probe to stop; thus, probe deceleration is affected by penetration depth.

The Sandia Laboratories' empirical formula (Eqn. 2.7, p.21) was investigated for predicting penetration depth of the soils tested. Penetrability index (S) was found for each of the 216 penetration tests. Mean value of S was 261.4, 178.4, and 249.6 for the clay loam, fine sandy loam, and silt loam soil, respectively. Using these mean values for S, the penetration depth that could be predicted for the fine sandy loam was less than that for the other soils, which agrees with the penetration results of Tables 8, 9, and 10. The standard deviation of S was 97.1, 51.1, and 79.8 for the clay loam, fine sandy loam, and silt loam soil, respectively. These standard deviation values are high because of the non-homogeneous soil conditions encountered and because the penetration depth is near the critical depth subject to surface effects.

The inverse relationship demonstrated in Tables 8, 9, and 10 between peak force and penetration depth was investigated as a basis for predicting the peak impact force on a probe. This relationship was selected since probe inertia forces depend upon probe deceleration. Numerous multiple linear regression models were examined using the IMSL subroutine RLMUL (IMSL, 1982). The best regression model found to predict the peak impact force on a probe is as follows:

$$F_p = 8.400(E) + 26.076(D) - 4.376(X) + 548.745 \qquad (5.1)$$

where:

F_p = predicted peak force, N
E = input energy, J
D = probe diameter, mm
X = observed penetration depth, mm.

This dynamic response equation was calculated at a risk level of five percent with a coefficient of determination (r^2) of 72.4 percent. When an averaged value of peak cone index for each soil type was included, r^2 increased to only 73.2 percent; thus, cone index was not included. Omission of probe diameter decreased r^2 to 65.1 percent. Consequently, probe diameter was included. The model does not require input of soil properties because it depends upon penetration depth. Soil properties, soil-probe friction, and other parameters are collectively indicated by the penetration depth response.

CHAPTER VI

DESIGN AND CONSTRUCTION OF FERTILIZER APPLICATOR

1. INJECTOR TOOLBAR AND FRAME

A toolbar constructed from 102 x 152 x 6.4-mm rectangular steel tube and 9.5-mm steel plate supported the injector components (Figure 15). Components included a soil engaging probe mechanism, a probe driving system, and a fluid dispenser system. Overall width of the toolbar was 2.5 m. The front side of the toolbar was equipped with a Category I three-point hitch (ASAE S217.10, 1987). The steel plate was welded parallel to the opposite or back side. Two rows of 11-mm diameter holes bored on 50-mm centers into the plate provided for component mounting with bolts. This scheme provided positive mounting for components that required close alignment. Use of the traditional toolbar and U-bolts or clamps was assumed inappropriate, since vibrations might cause a shift among mounted components.

Two frame members supporting depth control tires were bolted outboard from the other components on the toolbar. Each frame member supported two self-aligning flange bearings, a 36-mm diameter axle, and a regular agricultural drive tire (Code R-1, 152-mm width, 356-mm diameter) mounted on a four-lugged Toyota automobile wheel. During probe operation, the tires rolled over the ground and provided soil penetration depth control for the probe. Each frame member contained vertical length adjustment, so probe depth was variable.

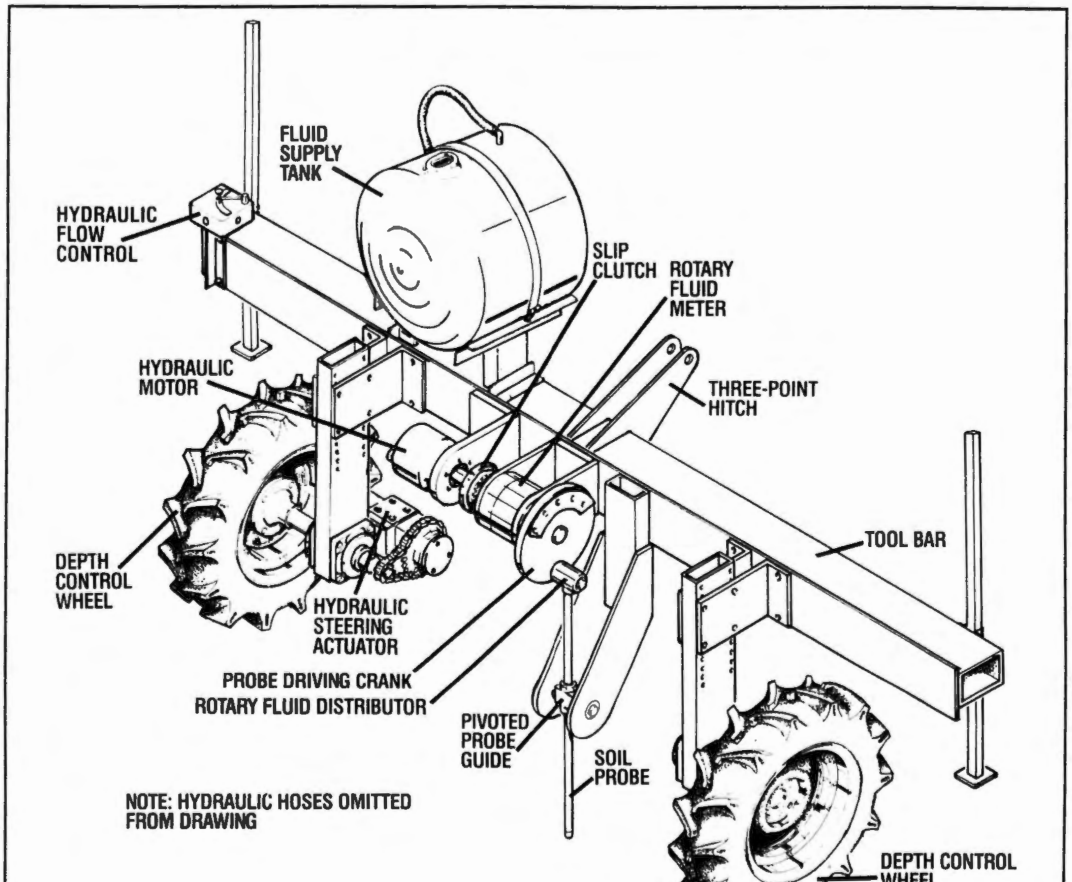

FIGURE 15. Prototype crank-driven, probe-type fluid fertilizer injector developed for minimum soil disturbance.

2. SOIL-ENGAGING PROBE MECHANISM

The probe-type injector employs a unique mechanism for opening the soil (Fig. 16). Actually, the mechanism is a kinematic inversion (Shigley and Uicker, 1980) of the slider-crank mechanism. A crank, rotating at constant angular velocity, drives a rod which passes through a rocking slide, pivoted at a fixed point (Hartog, 1948). The tip of the rod moves with simultaneous vertical and horizontal motion, yet the rod remains oriented nearly vertical throughout each cycle. Because the rod, or soil probe, serves as a soil opener, the mechanism operates on-the-go to incorporate fluid fertilizer while causing minimum soil disturbance.

The geometry of the mechanism determines the position and displacement of the probe tip. By inspection of Figure 16, probe tip position T depends on the following: 1) crank radius, r; 2) crank angle, θ; 3) probe length, l; and 4) distance, d, between point R at crank center and point U at pivot center. To relate these variables, the probe angle α is first determined in terms of θ as follows:

By examining triangle UVS (Fig. 16),

$$VS = r \sin(\theta) \tag{6.1}$$

$$UV = d - r \cos(\theta) \tag{6.2}$$

$$\tan(\alpha) = VS / UV \tag{6.3}$$

where,

VS = distance VS (Fig. 16), mm
UV = distance UV (Fig. 16), mm
r = crank radius, mm
d = distance RU (Fig. 16), mm
θ = crank angle, degrees
α = probe angle, degrees.

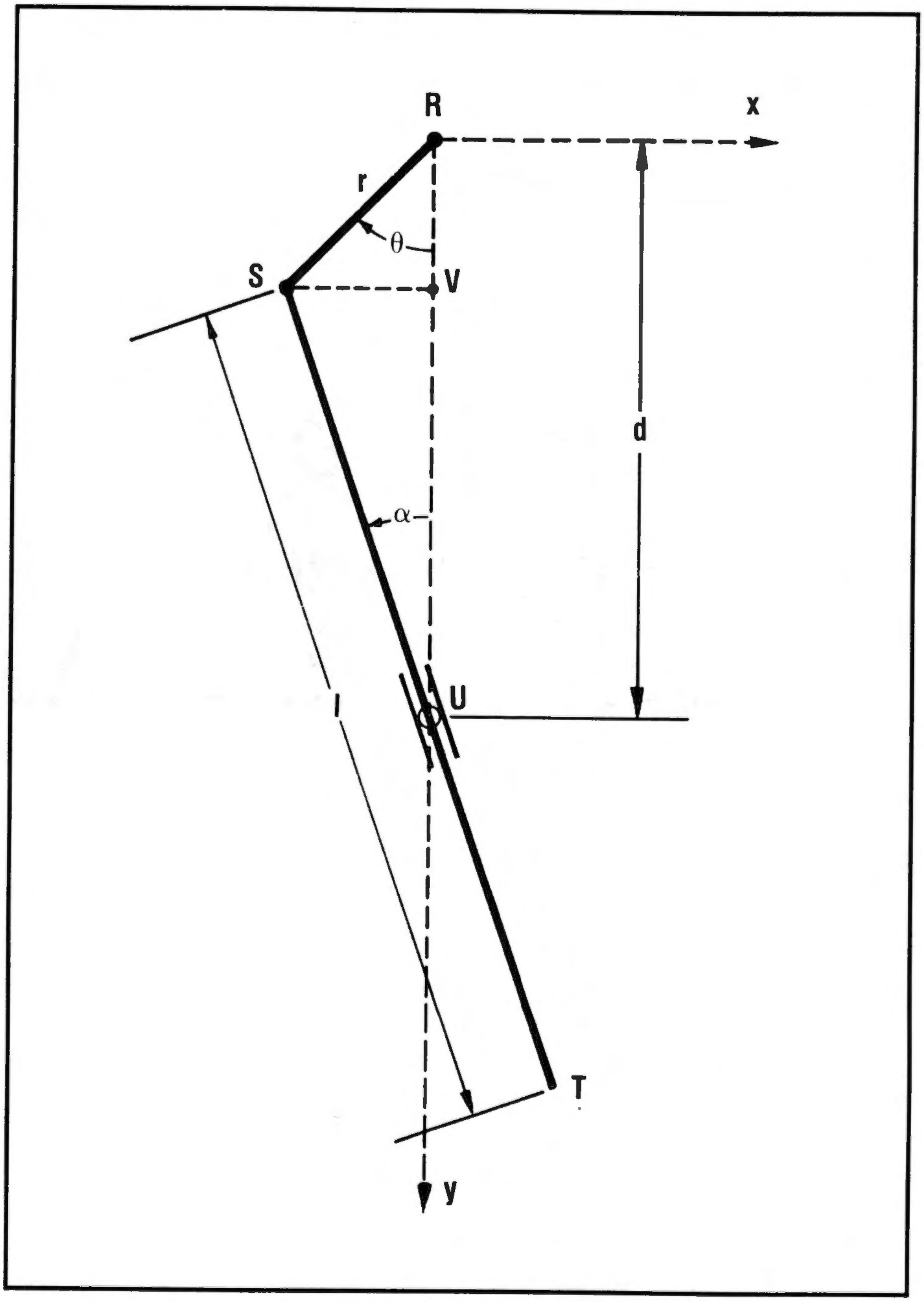

FIGURE 16. Linkage employed as a soil opener on the injector.

Solving for α,

$$\alpha = \arctan \{[r \sin(\theta)] / [d - r \cos(\theta)]\}. \qquad (6.4)$$

Then, the probe tip position can be expressed as:

$$X_t = l \sin(\alpha) - r \sin(\theta) \qquad (6.5)$$

$$Y_t = l \cos(\alpha) + r \cos(\theta) \qquad (6.6)$$

where,

X_t = horizontal displacement of probe tip, mm
Y_t = vertical displacement of probe tip, mm
l = probe length, mm.

Motion of the probe tip is visualized by plotting the path followed by the tip versus incremental changes in crank angle. Figure 17 plots the probe tip position X_t, Y_t for θ ranging from +90 to -90 degrees which corresponds to probe motion before and after soil engagement. By examining the ten-degree increments, note that the horizontal displacements are not uniform which will contribute to soil disturbance. Instantaneous horizontal tip velocity is proportional to the magnitude of horizontal tip displacement. Horizontal tip velocity offsets injector travel velocity during injector operation. Travel velocity was assumed constant. Differences between horizontal tip and travel velocity cause relative movement between the tip and soil surface, resulting in soil disturbance. However, the inclination of the probe is essentially vertical throughout soil engagement which will offset soil disturbance due to horizontal velocity differences.

The probe dimensions used in Figures 16 and 17 are: r = 101.6 mm, d = 457.2 mm, and l = 762.0 mm. These dimensions represent a compromise between depth of soil injection, injection

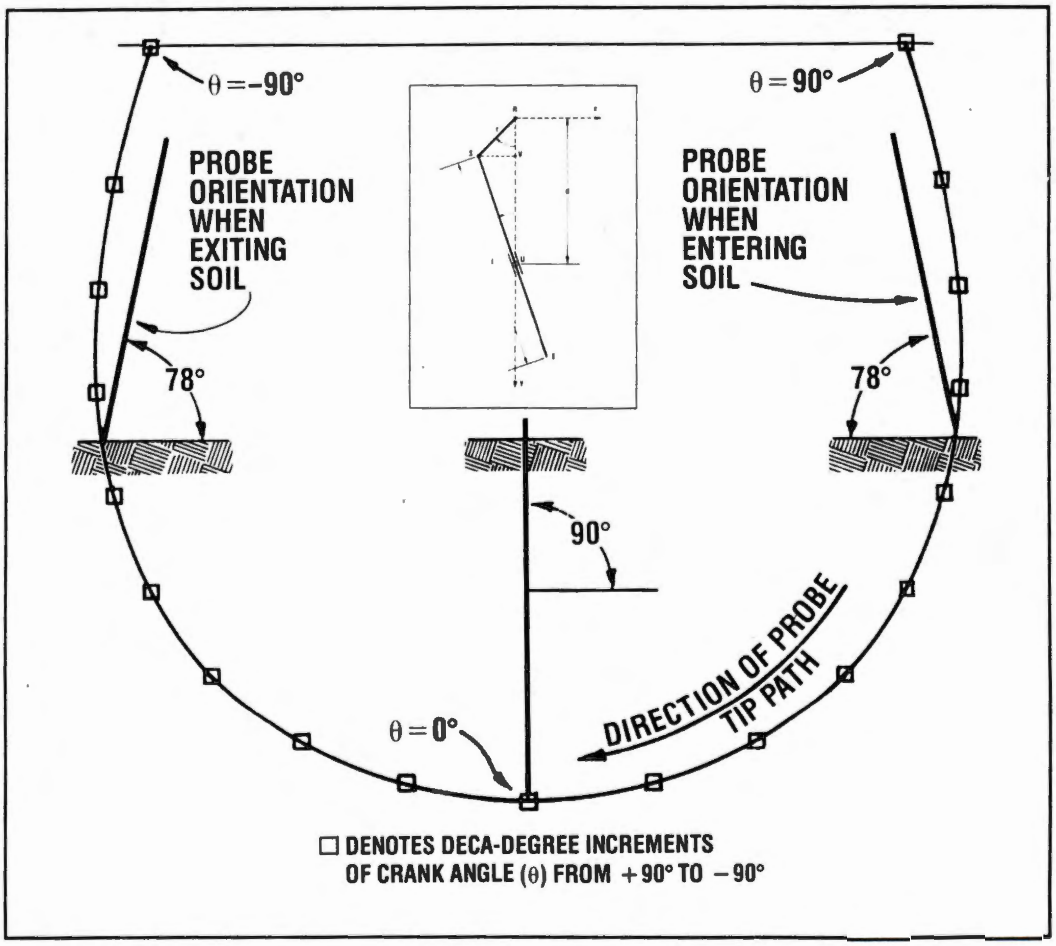

FIGURE 17. Diagram of injector probe tip position and displacement before and after soil engagement. Crank angle (θ) is defined in Figure 16.

interval, maximum probe angle, uniformity of horizontal displacement, and physical size of the injector. Other combinations of dimensions are possible. The combination selected yields a depth of soil injection of about 64 mm and a maximum probe angle of about 12 degrees.

For comparison, Figure 18 maps the path followed by the tip of a spoke on a wheel. The spoke enters the soil at an angle of about 45 degrees compared to about 78 degrees for the probe. This spoke angle is based on the wheel and spoke dimensions of the fourth generation Point Injector (Baker et al., 1986). Baker noted that the wheel rotates on the spoke tips, thereby causing soil disturbance along a line at each point of injection.

Structural members of the injector were sized using data obtained from dynamic soil penetration tests (Womac et al., 1987). The peak force observed in these tests was 1766 N when operating in a fine sandy loam soil using a 19.1-mm diameter probe. Although the penetration tests indicated a significant reduction in soil-probe impact force for probe diameters less than 19.1 mm, a probe diameter of 19.1 mm was selected for the injector for two reasons. First, this diameter provided ample space to accommodate a spring-loaded valve in the probe tip. Second, the entire probe was constructed from stock of this diameter to provide sufficient probe strength in moderately firm soil conditions. Using a uniform diameter probe simplified fabrication of the prototype injector used in this study.

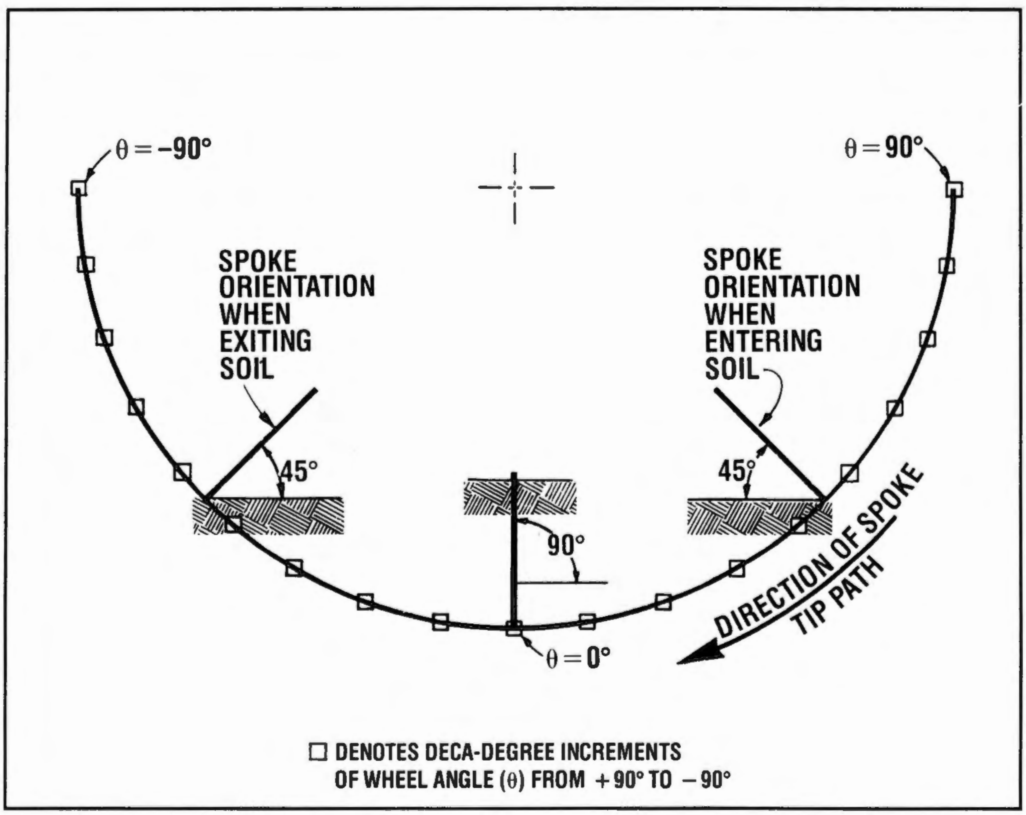

FIGURE 18. Diagram of Baker's spoked-wheel spoke tip position and displacement before and after soil engagement.

Axial loading of the probe was checked with a column formula. The slenderness ratio for the 762-mm long probe fabricated from 19.1-mm o.d. by 9.52-mm i.d. tubing is 36. Since Euler's column equation is generally valid for a slenderness ratio greater than 120, the probe is not defined as a slender column subject to failure by elastic buckling. However, the probe is defined as a short column that fails by inelastic buckling. The Euler-Engesser equation predicts inelastic buckling and is expressed as follows:

$$\sigma_{cr} = P_{cr}/A = (K\pi^2 E_t)/(L/r)^2 \tag{6.7}$$

where,

σ_{cr} = critical (buckling) stress, MPa
P_{cr} = critical load, MN
A = cross-sectional area of column, m^2
K = column restraint dependent variable
E_t = tangent modulus of elasticity, MPa
L = column length, m
r = least radius of gyration, m.

In this equation, the tangent modulus of elasticity is usually less than Young's modulus and must be determined at a particular strain from a stress-strain curve. This curve was not available for the probe material (304 stainless steel, annealed condition). Hence, the tangent modulus was arbitrarily assumed to equal 50,000 MPa, which is about one-fourth of Young's modulus (193,100 MPa). Then, assuming the column restraint variable equals one, the buckling stress for the probe equals 381 MPa. The yield strength of the probe material is 207 MPa and subsequently controls buckling. Maximum probe force recorded during dynamic soil penetration tests was 1766 N. This force results in an axial probe stress of 8.2 MPa, well below either buckling stress. So, inelastic buckling of the probe is unlikely to occur, provided the above assumptions represent the actual probe conditions.

The probe is also subject to bending stresses. The maximum moment arm on the probe occurs when the probe is fully extended downward into the soil. This dimension is 381 mm, extending from the bottom of the guide to the tip. If the maximum transverse force is arbitrarily assumed equal to the maximum measured axial force (1766 N), the maximum bending stress is 67 MPa. If the probe is subject to both bending (67 MPa) and compressive axial (8.2 MPa) stresses, a combined stress of 75 MPa results near the outer surface of one side of the probe. Under these stresses, the factor of safety is 2.76 when yield strength equals 207 MPa. However, the assumption about transverse force is only valid when the probe operates in soil free from rocks and other obstructions.

By inspection of the soil opener mechanism (Fig. 16, p.74), the probe is susceptible to damage when it strikes rocks or other solid objects. Ideally, the probe needs a shock absorbing overload protection device built within the probe, preferably near the tip. However, to simplify fabrication, the prototype described herein did not include this feature.

By examining the mounting arrangement of the probe (Fig. 16, p.74), the probe will tend to bend about the top and bottom ends of the pivoted guide. These bends will be in opposite directions resulting in an S-shaped probe. For example, suppose the probe strikes a rock as the injector travels through the field. A large transverse load causes the bottom end of the probe to bend backwards, with respect to the direction of travel. Subsequently, the top end tends to bend backwards in reaction to the moment at the bottom end. However, the flywheel or crank also affects bending stresses. The inertia of the flywheel will tend to overcome the moment causing backward bending of the top end and will ultimately cause forward bending of the top end. Thus, the combination of backward bending at the bottom end and forward bending at the top end causes an S-shaped bend to form in the probe at the rocking guide.

Maximum transverse force on the probe is dependent on the magnitude of the shock load. Ideally, the probe should be built from large stock (>38-mm diameter) to resist bending at the guide. The bottom end of the probe should be tapered to a smaller diameter to minimize soil disturbance. However, the prototype described herein was equipped with a small, uniform diameter probe (19.1-mm o.d., 9.5-mm i.d.) to simplify fabrication.

The injection interval or spacing of the holes punched into the soil depends on matching the injector travel velocity with the horizontal velocity component of the probe tip. The horizontal tip velocity is not uniform, as indicated by non-uniform displacement intervals depicted in Figure 17 (p.76). The probe initially enters the soil with a low horizontal velocity, then it accelerates to a maximum horizontal velocity when fully extended downward. Finally, the horizontal velocity reduces as the probe is being withdrawn from the soil. However, an average horizontal probe velocity offsets travel velocity. Hole spacing can vary from 200 to 600 mm, depending on the magnitude of soil disturbance deemed acceptable for the particular operating situation. Determination of the hole spacing corresponding to the least amount of soil disturbance was performed during injector evaluation.

Increasing dwell of the probe in the soil results in increasing soil disturbance because of increasing horizontal velocity variations between the probe and the ground. Dwell is the angular displacement of the probe crank through which the probe encounters soil. Dwell is controlled by adjusting depth of soil penetration. An optimum dwell exists that should result in an acceptable combination of soil disturbance and penetration depth. This was also examined during injector evaluation.

Compared to conventional tillage tools, the probe requires very little power to operate. The maximum energy used to dynamically drive the instrumented probe into the soil was about 86 N-m. If the probe mechanism encounters soil conditions similar to those during this measurement, less than one kilowatt is required to power the probe mechanism, assuming soil is actively penetrated one-fourth of one revolution of the probe crank operating at 400 rpm. The probe driving motor described in the next section develops almost four times the power required to drive the probe.

The probe mechanism was dynamically balanced by bolting counterweights to the flywheel opposite the crankpin. Table 11 lists the component masses of the mechanism. The bare flywheel mass was two and one-half times greater than the sum of the probe, distributor, and counterbalance masses. The rotating counterbalance

TABLE 11. Probe mechanism component masses measured when balancing injector.

Probe Mechanism Component	Mass (g)
Bare Flywheel	9439
Probe Shaft with Tip	1182
Rotating Fluid Distributor	1033
Rotating Counterbalance	1528

mass exceeded the rotating fluid distributor mass by 495 g. This additional mass is 42 percent of the probe shaft mass and was used to modify the shaking forces and inbalance created by the probe shaft mass. The shaft has both rotating and reciprocating components of motion. Typically in single-cylinder engines, from one-half to two-thirds of the reciprocating mass is added to the counterweight after balancing the rotating mass (Shigley and Uicker, 1980).

A Redington Model No. 1-4635, 5-digit mechanical counter was connected to the pivoted probe guide. A linkage transferred the back and forth rocking motion of the guide to the counter arm. Each revolution of the crank, in either direction, advanced the counter by one. The counter accommodates up to 1000 counts per minute.

3. PROBE DRIVING SYSTEM

A Hydreco Model 3M050 gear-type hydraulic motor drives the crankshaft of the injector. Figure 19 is a schematic of the hydraulic circuit used to power the motor with ground-speed-regulated amounts of pressurized hydraulic fluid. Ground speed equals injector travel velocity.

A Char-Lynn Model 212-1017 hydraulic power steering unit, supplied with pressurized fluid from the auxiliary hydraulic tractor supply and driven with a ground wheel via a chain drive, meters hydraulic fluid flow to the motor (Suggs and Peel, 1985). The steering unit displaces a fixed quantity of fluid per revolution, in a manner similar to a hydraulic pump. However, the unit cannot increase the pressure of the fluid flow; in fact, it actually

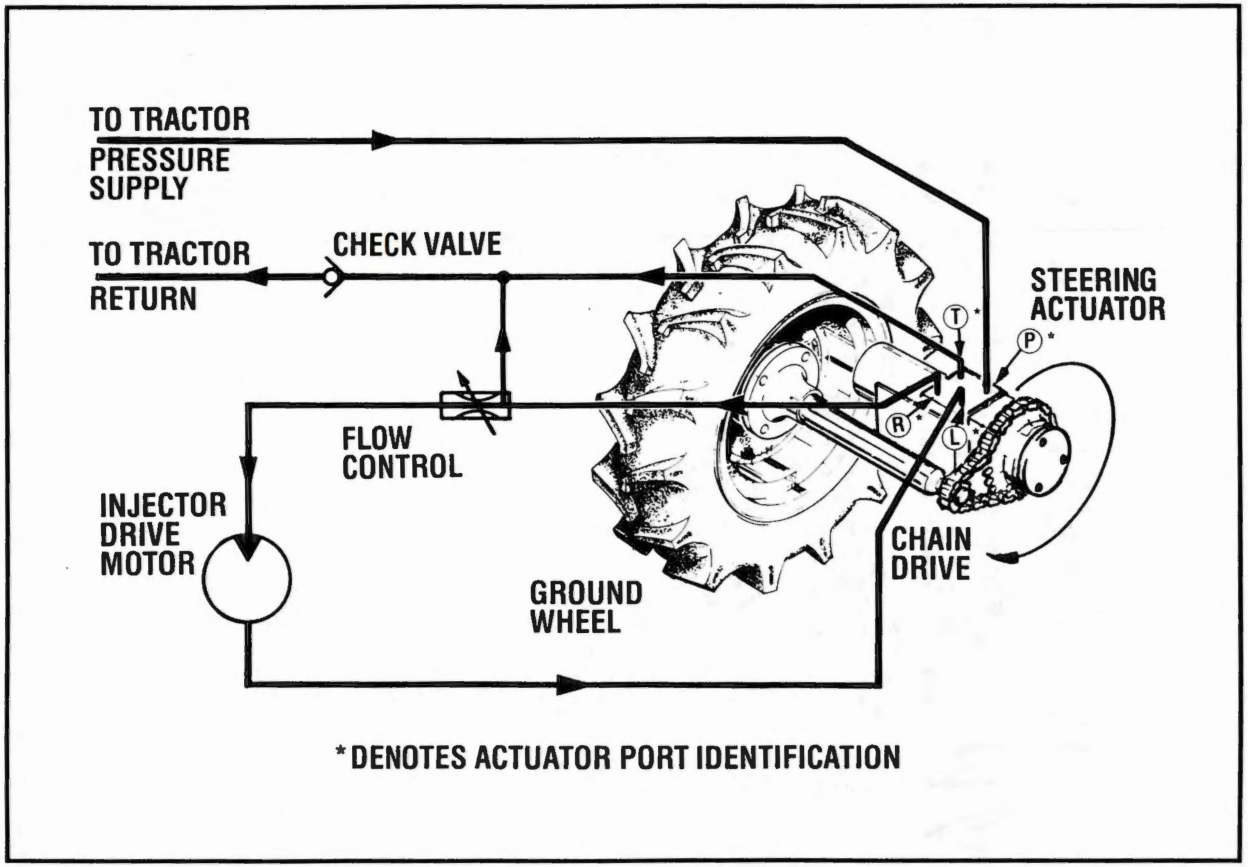

FIGURE 19. Schematic of hydraulic circuit used to operate injector drive motor.

decreases the pressure by about 350 kPa. A closed-loop system employing a standard pump was not selected because of possible slippage between the ground wheel and soil. When loaded, a pump resists shaft rotation, whereas the steering unit does not. Thus, rather than energize the injector with a system that relies on extreme tractive effort by a wheel, the tractor hydraulic system was utilized. Precise control of the probe crank speed with respect to the ground speed was assumed to be a critical link necessary for successful operation of the injector.

To mount a chain sprocket onto a recessed internal-splined shaft of the steering unit, a mating splined shaft was pressed into a double-row, deep-groove ball bearing which had been pressed into an aluminum block bolted to the unit. Thus, transverse forces on the splines and thrust loads on the input shaft of the unit were minimized. Metered output from the steering unit was directed through a flow control valve and then to the motor. Subsequently, the ratio between ground wheel speed and motor speed was proportional to the gear ratio of the chain drive and to the flow control setting. All components of the hydraulic circuit were connected with 12.7-mm nominal i.d. hydraulic hoses having two braids of wire reinforcement.

In addition to the hydraulic components, a Hilliard Type 321, Size 4 overload slip clutch, installed in the drive line between the hydraulic motor and rotary timing meter, provides a measure of safety in the event of probe overload. The maximum torque rating of the clutch is 103 N-m.

4. FLUID FERTILIZER DISPENSER SYSTEM

The dispenser system meters and regulates the flow of fluid fertilizer through the soil engaging probe. This system (Figure 20) consists of a pressure-regulated source, rotary timing meter, rotary fluid distributor, and probe-tip valve.

Pressure-Regulated Source

The pressure-regulated source was patterned after that used on a pesticide applicator. A 95-L polyethylene tank, mounted on the frame of the injector, supplies fluid through a polypropylene ball valve, an 80-mesh-screen line strainer having a polypropylene body, and a 19.1-mm i.d. reinforced rubber hose connected to a Hypro (Lear Siegler, Inc.) Model 6500N-T3 roller pump mounted on a tractor power-take-off shaft. The pump pressurizes the fluid to approximately 1380 kPa. Then, fluid flows from the pump through a hose, identical to the previously described supply hose, to a 19.1-mm nominal diameter, schedule 80, polyvinyl-choride (PVC) tee that directs the flow to an another ball valve and a second, identical tee. The ball valve, constructed of Type 316 stainless steel, diverts a portion of the excess pump output directly back into the tank via a tank agitator. The second tee directs the flow to the injector and a Teejet (Spraying Systems Co.) Model 9840 diaphragm-type, pressure-relief valve having an aluminum inlet body and bonnet. The pressure-relief valve, adjusted manually until the desired pressure registers on a gage (Ashcroft 3KA42666-006, 2760 kPa capacity, 316 stainless steel,

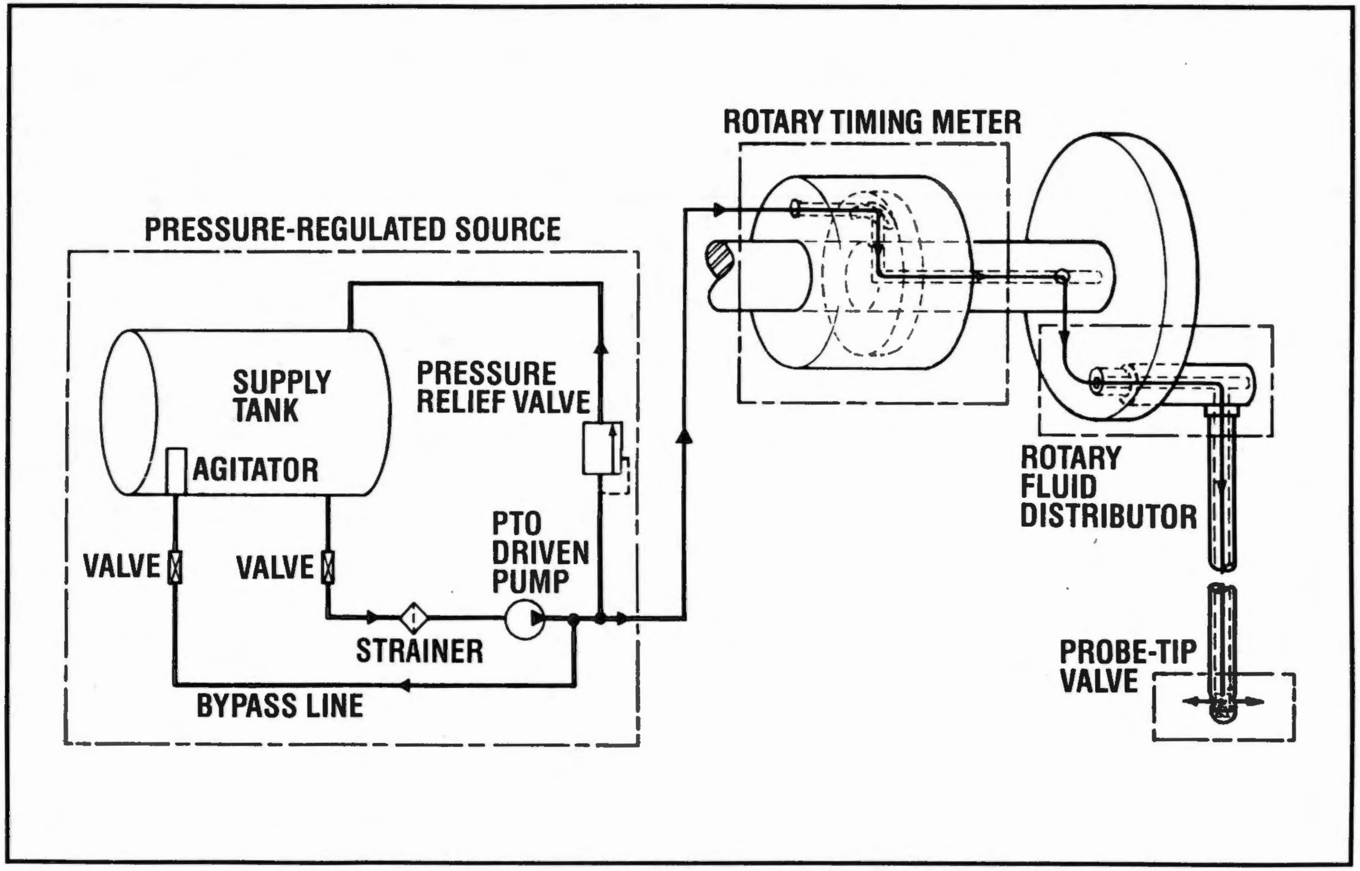

FIGURE 20. Schematic of fluid fertilizer dispenser system.

glycerine filled) installed in the gage port of the relief valve, dumps the remaining excess fluid back into the tank via a 12.7-mm i.d. reinforced rubber hose. All rubber hoses were connected with stainless steel hose barbs and worm-driven clamps.

Rotary Timing Meter

An in-house-fabricated rotary meter (Figure 21) controls fluid injection timing synchronized with the engagement of the probe with the soil. This meter functions as a rotating fluid union and fluid timing valve. No commercial meters that would handle the corrosive liquid fertilizer were available. Hence, a custom designed unit was necessary.

The fabricated meter consists of a disk-shaped rotor pressed onto a shaft supported on bearings in each end of the housing. This shaft also serves as the crankshaft for the probe mechanism. Fluid flows from the pressure-regulated source, via Parker Hose No. 919-6 consisting of an inner tube of extruded polytetrafluoroethylene (Teflon) with stainless steel wire braid outer cover, to a fixed-position port in the meter housing. Then, fluid flows from the fixed port into a tube pressed into a disk-shaped pressure plate that is free to move axially over the shaft and towards the rotor. A Parker Type B Polypak rod seal prevented fluid leakage between the housing and tube. To insure a self-adjusting positive seal, the pressure plate was spring-loaded against a thin sheet of virgin Teflon sandwiched between the plate and rotor. Next, depending on the

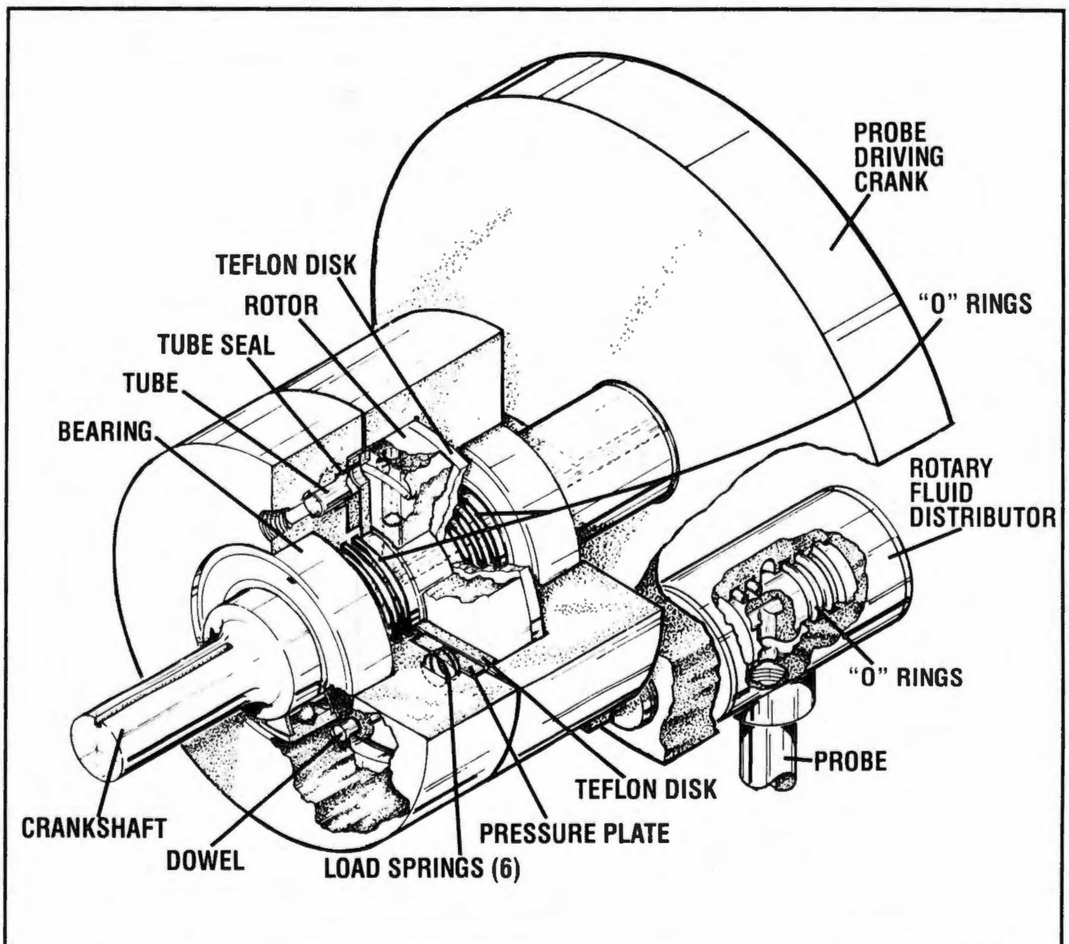

FIGURE 21. Sectioned perspective view of rotary fluid injection timing meter and rotary fluid distributor.

angular position of the rotor, fluid flows through the pressure plate tube into a slotted port machined into the face of the rotor. The length of the slot extends through 20 degrees of angular displacement of the rotor. Bottom dead center of the probe crank pin corresponds to the alignment of the fluid supply tube with the center of the rotor slot. Thus, fluid injection begins 10 degrees before bottom dead center (BBDC) and ends 10 degrees after bottom dead center (ABDC) of the crank pin. The meter was bolted in a bracket having slotted bolt holes so that the housing could be rotated with respect to the shaft and rotor assembly. These slots allowed the starting point of injection, normally 10 degrees BBDC, to be varied in a manner similar to an engine ignition distributor or fuel injection pump. Adjustable fluid timing may be needed to compensate for lags in fluid movement at high rotary speeds of the timing meter. Another thin sheet of virgin Teflon was sandwiched between the rotor and housing on the side opposite the pressure plate. Dowel pins restrained the pressure plate and each sheet of Teflon from rotation. Finally, fluid flows from the rotor through a drilled passage to the center of the crankshaft.

The meter housing, rotor, and pressure plate were machined from Type 7075 aluminum alloy. The crankshaft and pressure-plate tube were machined from stainless steel. Note from Figure 21 that this meter supports the flywheel assembly; consequently, the meter was equipped with 45.0-mm-bore, single-row, deep-groove ball bearings rated at 21200 N load capacity.

O-ring shaft seals were incorporated inboard and adjacent to each bearing. Parker No. 2-133 O-rings formed from Nitrile (Buna N) compound were installed in grooves machined into the meter housing. Grooves were installed in the stationary housing rather than the crankshaft to negate the effects of centrifugal force on the O-ring which causes the O-ring to rotate within the groove and prematurely fail. For rotary seals having surface velocities up to 61.0 m/min, Parker recommends O-ring related tolerances for industrial reciprocating O-ring seals. Since the maximum surface velocity exceeds 71.8 m/min (for 500 rpm speed), groove dimensions and diametral clearance were determined per Parker recommendations for rotary O-ring seals. When the meter was assembled, the O-rings fit too tightly as indicated by the fact that the shaft was difficult to manually rotate in the housing. Chassis grease had been applied to the rings. The machinist feared that excessive friction on the rings would cause the rings to prematurely fail. Thus, the meter was disassembled, and the groove diameters were enlarged until the shaft could be rotated manually when installed in the housing.

Rotary Fluid Distributor

The fluid path continues from the rotary timing meter through the center-drilled crankshaft to an external port located near the flywheel. An external tube (Parker Hose No. 919-6) carries fluid from the crankshaft port to another port drilled into one end of the crankpin that protrudes through the flywheel. About midway along the axis of the crankpin, a second crankpin port was drilled from the

radial crankpin surface to the center port. Fluid passes through these ports to a fluid distributor supported on the crankpin by needle bearings; thus, the distributor is free to rotate about the crankpin. Fluid flows through an internal distributor groove that encircles the outlet of the crankpin port to a threaded port positioned at right angles to the axis of rotation. This threaded port accommodates the uppermost end of the soil engaging probe.

O-ring seals, designed similar to the meter seals, prevent fluid loss at the rotary interface of the distributor and crankpin. Parker No. 2-214 O-rings formed from Buna N compound were installed in grooves machined into the fluid distributor. Maximum surface velocity of this seal is 39.9 m/min (for 500 rpm speed); subsequently, Parker O-ring design recommendations for industrial reciprocating seals were followed. The rings fit too tight and were subsequently custom fitted like those in the meter.

Probe Tip Valve

A normally-closed valve was integrated into the probe-tip (Figure 22) to provide fluid shutoff between injections. The valve consists of a spring-loaded poppet that covers two ports drilled transversely through the probe wall. Hydrostatic pressure, activated when the timing meter passes fluid, forces the poppet down into an open position and subsequently allows fluid to flow through the probe ports. Then, when the flow subsides, the spring force pushes the poppet up into a closed position until another surge. A pin, inserted transversely through the probe wall, limits the upward

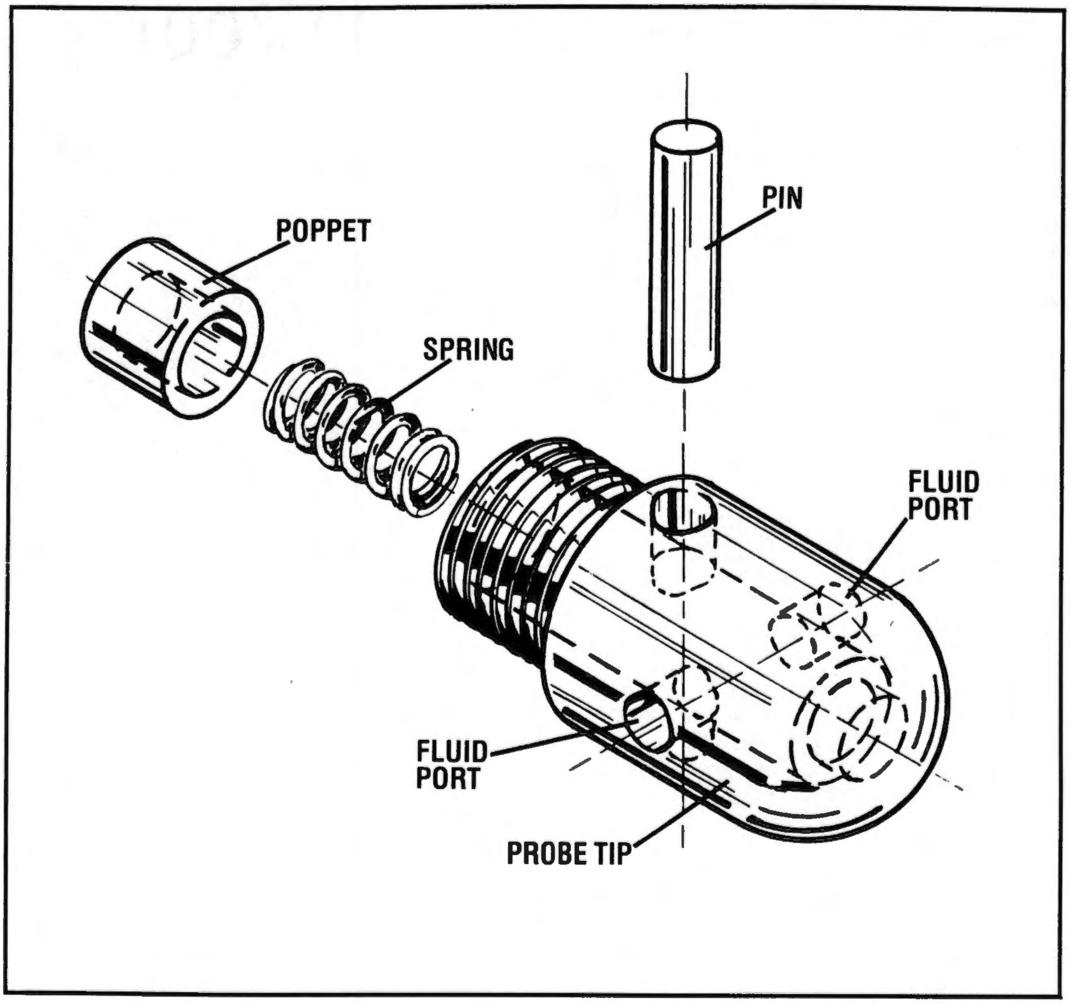

FIGURE 22. Exploded view of injector probe tip.

movement of the poppet and holds it in the tip. The poppet, pin and probe-tip were machined in-house from stainless steel.

A 6.1-mm o.d. stainless-steel compression spring preloads the poppet against the pin. This factory-made spring was constructed from 0.74-mm diameter wire and was factory calibrated at a spring rate of 2.21 N/mm. The spring preloads the poppet with a force of approximately 20 N. Theoretically, a hydrostatic pressure of about 273 kPa was required to crack open the valve, and a pressure of about 421 kPa was required to fully open it.

CHAPTER VII

EVALUATION OF FERTILIZER APPLICATOR

1. INJECTOR TOOLBAR AND FRAME

The toolbar and frame members operated without noticeable deflection during injector evaluation. However, three undesirable characteristics were observed. First, the toolbar vibrated in a motion that rotated perpendicular to an imaginary fore-aft axis passing through the tractor and injector. Rotation centered about the hitch. Although vibration amplitude at each end of the toolbar rarely exceeded one centimeter and was not felt by the tractor operator, this aspect should be considered by designers of multi-probed machines. Second, tire sinking of the depth control wheels strongly affected soil penetration depth by the probe and subsequent soil disturbance. Actually, the injector wheels tracked in a soil depression created by the tractor tires. Depth of the soil depression varied in the field, so height of the depth control wheels was compromised between the minimum and maximum required heights. The probe and depth control wheels should be mounted closer together letting one trail the other. Third, the toolbar with mounted components was top-heavy when unhitched from the tractor. Special, heavy-duty, triangular-shaped support stands, or cradles, were fabricated to prevent the injector from toppling during transport on a vehicle. Upright injector transport was required. Other transport positions were not possible because of possible component damage.

2. SOIL-ENGAGING PROBE MECHANISM

The probe mechanism was initially tested in a 0.6 by 7.3-m wooden sandbox filled with fine river sand to a depth of 80 mm. These tests were conducted with the injector hitched to a Massey Ferguson (MF) 265 tractor. Since the sandbox was built on the ground surface, the height of the depth control wheels of the injector was adjusted to the lowest position to allow clearance between the probe tip and sandbox bottom. Several passes were made through the box while adjusting injector crank speed to minimize soil disturbance. Injector speed and subsequent soil disturbance was strongly affected by gear selection and engine crank speed of the tractor. This problem is discussed in subsequent paragraphs pertaining to the probe driving system. However, during constant tractor operating settings, the probe contacted, penetrated, and exited the soil with very little soil disturbance. The resulting hole in the soil was slightly elongated to about 25 mm. Hole spacing was about 500 mm.

The injector was transported to the field for further evaluation. The Milan Experiment Station located in West Tennessee was chosen for the test site, because the soil there is relatively free from rocks and other probe damaging obstructions. The injector was hitched to a relatively new (<500 hrs) Case-IH 685 tractor (Figs. 23-24). The problems experienced with the MF 265 tractor regarding speed compensation by the injector were not noticed when using the Case-IH 685 tractor. However, to not compound other aspects of the evaluation, the tractor was operated under nearly constant operating

FIGURE 23. Side view of injector hitched to Case-IH 685 tractor.

FIGURE 24. Rear view of injector hitched to Case-IH 685 tractor.

conditions as indicated by the standard instruments supplied on the tractor. The tractor was operated in the third, low range gear at an engine speed of 2165 rpm. These settings were arbitrarily chosen to represent a typical operating condition. The higher engine speed insured delivery of a sufficient volumetric flow of hydraulic fluid to the probe drive mechanism. Furthermore, the gear selection versus engine speed chart posted on the tractor indicated an approximate ground speed of 5.8 km/h for these tractor operating settings.

The injector was primarily operated in a disked field. Figures 25-28 show results of injector operation. Figure 25 illustrates the dynamic motion of the probe being withdrawn from the soil. Note that the crank turns counter-clockwise, and that forward travel direction of the injector is toward the upper, right-hand corner of the photograph. Also, the chain-driven power steering actuator is pictured in the upper, left-hand corner. Figure 26 shows a row of seven holes formed by the injector. The holes are not easy to distinguish from the irregularities of the ground surface. They pass through a vertical, slightly diagonal row in the middle of the photograph. Hole spacing was about 400 mm. Figure 27 shows a single hole depth indicated with a scale having traditional English units. An average probe penetration depth of 65 mm was measured. Figure 28 shows a single hole width indicated with a scale having traditional English units. The path of injector travel coincided with the orientation of the scale (horizontal in photograph). The width of the hole in this direction was about 25 mm. The width of the hole in the direction perpendicular to the travel path was about 20 mm.

FIGURE 25. Probe exiting soil during field evaluation of injector.

FIGURE 26. Row of seven holes in soil demonstrating pattern of soil disturbance resulting from probe operation.

FIGURE 27. Depth of single hole formed by probe indicated with scale having traditional English units.

FIGURE 28. Width of single hole formed by probe indicated with scale having traditional English units.

Punched hole spacing affected the magnitude of soil disturbance. For spacing greater than about 400 mm, the horizontal speed of the probe tended to lag the travel speed of the injector. This lag caused the probe to drag in the soil. For spacing less than about 400 mm, the horizontal speed of the probe tended to lead the travel speed of the injector. This lead caused the probe to push soil. The severity of both soil disturbance cases increased in proportion to the deviation of spacing from 400 mm. However, increased soil disturbance may be acceptable in some application circumstances.

The author bent two probes during the several tests, including those performed in the sandbox and field. One probe hit the wooden end of the sandbox through operator negligence. Another struck an object, probably a hard, dried-out cornstalk, in a field containing heavy crop stubble. Removing the bent probes from the injector was not a simple task. The probes bent in an S-shape as expected. Thus, one end, usually the lowest one, had to be straighted before withdrawing the probe through the pivoted slide. The probes, built from type 304 stainless steel, were straightened by hand for removal. In addition to an increased probe diameter extending down through the pivoted slide, an overload trip release is obviously required for continuous probe operation. The release could be incorporated into the probe itself, or into the entire mechanism. Dynamic penetration data obtained in this study is available for determining optimum trip settings.

How practical is the developed mechanism for a field-going, production-agriculture machine? The mechanism is much more complex than the knife-type applicator used in current agricultural practice. Is this complexity justified? The answer to that question depends on the emphasis of certain agricultural issues. For example, combines and cotton pickers are also complex machines, yet they are necessary for modern agriculture to succeed. Labor savings provided the impetus for harvester technology development. The impetus driving the development of the probe-type injector was to allow fertilizer to be placed beneath the soil surface without significant soil disturbance and to improve environmental quality associated with the incorporation of chemicals. Regulation and enforcement of these environmental aspects provides additional justification to warrant the complexity of the injector. Other reasons such as anticipated increases in fertilizer use efficiency and smaller tractor requirements may provide additional justification.

3. PROBE DRIVING SYSTEM

The hydraulic-based probe driving system operated satisfactorily during injector testing. The system regulated probe crank speed according to the ground speed. Thus when the tractor ground speed was increased, the crank speed also increased to maintain nearly constant hole spacing intervals.

When the injector was initially tested with the MF 265, the injector crank speed was unexpectedly sensitive to the tractor throttle and gear settings. The problem was determined to be inadequate flow of hydraulic fluid to the injector. Maximum hydraulic flow capacity of the MF 265 was estimated at 38 L/min at a rated engine speed of 2000 rpm. Power-assisted steering on the tractor may have reduced the quantity available at the auxiliary ports. Generally, hydraulic flow rate depends on engine speed. When operating at engine speeds greater than about 1100 rpm, the pressure relief built into the hydraulic flow selector tripped the selector into the neutral position during periods of reduced flow demand. Reduced demand occurred at the start and finish of test runs when the steering actuator on the injector was no longer turned. Changing engine speed while operating through the relatively short and narrow sandbox was difficult to synchronize by the author.

The hydraulic pump on the Case-IH 685 tractor was rated at 59.8 L/min at a rated engine speed of 2400 rpm, according to the owner's manual. Power steering reduced output by 9.5 L/min. To insure that sufficient fluid was available, the tractor was operated at 2165 rpm. Unlike the MF 265 tractor, this tractor had a mechanism to hold the hydraulic flow selector in a preset position. Thus, about 44 L/min was constantly available for the injector. The hydraulic motor on the injector required no more than 23 L/min at an operating speed of about 300 rpm. For a ground speed of 5.8 km/h and a hole spacing of 400 mm, the injector crank turned at approximately 240 rpm. Ideally, a smaller displacement hydraulic motor should have been outfitted to the injector, but the author used the selected motor because it was available from in-house stock.

During injector start up, the first injection typically disturbed the soil more than subsequent injections. This initial disturbance occurred because the probe was sometimes dragged through the soil a distance that varied from three to six probe diameters. The source of this problem was found to be the hydraulic system. At very low speeds (< 30 rpm), the hydraulic motor operated with a jerking motion. The exact cause of this undesirable motion was not identified, although the power steering actuator was suspected as being the source of the problem. However, this occasional jerking motion was not considered to be a significant problem.

One advantage to using a probe drive separate from the probe is the possibility of exercising variable control between the two units. For example, Baker's Point Injector that resembles a wagon wheel with spokes protruding beyond the rim drives itself. Spoke operation and subsequent hole spacing will always be dependant on the geometry of the wheel. The probe-type injector offers greater variability than a fixed geometry wheel. The hydraulic link between the ground drive and probe mechanism could be controlled with an electronic-based control system that dictates when and where the probe injects.

The steering actuator support bracket constructed from 6.4-mm steel plate elastically deflected whenever the actuator severely resisted rotation. The power steering actuator was easily turned when supplied with a sufficient quantity of pressurized fluid. However, the actuator resisted rotation when no pressurized fluid was available, or when the actuator shaft speed exceeded the speed limited by flow (fluid flow divided by effective actuator displacement). Thus, injector modifications should include reinforcement of the original bracket, or a new bracket built out of thicker stock.

4. FLUID FERTILIZER DISPENSER SYSTEM

The fluid dispenser system was evaluated using tap water in the system. Fluid fertilizers have a specific gravity ranging from about 1.2 to 1.4, depending on the exact formulation. Thus, injector evaluation results obtained with fluid fertilizers will vary from those reported herein. Water was chosen for evaluation purposes to reduce the hazards associated with handling fertilizers.

Fluid output through the probe tip was observed while operating the injector above ground with the probe crank in a stationary, downward position. In this position, the internal ports were aligned, so that pressurized fluid flowed through the injector and out the tip. The resulting steady flow emitting from the tip was then characterized for two operating pressures. Figure 29 depicts the flow through the tip at a low fluid pressure (1030 kPa). Most of the flow exits the tip in a primary stream directed down towards the ground. Also, secondary streams having a combined flow of much less than the primary stream radiate from each tip opening. Flow primarily occurs in a vertical plane perpendicular to the direction of travel. Furthermore, the primary and secondary streams contribute to a fine mist formed several hundred millimeters out from the probe. This mist, as well as any secondary stream, is not desirable since potential losses of the fluid are increased. However, these

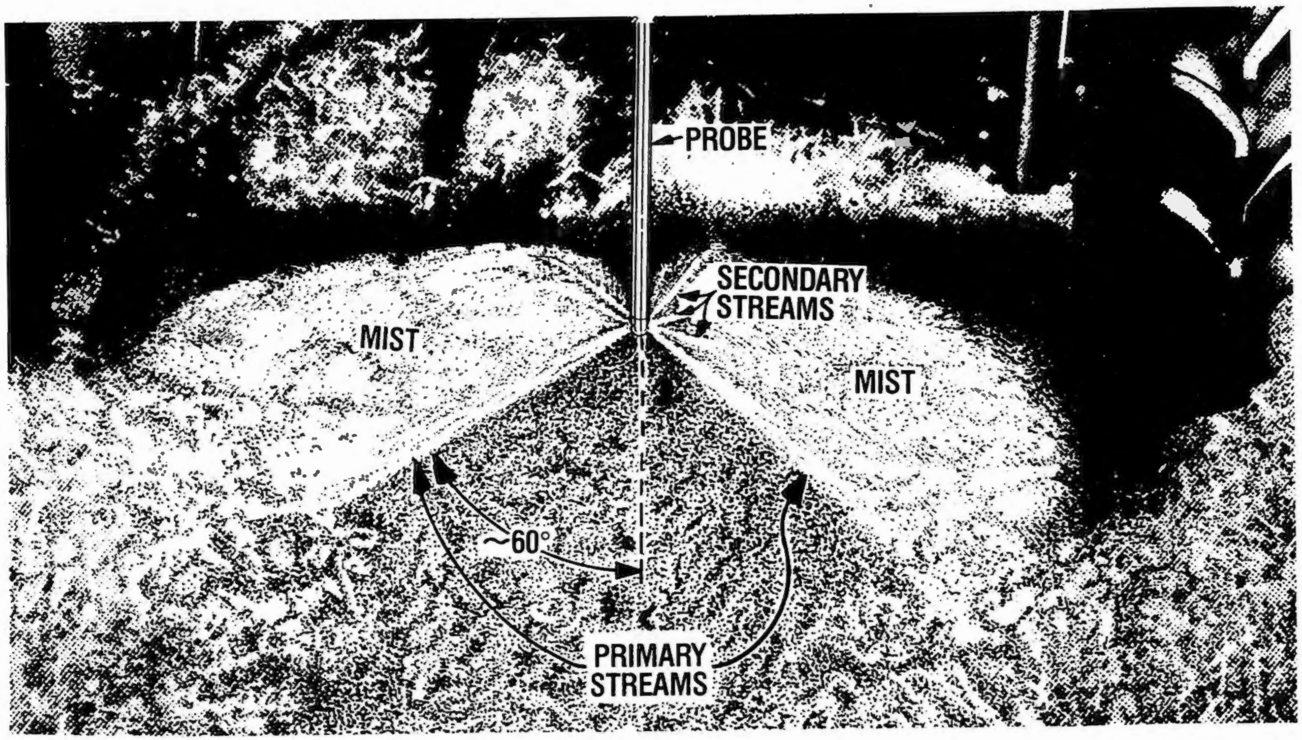

FIGURE 29. Characterization of fluid output from probe tip at low fluid pressure.

potential losses were not observed when the probe injected fluid below the ground surface. Figure 30 depicts the flow from the tip at high fluid pressures (1720 kPa). A primary stream carries most of the flow, similar to the low-pressure flow. However, the secondary streams are not as pronounced during the high-pressure flow. Instead, a mist is formed near the probe tip in place of the secondary streams. No fluid was detected leaving the ground when the injector probe squirted fluid at high pressure below the soil surface.

Examination of fluid placement in the soil was difficult. Formulabs fluorescent dye tablets were mixed in water at the rate of one tablet per 3.8 L. Then, this mixture was injected into the soil by the probe mechanism. Cross-sections of each punched hole were examined under a blacklight at night. The soil tended to soak up the mixture leaving only a thin film of residue exposed to the light. Detecting the thin film with the naked eye and/or photographically was very difficult for the author. Consequently, examination of fluid placement in the soil was suspended.

The fluid volume output through the dispenser system at the probe tip was measured in two ways. First, steady flow activated with the probe crank in a stationary, downward position was measured at three pressures. Figure 31 plots these results. The three groups of data correspond to the three pressures 1030, 1380, and 1720 kPa. Scatter among the data in each group was primarily attributed to fluid losses due to splatter. As the plot indicates, fluid did not begin to immediately flow from the tip when the pressure was

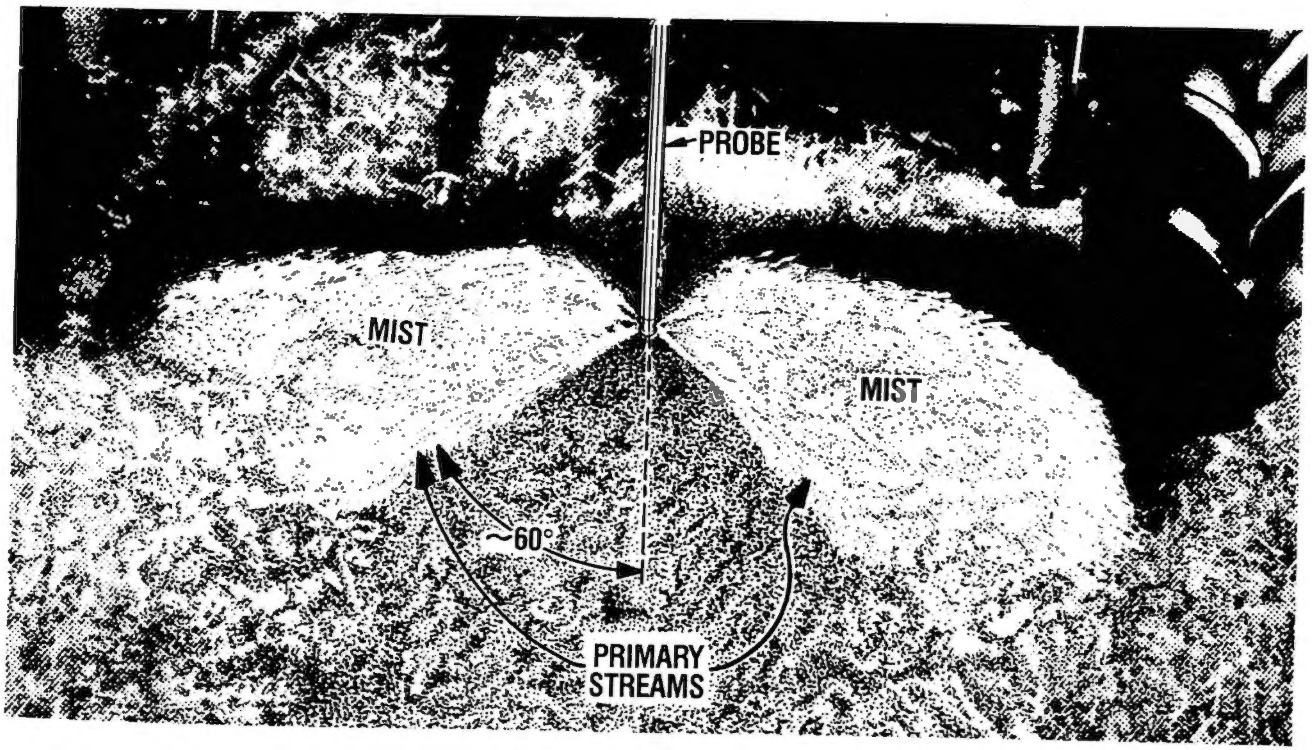

FIGURE 30. Characterization of fluid output from probe tip at high fluid pressure.

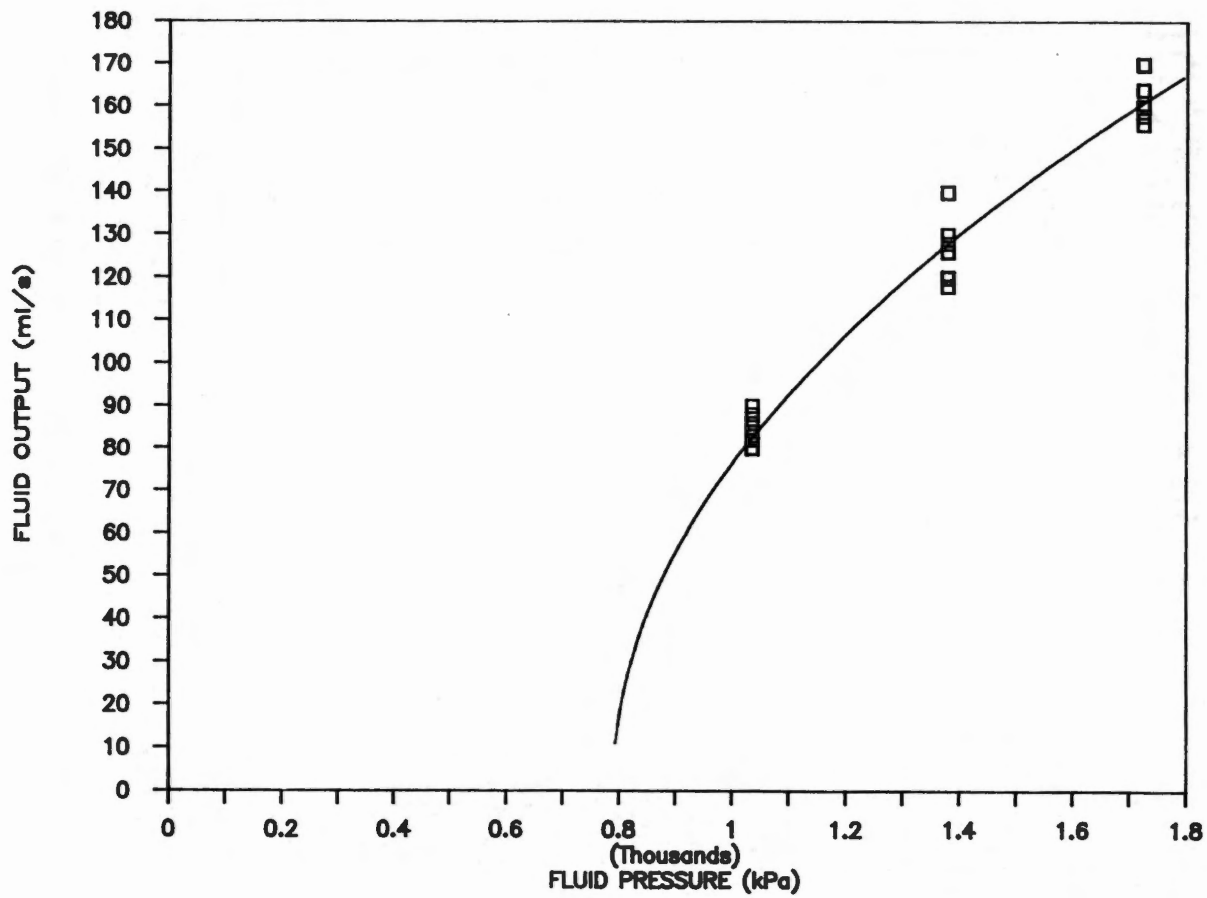

FIGURE 31. Steady fluid flow output from injector versus fluid operating pressure.

increased from zero. Flow only began after some probe tip valve cracking pressure was attained. The exact determination of this cracking pressure was difficult because the valve opened gradually. Initially, a fine mist escaped and then with further pressure increases the mist became a stream. This transition occurred at about 700 kPa. A modified orifice flow equation was fit through the data and extrapolated down to zero fluid output axis. The following best-fit curve was computed using the IMSL subroutine RNLIN (IMSL, 1988):

$$Q = k\,(P - P_c)^{0.5}$$

where,

Q = steady fluid output, ml/s
k = orifice constant = 5.2665
P = system pressure, kPa
P_c = cracking pressure = 788.5, kPa.

Second, the injector crank was operated with the probe above ground, and the resulting intermittent fluid flow was measured. This procedure simulated injector operation in the field. The ground wheel coupled to the hydraulic power steering actuator was turned manually. Determining a constant turning speed was difficult, if possible at all. Average speed was computed by dividing the time interval into the corresponding number of revolutions. This method was chosen to simulate a field calibration. Different speeds were examined. Figure 32 plots the average quantity of fluid output per injection versus the probe crank speed. As expected, fluid output decreases with increases in speed. This reduction occurs because a finite amount of time was required for stationary fluid to be set into motion in the system. These data show the difficulties of

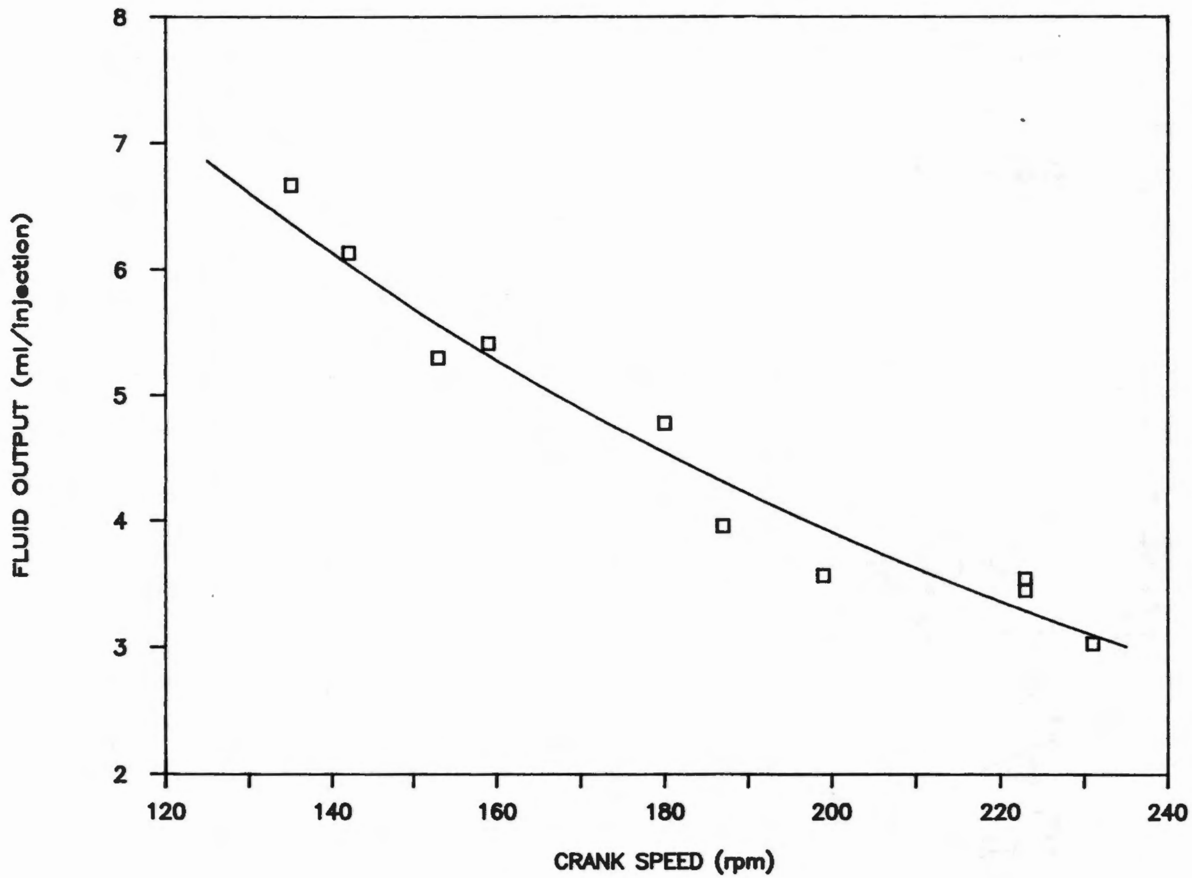

FIGURE 32. Intermittent fluid flow output from injector versus crank speed.

establishing and maintaining the calibration of a rotary timing meter for field use. The following decaying, exponential equation, computed with an r^2 of 0.955, was fitted to the data with a least squares method:

$$q = a\, e^{-bn}$$

where,

q = intermittent fluid output, ml/injection
a = constant = 18.45
b = constant = 0.0078
n = rotational crank speed, rpm.

Measurement of output using different fluids was not investigated. However, fluids having different characteristics, such as specific gravity and viscosity, may behave differently in the system as compared to water. Thus, the values in the above equations may only apply to water, although calibration using other fluids should be represented by similar curves. Fluid temperature may also affect calibration.

The pressure-regulated source operated satisfactorily during the limited amount of testing. The roller pump failed to pump on one occasion. The pump resumed normal operation after the system was shutdown and then immediately restarted.

The rotary timing meter functioned well. Advancing the timing of the fluid injection interval was not needed. Thus, fluid flow began at 10 degrees before bottom dead center of the crank pin. Flow continued for 20 degrees rotation of the crank as determined by the dimensions of the slot machined in the rotor. The triple O-ring seals on each shaft end did not leak, even at pressures and crank speeds as high as 2000 kPa and 400 rpm, respectively. Toward the end of the injector test period, the meter allowed small amounts of fluid to pass through the system when the rotor slot was in a closed position. The condition was more pronounced when the fluid was hotter than fifty degrees Celsius. The fluid became hot during extended periods of pumping and recirculation. Remnants of the fluorescent dye trace material may have recrystalized in the rotary valve causing damage to the Teflon seal material.

No problems were encountered with the rotary fluid distributor. The double O-ring seals did not leak.

The poppet-type valve incorporated into the probe tip performed flawlessly. The valve opened and closed with a snappy action preventing fluid from slinging out of the probe due to inertial forces. Also, the poppet sealed off the external fluid ports such that soil never plugged the outlets in the tip.

CHAPTER VIII

SUMMARY AND CONCLUSIONS

1. SUMMARY

An experimental machine for injecting fluid fertilizer into the soil at discrete increments with minimal soil disturbance was developed. Incorporation of nitrogen sources below the soil surface to reduce losses and reduction in soil disturbance for no-till cropping systems justified machine development. The design featured a probe-type injector that impacts a probe into the soil. Previously published literature lacks information and data regarding impact-loaded soils, especially agricultural soils. Thus, the injector design was based upon measurements of soil dynamic response to impact loading.

A microcomputer-based data acquisition system was developed and employed for high-frequency monitoring of a probe impacted into the *in situ* surface of clay loam, fine sandy loam, and silt loam soils. Data defining impact force on the probe versus depth of penetration were obtained for probe diameters ranging from 9.5 to 19.1 mm and probe striking velocities ranging from 2.0 to 5.0 m/s. Data analysis for 216 tests indicated that final probe penetration depth strongly affected peak probe force. A regression model based upon input energy, probe diameter, and penetration depth was developed to predict peak impact force on a probe.

Dynamic soil characteristics were measured to quantify the soil conditions used in the penetration tests. Soil specimens were tested in a torsional-type resonant column device, employing a method developed to test agricultural soils at low confining stresses. Measured shear modulus, damping ratio, and strain amplitude ranged from 13.1 to 38.1 MPa, 0.89 to 4.04 percent, and 4.9×10^{-5} to 11.9×10^{-5} cm/cm, respectively. Generally, shear modulus decreased and damping ratio increased with an increase in strain amplitude.

A prototype injector employing a kinematically inverted slider-crank mechanism was evaluated. Vertical orientation of the mechanism allowed a member, or probe, to engage soil during injector travel. Horizontal probe tip velocity offset injector travel velocity. A hydraulic-based actuator system controlled this velocity relationship. The probe released fluid through the tip during soil penetration. A custom-built fluid dispenser system integrated with the probe mechanism consisted of a pressure-regulated source, rotary timing valve, rotary fluid distributor, and probe tip valve. Fluid injection occurred in 400-mm intervals at a soil depth of 65 mm. Steady flow through the probe tip was described with a modified orifice flow equation. Reduction in intermittent flow rate with increasing crank speed was described with a decaying exponential function.

2. CONCLUSIONS

Development of a fluid fertilizer injector based upon the dynamic response of impact loaded *in situ* soil resulted in the following conclusions:

1. A machine can inject fluid fertilizers into the soil at discrete increments with minimal soil disturbance.
2. Fluid injection machines can use single, high-velocity probes to penetrate soil.
3. Soil-engaging, high-velocity probes need an overload release mechanism incorporated into the probe design.
4. A ground-speed-compensating hydraulic circuit can control and actuate a single probe to operate with minimal soil disturbance.
5. Initiation and termination of fluid flow can be synchronized with probe orientation and subsequent soil penetration.
6. Steady fluid flow through an injector mechanism can be described with a modified orifice flow equation.
7. Intermittent fluid flow through an injector mechanism can be described with a decaying exponential function.
8. Peak probe forces during soil impact can be predicted.
9. Peak probe forces during soil penetration are proportional to the soil stiffness as measured by a standard dynamic soil test.

BIBLIOGRAPHY

BIBLIOGRAPHY

Adeli, H., A.M. Amin and R.L. Sierakowski. 1986. Earth penetration by solid impactors. The Shock and Vibration Digest 18(9):15-22.

Angle, J.S., G. McClung, M.S. McIntosh, P.M. Thomas, and D.C. Wolf. 1984. Nutrient losses in runoff from conventional and no-till corn watersheds. Journal of Environmental Quality 13(3):431-435.

Aref, K.S., W.J. Chancellor, and D.R. Nielson. 1975. Dynamic shear strength properties of unsaturated soils. Transactions of the ASAE 18(5):818-823.

ASAE Standards. 1987. *ASAE Standards 1987 - 34th edition*. Editors: R.H. Hahn, and E.E. Rosentreter. American Society of Agricultural Engineers, St. Joseph, MI.

Baker, J.L., T.S. Colvin, S.J. Marley, and M. Dawelbeit. 1983. Use of a point-injector fertilizer applicator for better fertilizer management with conservation tillage. Paper No. MCR 83-114, American Society of Agricultural Engineers, St. Joseph, MI.

Baker, J.L. and D.R. Timmons. 1984. Effect of method, timing, and number of fertilizer applications on corn yield and nutrient uptake. Agronomy Abstracts, p 197.

Baker, J.L., T.S. Colvin, S.J. Marley, and M. Dawelbeit. 1985. Improved fertilizer management with a point-injector applicator. Paper No. 85-1516, American Society of Agricultural Engineers, St. Joseph, MI.

Baker, J.L., D.R. Timmons and R.M. Cruse. 1986. A comparison of point injection with conventional methods of applying fluid fertilizer in no-till corn. The 1986 Symposium Proceedings: The management of Fluid Fertilizers for efficient crop production, Fluid Fertilizer Foundation, Florida, March 11-13, p 76-85.

Bandel, V.A., S. Dzienia and G. Sanford. 1980. Comparison of N fertilizers for no-till corn. Agronomy Journal 72:337-341.

Blevins, R.L., D. Cook, S.H. Phillips and R.E. Phillips. 1971. Influence of no-tillage on soil moisture. Agronomy Journal 63:593-596.

Bowles, J.E. 1982. *Foundation Analysis and Design*. McGraw-Hill Book Co., New York, NY.

Bridges, J.D. 1982. *Fertilizer Trends 1982*. National Fertilizer Development Center, Tennessee Valley Authority, Muscle Shoals, AL.

Cameron, K.C. and A. Wild. 1984. Potential aquifer pollution from nitrate leaching following the plowing of temporary grassland. Journal of Environmental Quality 13(2):274-278.

Chancellor, W.J., J.A. Vomocil, and K.S. Aref. 1969. Energy disposition in compression of three agricultural soils. Transactions of the ASAE 12(4):524-528, 532.

Chichester, F.W., J.E. Morrison, Jr. and T.J. Gerik. 1984. Minimum disturbance fertilizer knifing for no-till. Paper No. 84-1009, American Society of Agricultural Engineers, St. Joseph, MI.

Clark, R.L. and J.T. Reid. 1984. Topographic mapping of soil properties. Paper No. 84-1029, American Society of Agricultural Engineers, St. Joseph, MI.

Clark, S.J. and L. Wagner. 1983. Computer simulation approach in soil dynamics. Paper No. 83-1538, American Society of Agricultural Engineers, St. Joseph, MI.

Curley, R.D. and D. Smith. 1985. Precision placement: key to conservation-till. Solutions Magazine, Inc. 29(7):18-19, 22-24.

Das, B.M. 1983. *Fundamentals of Soil Dynamics*. Elsevier Science Publishing Co., Inc., New York, NY.

Dawelbeit, M., J.L. Baker and S.L. Marley. 1981. Design and development of a point-injector for liquid fertilizer. Paper No. 81-1010, American Society of Agricultural Engineers, St. Joseph, MI.

Dickey, E.C., C.R. Fenster, J.M. Laflen and R.H. Mickelson. 1983. Effects of tillage on soil erosion in a wheat-fallow rotation. Transactions of the ASAE 26(3):814-820.

DMI, Inc. 1985. Colt-r-nife product sales literature. DMI, Inc., Goodfield, IL.

Doran, J.W. 1980. Soil microbial and biochemical changes associated with reduced tillage. Soil Science Society of America Journal 44:765-771.

Dowding, E.A., K.N. Hawley, R.E. McDole, C.L. Peterson. 1984. Fertilizer placement experiments under conservation tillage. Paper No. 84-2558, American Society of Agricultural Engineers, St. Joseph, MI.

Drnevich, V.P. 1978. Resonant column testing - problems and solutions. Dynamic Geotechnical Testing, ASTM STP 654, American Society for Testing and Materials. pp 384-398.

Drnevich, V.P., B.O. Hardin and D.J. Shippy. 1978. Modulus and damping of soils by the resonant-column method. Dynamic Geotechnical Testing, ASTM STP 654, American Society for Testing and Materials. pp 91-125.

Ernst, J.W. and H.F. Massey. 1960. The effects of several factors on volatilization of ammonia formed from urea in the soil. Soil Science Society of America Proceedings 24:87-90.

Fee, R. 1982. How to fertilize for conservation tillage. Successful Farming in the South, October 1982, p16-19. Meredith Corp., Des Moines, IA.

Fee, R. 1983. Nitrogen: new rules for conservation tillage. Successful Farming in the South, March 1983, p15-22. Meredith Corp., Des Moines, IA.

Fleischer Manufacturing, Inc. 1985. Buffalo Farm Equipment product sales literature. Fleischer Manufacturing, Inc., Columbus, NE.

Flennikin, J.M., R.E. Hefner, and J.A. Weber. 1977. Dynamic soil strength parameters from unconfined compression tests. Transactions of the ASAE 20(1):21-25, 29.

Fountaine, E.R. and N.J. Brown. 1959. Shearing resistance of top soils under small normal loads. Journal of Agricultural Engineering Research 4:53-59.

Fox, R.H. and L.D. Hoffman. 1981. The effect of fertilizer source on grain yield, N uptake, soil pH and lime requirements in no-till corn. Agronomy Journal 73:891-895.

Freeland, R.S., F.D. Tompkins, and L.R. Wilhelm. 1987. Keeping test errors within acceptable limits. Agricultural Engineering 68(2):13-15.

Gallaher, R.N. 1977. Soil moisture conservation and yield of crops no-till planted in rye. Soil Science Society of America Journal 41:145-147.

Gupta, C.P. and A.C. Pandya. 1967. Behavior of soil under dynamic loading: its application to tillage implements. Transactions of the ASAE 10(3):352-358,363.

Hall, J.R.,Jr. and F.E. Richart, Jr. 1963. Dissipation of elastic wave energy in granular soils. Journal of the Soil Mechanics and Foundations Division, Proceedings of the American Society of Civil Engineers 89:27-55.

Hardin, B.O. and W.L. Black. 1968. Vibration modulus of normally consolidated clay. Journal of the Soil Mechanics and Foundations Division, Proceedings of the American Society of Civil Engineers 94:353-369.

Hardin, B.O. and V.P. Drnevich. 1972a. Shear modulus and damping in soils: measurement and parameter effects. Journal of the Soil Mechanics and Foundations Division, Proceedings of the American Society of Civil Engineers 98:603-624.

Hardin, B.O. and V.P. Drnevich. 1972b. Shear modulus and damping in soils: design equations and curves. Journal of the Soil Mechanics and Foundations Division, Proceedings of the American Society of Civil Engineers 98:667-692.

Hargrove, W.L. and D.E. Kissel. 1979. Ammonia volatilization from surface applications of urea in the field and laboratory. Soil Science Society of America Journal 43:359-363.

Hartog, J.P.Den. 1948. *Mechanics*. Dover Publications, Inc., NY.

Hendrick, J.G. and G.E. VandenBerg. 1961. Strength and energy relations of a dynamically loaded clay soil. Transactions of the ASAE 4(1):31-32,36.

Hergert, Gary W. 1986. Nitrate leaching through sandy soil as affected by sprinkler irrigation management. Journal of Environmental Quality 15(3):272-278.

Holtz, R.D. and W.D. Kovacs. 1981. *An Introduction to Geotechnical Engineering*. Prentice-Hall, Inc., Englewood Cliffs, NJ.

Hubbard, R.K. and J.M. Sheridan. 1983. Water and nitrate-nitrogen losses from a small, upland, coastal plain watershed. Journal of Environmental Quality 12(2):291-295.

IMSL. 1982. Subroutine RLMUL, Users Manual - edition 9.2. International Mathematics and Statistics Library, Inc., Houston, TX.

IMSL. 1988. Subroutine RNLIN, Users Manual - edition 10.0. International Mathematics and Statistics Library, Inc., Houston, TX.

Jackson, M.L. 1958. *Soil Chemical Analysis*. Prentice-Hall, Inc., Englewood Cliffs, NJ.

Jumikis, A.R. 1969. *Theoretical Soil Mechanics*. Van Nostrand Reinhold Company, New York, NY.

Kang, B.T. and M. Yunusa. 1977. Effect of tillage methods and phosphorus fertilization on maize in humid tropics. Agronomy Journal 69:291-294.

Kolsky, H. 1963. *Stress Waves in Solids*. Dover Publications, Inc., New York, NY.

Lambe, T.W. and R.V. Whitman. 1979. *Soil Mechanics, S.I. Version*. John Wiley and Sons, New York, NY.

Lessiter, F. 1984a. Four nitrogen sources compared. No-Till Farmer, January 1984, p 2. No-Till Farmer, Inc., Waukesha WI.

Lessiter, F. 1984b. What's "new" in equipment lines. No-Till Farmer, July 1984, p 6. No-Till Farmer, Inc., Waukesha, WI.

Lessiter, F. 1984c. "Shoot fertilizer through your stubble. No-Till Farmer, August 1984, p 6. No-Till Farmer, Inc., Waukesha, WI.

Longwell, T.J., W.L. Parks, and M.E. Springer. 1963. Moisture Characteristics of Tennessee Soils. Experiment Station Bulletin No. 367, The University of Tennessee Agricultural Experiment Station, Knoxville.

Lowrance, R.R., R.L. Todd, and L.E. Asmussen. 1984a. Nutrient cycling in an agricultural watershed: I.phreatic movement. Journal of Environmental Quality 13(1):22-27.

Lowrance, R.R., R.L. Todd, and L.E. Asmussen. 1984b. Nutrient cycling in an agricultural watershed: II.streamflow and artificial drainage. Journal of Environmental Quality 13(1):22-27.

MacIver, G.N. and G.P. Hale. 1970. *Laboratory Soils Manual - Engineer Manual EM 1110-2-1906*. U.S. Army Engineer Waterways Experiment Station (WES), Department of the Army. Washington, D.C.

McDowell, L.L. and K.C. McGregor. 1980. Nitrogen and phosphorus losses in runoff from no-till soybeans. Transactions of the ASAE 23(3): 643-648.

McGregor, K.C. and J.D. Greer. 1982. Erosion control with no-till and reduced till corn for silage and grain. Transactions of the ASAE 25(1):154-159.

Mengel, D.B., D.W. Nelson and D.M. Huber. 1982. Placement of nitrogen fertilizers for no-till and conventional till corn. Agronomy Journal 74:515-518.

Moschler, W.W., and G.M. Shear, D.C. Martens, G.D. Jones and R.R. Wilmouth. 1972. Comparative yield and fertilizer efficiency of no-till and conventionally tilled corn. Agronomy Journal 64:229-231.

Nichols, T.A., A.C. Bailey and C.E. Johnson. 1985. Soil stress state determination under wheel loads. Paper No. 85-1553, American Society of Agricultural Engineers, St. Joseph, MI.

Nicholson, R.I., L.L. Bashford, and L.N. Mielke. 1984. Energy requirements for tillage from a reference implement. Paper No. 84-1028, American Society of Agricultural Engineers, St. Joseph, MI.

Owens, L.B., W.M. Edwards, and R.W. van Keuren. 1984. Peak nitrate-nitrogen values in surface runoff from fertilized pastures. Journal of Environmental Quality 13(2):310-312.

Owens, L.B., R.W. van Keuren, and W.M. Edwards. 1983. Nitrogen loss from a high-fertility, rotational pasture program. Journal of Environmental Quality 12(3):346-350.

Pang, S.S., A. Kumano, W. Goldsmith, and U. Rask. 1986. Performance of a pickax. Rock Mechanics and Rock Engineering 19:27-52.

Perumpral, J.V. 1983. Cone penetrometer application - a review. ASAE Paper No. 83-1549, American Society of Agricultural Engineers, St. Joseph, MI.

Pesek, J., G. Stanford and N.L. Case. 1971. Nitrogen production and use. p. 217-266. In: R.A. Olsen (editor). Fertilizer Technology and Use. Soil Science Society of America, Inc. Madison, WI.

Richart, F.E.,Jr. and R.D. Woods. 1970. *Vibrations of Soils and Foundations*, Prentice-Hall, Inc., Englewood Cliffs, NJ.

Rogers, C.O., S.S. Pang, A. Kumano, and W. Goldsmith. 1986. Response of dry- and liquid-filled porous rocks to static and dynamic loading by variously-shaped projectiles. Rock Mechanics and Rock Engineering 19:235-260.

Rogers, R.B. and B. Rinholm. 1987. Pulse bander development. ASAE Paper No. 87-1607, American Society of Agricultural Engineers, St. Joseph, MI.

Rowe, R.J. and K.K. Barnes. 1961. Influence of speed on elements of draft of a tillage tool. Transactions of the ASAE 4(1):55-57.

Sanglerat, G. 1972. *The Penetrometer and Soil Exploration: Interpretation of Penetration Diagrams - Theory and Practice*. Elsevier Publishing Company, Amsterdam, The Netherlands.

Schreiber, J.D. 1985. Leaching of nitrogen, phosphorus, and organic carbon from wheat straw residues: II. loading rate. Journal of Environmental Quality 14(2):256-260.

Schreiber, J.D. and L.L. McDowell. 1985. Leaching of nitrogen, phosphorus, and organic carbon from wheat straw residues: I.rainfall intensity. Journal of Environmental Quality 14(2):251-256.

Seed, H.B. and I.M. Idriss. 1970. Soil moduli and damping factors for dynamic response analyses. Report No. EERC 70-10, Earthquake Engineering Research Center, University of California, Berkeley, CA.

Shear, G.M. and W.W. Moschler. 1969. Continuous corn by the no-tillage and conventional tillage methods: a six year comparison. Agronomy Journal 61:524-527.

Shigley, J.E. and J.J. Uicker,Jr. 1980. *Theory of Machines and Mechanisms*. McGraw-Hill Book Company, New York, NY.

Singh, T.A., G.W. Thomas, W.W. Moschler and D.C. Martens. 1966. Phosphorus uptake by corn (Zea mays L.) under no-tillage and conventional practices. Agronomy Journal 58:147-148.

Slack, A.V. 1972. Fertilizer products. p47-63. In: W.C. White and D.N. Collins (editors). *The Fertilizer Handbook*. The Fertilizer Institute, Washington, D.C.

Smith, K.A. 1983. *Soil Analysis-Instrumental Techniques and Related Procedures*, K.A. Smith-Editor. Marcel-Dekker, Inc., New York, NY.

Soehne, W. 1956. Some principles of soil mechanics as applied to agricultural engineering. Grundlagen der Landtechnik 7:11-27 (Natl. Inst. Agr. Engin. English Translation No. 53).

Solutions, Inc. 1984. New products. Editor: Ned van Buren, Solutions Magazine, Inc, Peoria IL 61615. November/December 1984.

Stafford, J.V. 1979. The performance of a rigid tine in relation to soil properties and speed. Journal of Agricultural Engineering Research 24:41-56.

Stafford, J.V. and D.W. Tanner. 1983a. Effect of rate on soil shear strength and soil-metal friction: i. shear strength. Soil and Tillage Research 3:245-260.

Stafford, J.V. and D.W. Tanner. 1983b. Effect of rate on soil shear strength and soil-metal friction: ii. soil-metal friction. Soil and Tillage Research 3:321-330.

Suggs, C.W. and H.B. Peel, Jr. 1985. Speed control for hydraulically powered outboard wheel. Paper No. 85-1585, American Society of Agricultural Engineers, St. Joseph, MI.

Terman, G.L. and C.M. Hunt. 1964. Volatilization losses of nitrogen from surface-applied fertilizers, as measured by crop response. Soil Science Society of America Proceedings 28:667-672.

Terzaghi, K. 1943. *Theoretical Soil Mechanics*. John Wiley and Sons, Inc., New York, NY.

Timmons, D.R. 1984. Nitrate leaching as influenced by water application level and nitrification inhibitors. Journal of Environmental Quality 13(2):305-309.

Touchton, J.T. and W.L. Hargrove. 1982. Nitrogen sources and methods of application for no-tillage corn production. Agronomy Journal 74:823-826.

Townsend, J.S. and J.M. Bethge. 1984. Furrow opener for proper seed and fertilizer placement in no-till. Paper No. 84-1511, American Society of Agricultural Engineers, St. Joseph, MI.

Triplett, G.B., Jr. and D.M. Van Doren, Jr. 1969. Nitrogen, phosphorus and potassium fertilization of non-tilled maize. Agronomy Journel 61:637-639.

Turnage, G.W. and D.R. Freitag. 1969. Effects of cone velocity and size on soil penetration resistance. Paper No. 69-670, American Society of Agricultural Engineers, St. Joseph, MI.

TVA. 1978. *Engineering Soils Testing-3rd edition, Technical Manual SM-106*. Singleton Materials Engineering Laboratory, Division of Construction, Tennessee Valley Authority, Knoxville, TN.

Wanzel, R.J. 1988. Point injector rolls out. Solutions Magazine, Inc. 32(4):14-15.

Wilkens, D.E., P.E. Rasmussen, B.L. Klepper, and D.A. Haasch. 1982. Grain drill opener design for fertilizer placement. Paper No. 82-1516, American Society of Agricultural Engineers, St. Joseph, MI.

Winterkorn, H.F. and Hsai-Yang Fang. 1975. *Foundation Engineering Handbook*. Van Nostrand Reinhold Company, New York, NY.

Wismer, R.D. and H.J. Luth. 1972. Performance of plane soil cutting blades in clay. Transactions of the ASAE 15(2):211-216.

Womac, A.R., F.D. Tompkins, E.C. Drumm, R.S. Freeland and J.B. Wilkerson. 1987. Measuring dynamic response of soil subjected to impact loading. Paper No. 87-1010, American Society of Agricultural Engineers, St. Joseph, MI.

Wu, Tien Hsing. 1971. *Soil Dynamics*. Allyn and Bacon, Inc., Boston, MA.

Yost, R.S., E.J. Kamprath, E. Lobato and G. Naderman. 1979. Phosphorus response of corn on an oxisol as influenced by rates and placement. Soil Science Society of America Journal 43:338-343.

Young, S.C., C.E. Johnson, and R.L. Schafer. 1984. Real-time quantification of soil physical condition. Paper No. 84-1037, American Society of Agricultural Engineers, St. Joseph, MI.

APPENDIX

APPENDIX

Table 12. Test parameters and results of dynamic response of soil subjected to impact loading.

Impact Test*	Dropped Mass (kg)	Probe Velocity (mm/s)	Impact Energy (N-m)	Maximum Depth (mm)	Peak Force (N)
cl6f1	5.8133	4596.4	61.41	93.90	1165.33
cl6f2	5.8133	4278.2	53.20	95.78	904.65
cl6f3	5.8133	4709.2	64.46	107.05	886.10
cl5f1	5.7470	4720.1	64.02	109.87	843.86
cl5f2	5.7470	4700.9	63.50	112.69	935.56
cl5f3	5.7470	4465.1	57.29	94.84	904.65
cl4f1	5.6913	4729.4	63.65	99.54	942.77
cl4f2	5.6913	4729.4	65.49	97.67	1057.14
cl4f3	5.6913	4808.6	65.80	108.94	979.87
cl3f1	5.6480	4791.3	64.83	130.53	903.62
cl3f2	5.6480	4749.7	63.71	156.83	815.01
cl3f3	5.6480	4756.8	63.90	134.29	836.65
cl6e1	7.4375	4352.5	70.45	99.54	1242.61
cl6e2	7.4375	4462.0	74.04	108.93	1071.57
cl6e3	7.4375	4591.8	78.41	100.43	1300.31
cl5e1	7.3712	4588.3	77.59	135.23	866.53
cl5e2	7.3712	4583.2	77.42	113.63	1095.26
cl5e3	7.3712	4577.6	77.23	116.44	1090.11
cl4e1	7.3155	4524.0	74.86	127.71	949.99
cl4e2	7.3155	4623.8	78.20	145.56	699.61

Table 12. (Continued)

Impact Test*	Dropped Mass (kg)	Probe Velocity (mm/s)	Impact Energy (N-m)	Maximum Depth (mm)	Peak Force (N)
c14e3	7.3155	4630.3	78.42	135.22	933.50
c13e1	7.2722	4567.9	75.87	138.98	865.50
c13e2	7.2722	4647.9	78.55	154.94	783.07
c13e3	7.2722	4611.6	77.33	158.70	866.53
c16d1	9.1175	3814.4	66.33	108.93	1030.35
c16d2	9.1175	4034.9	74.22	107.99	1236.42
c16d3	9.1175	4042.0	74.48	106.11	1208.60
c15d1	9.0512	4109.8	76.44	128.66	1046.84
c15d2	9.0512	3972.8	71.43	104.23	1021.08
c15d3	9.0512	3971.7	71.39	108.93	897.44
c14d1	8.9955	4084.9	75.05	127.71	996.35
c14d2	8.9955	4129.5	76.70	135.22	1005.62
c14d3	8.9955	4066.0	74.36	130.53	871.68
c13d1	8.9522	4099.9	75.24	209.41	729.49
c13d2	8.9522	4147.3	76.99	213.16	753.19
c13d3	8.9522	4139.2	76.69	216.92	733.61
c16c1	10.7975	3643.3	71.66	110.81	1012.84
c16c2	10.7975	3634.1	71.30	102.36	1218.91
c16c3	10.7975	3674.9	72.91	94.84	1306.49
c15c1	10.7312	3646.3	71.34	105.18	1088.05
c15c2	10.7312	3633.8	70.85	99.54	1216.85
c15c3	10.7312	3643.0	71.21	104.24	1060.23

Table 12. (Continued)

Impact Test*	Dropped Mass (kg)	Probe Velocity (mm/s)	Impact Energy (N-m)	Maximum Depth (mm)	Peak Force (N)
cl4cl	10.6755	3749.2	75.03	145.56	819.13
cl4c2	10.6755	3747.2	74.95	115.51	1139.57
cl4c3	10.6755	3732.4	74.36	153.07	799.55
cl3cl	10.6322	3782.5	76.06	200.02	676.94
cl3c2	10.6322	3730.7	73.99	181.24	703.73
cl3c3	10.6322	3722.1	73.65	167.16	813.98
cl6bl	12.4775	2825.9	49.82	89.21	862.41
cl6b2	12.4775	2723.6	46.28	74.18	990.17
cl6b3	12.4775	2650.2	43.82	69.49	988.11
cl5bl	12.4112	2850.7	50.43	61.03	1000.47
cl5b2	12.4112	2880.2	51.48	96.72	823.25
cl5b3	12.4112	2897.5	52.10	112.69	672.82
cl4bl	12.3555	2931.8	53.10	138.04	552.27
cl4b2	12.3555	2745.6	46.57	95.78	723.31
cl4b3	12.3555	2749.7	46.71	111.75	796.46
cl3bl	12.3122	2920.3	52.50	140.86	650.15
cl3b2	12.3122	2864.1	50.50	125.84	634.70
cl3b3	12.3122	2928.9	52.81	129.59	671.79
cl6al	20.8775	2113.1	46.61	85.45	803.68
cl6a2	20.8775	2040.4	43.46	85.46	923.20
cl6a3	20.8775	2049.8	43.86	84.51	1031.38
cl5al	20.8112	2304.7	55.27	61.04	1170.48

Table 12. (Continued)

Impact Test*	Dropped Mass (kg)	Probe Velocity (mm/s)	Impact Energy (N-m)	Maximum Depth (mm)	Peak Force (N)
cl5a2	20.8112	1936.5	39.02	60.10	1466.19
cl5a3	20.8112	2139.2	47.62	92.97	904.65
cl4a1	20.7555	2222.3	51.25	115.50	808.83
cl4a2	20.7555	2536.5	66.77	259.18	619.24
cl4a3	20.7555	2208.3	50.61	108.94	779.98
cl3a1	20.7122	2261.8	52.98	135.22	778.95
cl3a2	20.7122	2162.9	48.45	115.50	688.28
cl3a3	20.7122	2317.3	55.61	128.65	764.52
fsl6f1	5.8133	5025.9	73.42	70.42	1512.56
fsl6f2	5.8133	5034.1	73.66	81.70	1343.58
fsl6f3	5.8133	5091.5	75.35	78.88	1411.58
fsl5f1	5.7470	5070.9	73.89	85.45	1256.00
fsl5f2	5.7470	5187.3	77.32	87.33	1176.66
fsl5f3	5.7470	5232.0	78.66	78.89	1466.19
fsl4f1	5.6913	5137.6	75.11	93.91	1055.08
fsl4f2	5.6913	5196.8	76.85	77.94	1171.51
fsl4f3	5.6913	5135.9	75.06	90.15	1087.02
fsl3f1	5.6480	5064.7	72.44	122.08	767.61
fsl3f2	5.6480	5153.4	75.00	123.96	783.07
fsl3f3	5.6480	5146.9	74.81	116.44	918.04
fsl6e1	7.4375	4753.0	84.01	81.70	1492.98
fsl6e2	7.4375	4743.6	83.68	77.94	1657.84

Table 12. (Continued)

Impact Test*	Dropped Mass (kg)	Probe Velocity (mm/s)	Impact Energy (N-m)	Maximum Depth (mm)	Peak Force (N)
fsl6e3	7.4375	4797.5	85.59	85.45	1453.83
fsl5el	7.3712	4727.5	82.37	100.48	1096.30
fsl5e2	7.3712	4716.8	82.00	96.72	1126.18
fsl5e3	7.3712	4654.9	79.86	103.29	1102.48
fsl4el	7.3155	4763.0	82.98	119.26	881.98
fsl4e2	7.3155	4805.0	84.45	108.93	937.62
fsl4e3	7.3155	4733.0	81.94	122.08	1022.11
fsl3el	7.2722	4778.6	83.03	141.80	781.01
fsl3e2	7.2722	4799.8	83.77	110.81	968.53
fsl3e3	7.2722	4774.8	82.90	133.34	841.80
fsl6dl	9.1175	4188.6	79.98	78.88	1376.55
fsl6d2	9.1175	4082.5	75.98	71.37	1612.50
fsl6d3	9.1175	4190.4	80.05	67.61	1758.81
fsl5dl	9.0512	4273.8	82.66	88.28	1339.46
fsl5d2	9.0512	4228.8	80.93	89.21	1427.04
fsl5d3	9.0512	4195.0	79.64	89.21	1305.46
fsl4dl	8.9955	4200.3	79.35	119.26	942.77
fsl4d2	8.9955	4221.9	80.17	112.68	895.38
fsl4d3	8.9955	4241.9	80.93	91.09	1191.09
fsl3dl	8.9522	4199.8	78.95	139.92	773.79
fsl3d2	8.9522	4224.7	79.89	129.59	790.28
fsl3d3	8.9522	4223.6	79.85	115.50	799.55

Table 12. (Continued)

Impact Test*	Dropped Mass (kg)	Probe Velocity (mm/s)	Impact Energy (N-m)	Maximum Depth (mm)	Peak Force (N)
fs16c1	10.7975	3686.2	73.36	71.36	1668.14
fs16c2	10.7975	3750.7	75.95	62.91	1752.63
fs16c3	10.7975	3824.8	78.98	73.25	1546.56
fs15c1	10.7312	3780.8	76.70	79.82	1251.88
fs15c2	10.7312	3774.9	76.46	101.42	1142.66
fs15c3	10.7312	3543.7	67.38	121.13	865.50
fs14c1	10.6755	3851.0	79.16	114.56	861.37
fs14c2	10.6755	3762.2	75.55	103.30	937.62
fs14c3	10.6755	3754.7	75.25	111.75	941.74
fs13c1	10.6322	3847.6	78.70	143.68	732.58
fs13c2	10.6322	3847.4	78.69	138.04	748.04
fs13c3	10.6322	3904.6	81.05	156.83	685.18
fs16b1	12.4775	2876.8	51.63	61.04	1247.76
fs16b2	12.4775	3016.0	56.75	63.86	1298.24
fs16b3	12.4775	2999.8	56.14	61.98	1433.22
fs15b1	12.4112	2942.5	53.73	66.67	1158.12
fs15b2	12.4112	2959.4	54.35	61.98	1229.21
fs15b3	12.4112	2887.5	51.74	66.68	1131.33
fs14b1	12.3555	3093.8	59.13	82.63	877.86
fs14b2	12.3555	3003.0	55.71	89.21	961.32
fs14b3	12.3555	2957.9	54.05	68.55	1101.45
fs13b1	12.3122	2996.1	55.26	88.28	852.10

Table 12. (Continued)

Impact Test*	Dropped Mass (kg)	Probe Velocity (mm/s)	Impact Energy (N-m)	Maximum Depth (mm)	Peak Force (N)
fsl3b2	12.3122	2987.6	54.95	82.64	857.25
fsl3b3	12.3122	2997.2	55.30	77.01	982.96
fsl6a1	20.8775	2013.2	42.31	39.44	1602.20
fsl6a2	20.8775	2072.1	44.82	51.64	1691.84
fsl6a3	20.8775	2072.3	44.83	49.77	1766.02
fsl5a1	20.8112	2179.5	49.43	46.01	1766.02
fsl5a2	20.8112	2262.0	53.24	62.92	1340.49
fsl5a3	20.8112	2155.8	48.36	64.80	1040.66
fsl4a1	20.7555	2162.5	48.53	68.55	962.35
fsl4a2	20.7555	2344.6	57.05	83.58	986.05
fsl4a3	20.7555	2131.7	47.16	72.31	976.77
fsl3a1	20.7122	2278.8	53.78	106.11	623.36
fsl3a2	20.7122	2174.5	48.97	80.76	752.16
fsl3a3	20.7122	2211.3	50.64	103.30	687.25
sl6f1	5.8133	4789.9	66.69	106.11	1155.03
sl6f2	5.8133	4779.9	66.41	96.73	1066.42
sl6f3	5.8133	4751.8	65.63	82.64	1105.57
sl5f1	5.7470	4783.1	65.74	118.32	1227.15
sl5f2	5.7470	4798.3	66.16	104.23	1231.27
sl5f3	5.7470	4760.5	65.12	96.72	1090.11
sl4f1	5.6913	4763.5	64.57	115.50	983.99
sl4f2	5.6913	4815.2	65.98	123.02	872.71

Table 12. (Continued)

Impact Test*	Dropped Mass (kg)	Probe Velocity (mm/s)	Impact Energy (N-m)	Maximum Depth (mm)	Peak Force (N)
sl4f3	5.6913	4866.4	67.39	107.06	1116.90
sl3f1	5.6480	4660.9	61.35	118.32	931.44
sl3f2	5.6480	4633.7	63.69	140.86	710.94
sl3f3	5.6480	4841.7	66.20	155.89	629.55
sl6e1	7.4375	4536.5	76.53	102.35	1226.12
sl6e2	7.4375	4536.2	76.52	96.73	1371.40
sl6e3	7.4375	4568.6	77.62	104.23	1482.68
sl5e1	7.3712	4577.0	77.21	106.12	1292.06
sl5e2	7.3712	4582.6	77.40	102.36	1254.97
sl5e3	7.3712	4559.8	76.63	101.42	1292.06
sl4e1	7.3155	4533.9	75.19	169.03	624.39
sl4e2	7.3155	4612.8	77.83	113.63	912.89
sl4e3	7.3155	4566.1	76.26	138.98	893.32
sl3e1	7.2722	4585.3	76.45	162.46	677.97
sl3e2	7.2722	4415.4	70.89	157.77	755.25
sl3e3	7.2722	4626.2	77.82	179.36	672.82
sl6d1	9.1175	4022.7	73.77	102.35	1054.05
sl6d2	9.1175	4092.7	76.36	113.62	1113.81
sl6d3	9.1175	4055.6	74.98	107.05	1085.99
sl5d1	9.0512	4021.5	73.19	118.32	975.74
sl5d2	9.0512	4051.0	74.27	101.42	1103.51
sl5d3	9.0512	3923.3	69.66	109.86	868.59

Table 12. (Continued)

Impact Test*	Dropped Mass (kg)	Probe Velocity (mm/s)	Impact Energy (N-m)	Maximum Depth (mm)	Peak Force (N)
sl4d1	8.9955	4133.0	76.83	156.13	901.56
sl4d2	8.9955	4151.5	77.52	144.62	856.22
sl4d3	8.9955	4130.3	76.73	142.73	854.16
sl3d1	8.9522	4183.5	78.34	157.76	881.98
sl3d2	8.9522	4230.5	80.11	191.57	680.03
sl3d3	8.9522	4318.8	83.49	241.34	621.30
sl6c1	10.7975	3657.2	72.21	76.07	1324.00
sl6c2	10.7975	3765.8	76.56	101.42	1136.48
sl6c3	10.7975	3950.4	84.25	81.70	1332.25
sl5c1	10.7312	3772.4	76.36	96.73	1099.39
sl5c2	10.7312	3850.9	79.57	100.48	1215.82
sl5c3	10.7312	3878.2	80.70	109.87	1109.69
sl4c1	10.6755	3818.5	77.83	144.61	752.16
sl4c2	10.6755	3836.4	78.56	138.04	910.83
sl4c3	10.6755	3835.6	78.53	113.63	949.99
sl3c1	10.6322	3932.2	82.20	189.69	733.61
sl3c2	10.6322	3862.0	79.29	166.22	692.40
sl3c3	10.6322	3892.1	80.53	179.36	683.12
sl6b1	12.4775	2975.6	55.24	88.27	1041.69
sl6b2	12.4775	2900.6	52.49	92.02	905.68
sl6b3	12.4775	2879.5	51.73	83.58	895.38
sl5b1	12.4112	2934.8	53.45	97.66	852.10

Table 12. (Continued)

Impact Test*	Dropped Mass (kg)	Probe Velocity (mm/s)	Impact Energy (N-m)	Maximum Depth (mm)	Peak Force (N)
sl5b2	12.4112	2924.9	53.09	94.85	759.37
sl5b3	12.4112	2892.8	51.93	95.78	812.95
sl4b1	12.3555	2925.7	52.88	129.59	801.61
sl4b2	12.3555	2983.5	54.99	129.59	686.21
sl4b3	12.3555	2983.2	54.98	129.59	791.31
sl3b1	12.3122	3015.8	55.99	138.05	749.07
sl3b2	12.3122	3013.1	55.89	155.88	807.80
sl3b3	12.3122	3010.1	55.78	152.12	704.76
sl6a1	20.8775	2165.5	48.95	83.57	918.04
sl6a2	20.8775	2472.4	63.81	92.97	1000.47
sl6a3	20.8775	2531.6	66.90	101.41	1064.35
sl5a1	20.8112	2604.2	70.57	145.55	853.13
sl5a2	20.8112	2511.8	65.65	123.02	873.74
sl5a3	20.8112	2520.2	66.09	114.56	925.26
sl4a1	20.7555	2586.2	69.41	154.00	884.04
sl4a2	20.7555	2534.6	66.67	149.31	829.43
sl4a3	20.7555	2513.4	65.56	134.28	863.44
sl3a1	20.7122	2665.5	73.58	174.67	648.09
sl3a2	20.7122	2648.8	72.66	180.30	620.27
sl3a3	20.7122	2626.8	71.46	179.36	680.03

*Test conditions are encoded into the test name. Converting the code requires that the name be read from left to right. The following symbol scheme describes test conditions: cl, fsl, and sl represent clay loam, fine sandy loam, and silt loam, respectively; 3, 4, 5, and 6 represent probe diameters of 9.5, 12.7, 15.9, and 19.1 mm, respectively; a, b, c, d, e, and f represent probe drop heights of approximately 230, 460, 790, 1020, 1370, and 1680 mm, respectively; and 1, 2, and 3 represent replications. For example, impact test sl3a3 was conducted in silt loam, with a 9.5-mm diameter probe, at a drop height of 230 mm, and was the third replication.

VITA

Alvin Ray Womac was born in Athens, Tennessee on January 22, 1959. He attended schools in Athens and was graduated from McMinn County High School in 1977. He entered The University of Tennessee, Knoxville in September 1977 and received a Bachelor of Science degree in Agricultural Engineering in June 1981. Being hired as an Assistant in Extension, he then entered The Graduate School at The University of Tennessee, Knoxville where he completed the Master of Science degree in Agricultural Engineering in December 1983. He continued his graduate studies toward the Doctor of Philosophy Degree at The University of Tennessee, Knoxville as a Graduate Research Assistant and an Instructor. He is a member of the American Society of Agricultural Engineers, American Society of Civil Engineers, and The American Society of Mechanical Engineers. Also, he is registered by the State of Tennessee as an Engineer-In-Training. He is married to the former Eleanore Jane Pobst of Bristol, Tennessee.